Table of Contents

ABBREVIATIONS

$[Ca^{2+}]c$	Cytoplasmic calcium concentration
$[Ca^{2+}]er$	Endoplsmic reticulum calcium concentration
$[Ca^{2+}]m$	Mitochondrial calcium concentration
ADP	Adenosine diphosphate
ANT	Adenine nucleotide translocator
Apaf-1	Apoptotic protease activating factor
ATAD3A	ATPase family, AAA domain containing 3A
ATP	Adenosine triphosphate
ATP5A	ATP synthase, H+ transporting, mitochondrial F1 complex, alpha subunit
Bcl-2/Xl	B cell leukemia/lymphoma 2/Extra large
BH1-4	Bcl-2 homology domain 1-4
BiP	Endoplasmic reticulum HSC70-cognate binding protein
BRET	Bioluminescence resonant energy transfer
CCH	Carbachol
CNS	Central nervous system
DBD	DNA binding domain
DCF	Dicloro-fluoroscein
DHE	Dihydroethidium
DOA	Dominant optic atrophy
DRP1	Dynamin related protein 1
EAE	Experimental autoimmune encephalomyelitis
EM	Electron microscopy
ER	Endoplasmic reticulum
ETC	Electron transport chain
FACL4	Fatty acid-CoA ligase 4
FAD	Flavin adenine dinucleotide
FCCP	Carbonylcyanide-p-trifluoromethoxyphenylhydrazone
FIS1	Mitochondrial fission 1 protein
FRET	Fluorescence resonant energy transfert
GFAP	Glial fibrillary acid protein
GFP	Green fluorescent protein
GTP	Guanosine triphosphate

HA	Hemagglutinin
HIF1α	Hypoxia-inducible factors 1 alpha
HSP60	Heat shock protein 60
IAP	Inhibitor of apoptosis protein
IMM	Inner mitochondrial membrane
INFG	Interferon gamma
IP3R	Inositol phosphate 3 receptor
MAM	Mitochondria associated membrane
MAPK	Mitogen activated protein kinase
MBP	Myelin basic protein
Mcl-1	Myeloid cell leukemia sequence 1
MCU	Mitochondrial Calcium Uniporter
MEF	Mouse embryonic fibroblast
MFN1/2	Mitofusin 1/2
Mmm	Mitochondrial morphology maintenance
$\Delta\Psi_m$	Mitochondrial membrane potential
MS	Multiple sclerosis
MTCO1	Mitochondrially encoded cytochrome c oxidase I
NADH	Nicotinamide adenine dinucleotide
NCX	Sodium Calcium exchanger
NDUF8B	NADH dehydrogenase [ubiquinone] 1 beta subcomplex subunit 8
NG2	Chondroitin sulfate proteoglycan NG2
NLS	Nuclear localization sequence
OMM	Outer mitochondrial membrane
OPA1	Optic atrophy 1
OSP	Oligodendrocyte specific protein
OXPHOS	Oxidative phosphorylation
PACS-2	Phosphofurin acidic cluster sorting protein 2
PMCA	Plasma membrane Ca^{2+} ATPase
PML	Promyelocytic leukemia protein
PP2A	Protein phosphatase 2 a
PTP	Permeability Transition Pore
PUMA	P53 upregulated modulator of apoptosis
RNS	Reactive nitrogen species

ROS	Reactive oxygen species
RyRs	Ryanodine receptor
SDHB	Succinate dehydrogenase [ubiquinone] iron-sulfur subunit B
SERCA	Sarco/Endoplasmatic Reticulum Calcium ATPasi
Sig-1R	Sigma 1 receptor
SR	Sarcoplasmic reticulum
TCA	Tricarboxylic acid cycle
TNFR1	Tumour necrosis factor alpha receptor 1
TNFR2	Tumour necrosis factor alpha receptor 2
TUNEL	Terminal deoxynucleotidyl transferase dUTP nick end labeling
UBC6	Ubiquitin-conjugating enzyme E2 6
UQCRC2	Ubiquinol-cytochrome c reductase core protein II
VDAC	Voltage dependent anion channel
YFP	Yellow fluorescent protein

Abstract

In recent years, mitochondria have gained much interest as organelles involved not only in the processes of obtaining energy, but also associated with novel roles in cell physiopathology. These roles range from mitochondria being the site for lipid synthesis, through constituting a buffering system for intracellular calcium, and from being a mediator of reactive oxygen species signalling to a regulator of different cell death types. This group of roles requires a highly regulated system of signalling mechanisms. One of these emerging mechanisms is the communication between the mitochondria and the endoplasmic reticulum. In fact, mitochondria and endoplasmic reticulum are tightly associated, in a region called mitochondria associated membranes, where several signalling events allow continuous communication between the two organelles. Among these signalling events, calcium signalling has been considered of great importance. Advanced techniques of molecular biology allow the development of tools for the investigation of these complex subcellular compartments. Particularly useful are those based on the green fluorescent protein and the calcium sensitive luminescent protein, aequorin.

In this work, the aforementioned tools have been used to investigate mitochondrial physiology, especially its communications with the endoplasmic reticulum. Two different cellular events were studied: i) the regulation of apoptosis by a strategic oncosuppressor, p53 and ii) differentiation of oligodendrocytes progenitor cells into adult oligodendrocytes during stress condition generated by cytokines.

Performed experiments allowed the describing of the endoplasmic reticulum as a new intracellular localization site of p53, where it increases the luminal calcium concentration, promoting the sensitivity to calcium dependent apoptotic stimuli. Simultaneously, it has been revealed how mitochondria are a target for TNFα in oligodendrocytes progenitors, where it promotes reactive oxygen species production and impairment of the respiratory chain activity, inhibiting cell differentiation without promoting cell death.In conclusion, these approaches reveal completely new relations between mitochondria, calcium signalling and cell physiology, shedding new light on the role for this fascinating organelle.

Riassunto

I mitocondri, sebbene da sempre considerati la principale sorgente energetica intracellulare, negli ultimi anni sono stati sempre più investiti di ruoli completamente nuovi per la patofisiologia cellulare. Questi vanno dalla sintesi dei lipidi, a sistema di buffer intracellulare del calcio, da mediatori della segnalazione via ROS a regolatore di vari meccanismi di morte intracellulare. Questo insieme di ruoli richiedono un regolato sistema di vie di segnalazione, di cui una delle emergenti, è la comunicazione con il reticolo endoplasmatico. Infatti mitocondri e reticolo endoplasmatico sono strettamente associate, in quella regione chiamata MAM, dove diversi eventi segnalatori avvengono permettendo una comunicazione continua tra I due organelli, primo fra tutti la segnalazione via calcio. Le recenti tecniche di biologia molecolare hanno permesso lo sviluppo di strumenti per lo studio di questi complessi sottodistretti cellulari, in modo particolare basati sulla proteina fluorescente verde e sulla sonda luminescente calcio-sensibile equorina.

In questo lavoro tali strumenti sono stati usati per studiare la fisiologia mitocondriale, specialmente le sue comunicazioni con il reticolo endoplasmico, in due eventi cellulari completamente diversi: la regolazione dell'apoptosi da parte dell'oncosoppressore, p53, e il differenziamento da progenitore dell'oligodendrocita ad oligodendrocita durante esposizione a citochine proinfiammatorie.

In particolare questi strumenti ci hanno permesso di osservare come il reticolo endoplasmico debba essere considerata una nuova localizzazione intracellulare di p53, dove aumenta la concentrazione di calcio intraluminale, promuovendo la sensibilità a stimoli apoptotici calcio dipendenti. Contemporaneamente si è ossevato come I mitocondri siano un target del TNFα nei progenitori, inducendo un'aumento di ROS e deregolazione della catena respiratoria , con conseguente arresto del differenziamento cellulare.

Concludendo tali approcci hanno permesso di rivelare relazioni completamente nuove tra mitocondri, segnalazione via calcio e fisiologia cellulare, sottolineando il ruolo di questo organello nella fisiopatologia cellulare.

Introduction

Mitochondrial structure

Mitochondria are organelles with extremely complex structures and functions. They are derived from an α-proteobacterium-like ancestor, due to an ancient "invasion" that occurred more than a billion years ago (1). The acquisition of mitochondria (and plastids) was a key event in the evolution of the eukaryotic cell, supplying it with bioenergetic and biosynthetic factors.

At subcellular resolution it appear composed by an outer membrane (OMM), mostly permeable to ions and metabolites up to 10 kDa, then an highly selective inner mitochondrial membrane (IMM), characterized by invaginations called cristae and which enclose the mitochondrial matrix. The space between these two structures is traditionally called the intermembrane space (IMS). The IMM is further subdivided into two distinct compartments: the peripheral inner boundary membrane and the cristae (2). Cristae are not simply random folds, but rather internal compartments formed by profound invaginations originating from very tiny "point-like structures" in the inner membrane. These narrow tubular structures, called cristae junctions, can limit the diffusion of molecules from the intra-cristae space towards the IMS, thus creating a microenvironment where mitochondrial electron transport chain (ETC) complexes (as well as other proteins) are hosted and protected from random diffusion. The inner boundary membrane is enriched with structural proteins and components of the import machinery of mitochondria (3).

Mitochondrial morphology in living cells is heterogeneous and can range from small spheres to interconnected tubules (4). This heterogeneity results from the balance between fusion and fission, and represents a process termed mitochondrial dynamics (5). Growing evidence indicates that mitochondrial morphology is critical for the physiology of the cell and changes in mitochondrial shape have been related to many different processes such as development, neurodegeneration, calcium (Ca^{2+}) signalling, ROS production, cell division, and apoptotic cell death (6).

Mitochondrial shape is controlled by the recently identified "mitochondria-shaping proteins", which regulate the fusion-fission equilibrium of the organelle. In mammals, key components of the fusion machinery include the homologues MFN1 and MFN2 (7). The only dynamin-like GTPase currently identified in the IMM is OPA1, a fusion protein which is mutated in dominant optic atrophy (DOA), the most common cause of inherited optic neuropathy. Post-transcriptional mechanisms, including proteolytic processing, tightly regulate OPA1 activity. In mammalian cells, mitochondrial division is regulated by DRP1 and FIS1 (8, 9). The large GTPase DRP1 is a cytosolic dynamin-related protein whose inhibition or downregulation results in a highly interconnected mitochondrial

network (9). The same phenotype is caused by downregulation of FIS1 (8), a protein of the OMM, proposed to act as a mitochondrial receptor for DRP1 (10). For example, mitochondrial dynamics seem to influence production of ROS and cellular longevity. DRP1-dependent fragmentation of the mitochondrial reticulum is a crucial component for accumulation of ROS in pathological conditions (11). How mitochondrial fission is required for ROS production and lifespan remains unclear, although a link between the two processes seems plausible. Hence, factors other than mitochondrial metabolism *per se* could have a role in the pathogenesis of ROS-related diseases (11).
Interestingly, many ROS (as well as Reactive Nitrogen Species, RNS) sources and targets are localized in the mitochondria or ER and are relevant for different pathways (12).

Mitochondria are the site for major energy production

Within cells, energy is provided by oxidation of "metabolic fuels" such as carbohydrates, lipids and proteins. It is then used to sustain energy-dependent processes, such as the synthesis of macromolecules, muscle contraction, active ion transport or thermogenesis. The oxidation process results in free energy production that can be stored in phosphoanhydrine "high-energy bonds" within molecules such as nucleoside diphosphate and nucleoside triphosphate (*i.e.*, adenosine 5' diphosphate and adenosine 5' trisphosphate, ADP and ATP, respectively), phosphoenolpyruvate, carbamoyl phosphate, 2,3-bisphosphoglycerate, and other phosphates like phosphoarginine or phosphocreatine. Among them, ATP is the effective central link—the exchange coin—between energy producing and the energy demanding processes that effectively involve formation, hydrolysis or transfer of the terminal phosphate group.
In general, the main energy source for cellular metabolism is glucose, which is catabolized in the three subsequent processes: glycolysis, tricarboxylic acid cycle (TCA or Krebs cycle), and finally oxidative phosphorylation to produce ATP. In the first process, when glucose is converted into pyruvate the amount of ATP produced is low. Subsequently, pyruvate is converted to acetyl coenzyme A (acetyl-CoA) which enters the TCA cycle, enabling the production of NADH. Finally, NADH is used by the respiratory chain complexes to generate a proton gradient across the inner mitochondrial membrane, necessary for the production of large amounts of ATP by mitochondrial ATP synthase. In addition, it should be mentioned that acetyl-CoA could be generated also by lipid and protein catabolism.

Citric Acid Cycle

The TCA, also known as the citric acid cycle, was elucidated by Sir Hans Krebs in 1940 when he concluded, "*the oxidation of a triose equivalent involves one complete citric acid cycle*" (13). The

"*triose*" deriving from glycolysis is completely oxidized into three molecules of CO_2 during a sequence of reactions that allow the reduction of cofactors NAD and flavin adenine nucleotide (FAD), providing energy for the respiratory chain in the form of electrons. In 1949 it was demonstrated by Kennedy and Lehningher that the entire cycle occurs inside mitochondria (14).

The starting material for the citric acid cycle is directly provided by the pyruvate coming from glycolysis through the activity of the pyruvate dehydrogenase complex. This enzymatic complex, composed of multiple copies of the three enzymes pyruvate dehydrogenase (E1), dihydrolipoyl transacetylase, (E2) and dihydrolipoyl dehydrogenase (E3), oxidizes pyruvate to acetyl-CoA and CO_2 in an irreversible reaction in which the carboxyl group is removed from pyruvate as a molecule of CO_2. This reaction is strictly related to the cycle, even if is not comprised in it. The acetyl group introduces two carbons in each turn of the cycle; these carbons will then leave the cycle as CO_2.

The first reaction of the citric acid cycle is the condensation of one Acetyl-CoA and a molecule of citrate to generate oxaloacetate and is catalysed by citrate synthase. Citrate is then transformed into isocitrate by aconitase through the formation of cis-aconitate. This step is reversible and could lead to the formation of both citrate and isocitrate. Only the fast consumption of isocitrate by its dehydrogenase can force the reaction to the proper direction. Isocitrate dehydrogenase catalyses the first irreversible oxidation leading to the decarboxylation of isocitrate, generating CO_2 and α-ketoglutarate. The second carbon leaves the cycle in the following step, when the newly generated α-ketoglutarate is immediately decarboxylated by the α-ketoglutarate dehydrogenase complex in a reaction similar to the pyruvate decarboxylation. In fact, both these complexes share high similarities in enzyme amino acid composition and in the organization of the different subunits. Energy released from both oxidations is used to generate NADH from NAD that directly feeds into the respiratory chain.

The following step is catalysed by succinyl-Coa synthetase and utilizes the energy derived from the CoA removal to phosphorylate GDP (or ADP) to GTP (or ATP). Selectivity for the nucleotide is determined by the isozyme involved. It has been well established that at least two isozymes of succinyl-CoA synthetase are expressed in animal tissues (15) and the proportion between them seems to be tissue specific.

The succinate generated in the previous step is the 4 carbon compound that is then converted, by three sequential reactions, to oxaloacetate to conclude the cycle. The first of these steps is the oxidation of succinate to fumarate by succinate dehydrogenase. This enzyme, tightly bound to the inner mitochondrial membrane (IMM), catalyses FAD reduction to $FADH_2$ that provides electrons for the respiratory chain. Fumarate is then hydrated by fumarate hydratase to L-malate. It is particularly interesting that both succinate dehydrogenase and fumarate hydratase are

oncosuppressor genes. It has been demonstrated that inactivation of these oncosuppressors leads to the accumulation of succinate and fumarate that spread in the cytosol and promote hypoxia-inducible factor 1α (HIF1α) accumulation by inactivating prolyl hydroxilase enzymes (promoter of HIF1α degradation); HIF1α in turn promotes a pseudo-hypoxic condition that favours tumour development (16). The last event that completes the citric acid cycle is the oxidation of L-malate to oxaloacetate. This reaction is performed by L-malate dehydrogenase, which induces the reduction of another molecule of NAD to NADH. The resulting molecule of oxaloacetate is suitable for starting another cycle through condensation with an acetyl group.

During all these processes, only one molecule of ATP (or GTP) is produced, but three molecules of NADH and one of FADH2 (plus one molecule of NADH from pyruvate dehydrogenase), which provide electrons for respiratory chain, are also generated and subsequently result in the production of large amounts of ATP (discussed later).

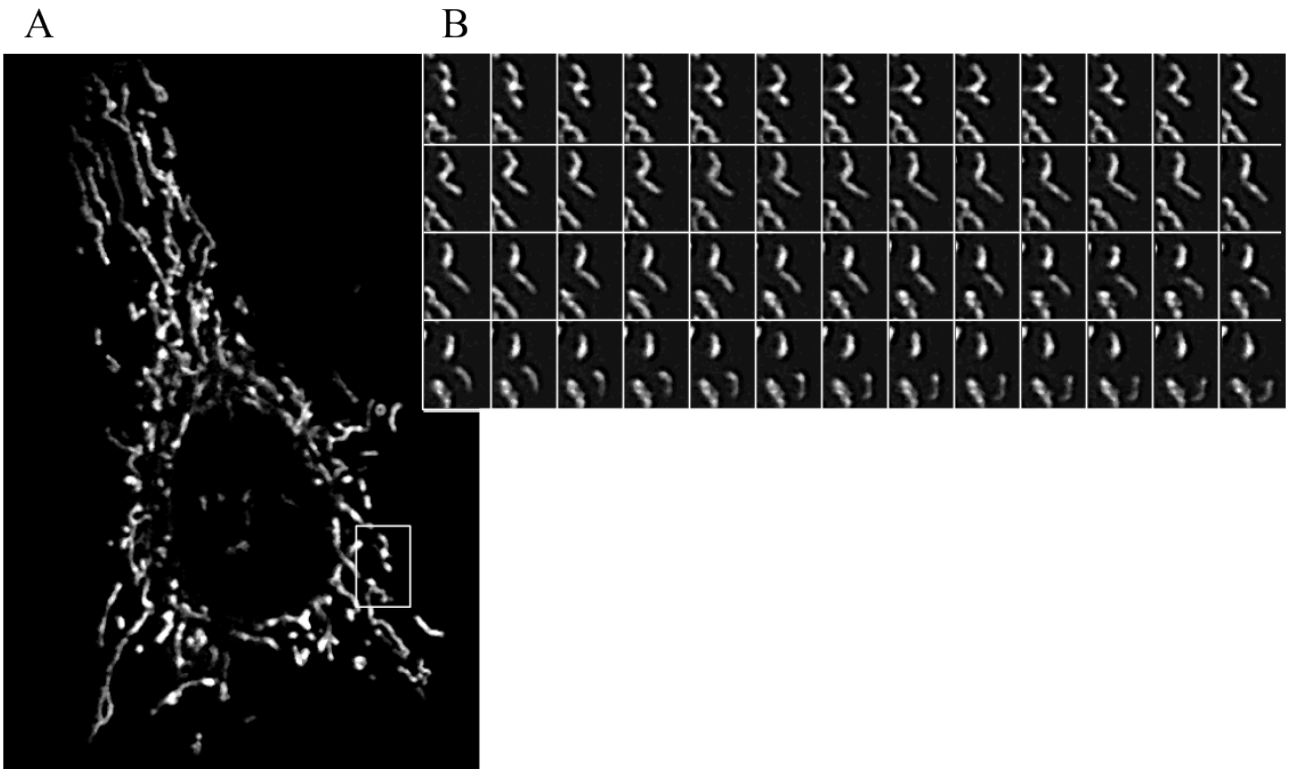

Fig1. Dynamic remodelling within mitochondrial network. (A) fast confocal imaging of mitochondria stained with mtDsRed. (B) Time series of cell portion enlightened in A showing mitochondrial fission, each step is separated by 1sec delay

Respiratory chain and Oxidative Phosphorylation

Respiratory chain comprises a series of components (complexes) conducting electron transfer across the membrane and involved in oxidative phosphorylation (OXPHOS), a process that occurs in aerobic conditions. In eukaryotic cells, electron transport occurs in mitochondria and chloroplasts, whereas in bacteria it is carried out across the plasma membrane. As mentioned, the electron transfer is considered a part OXPHOS, the process through which ADP is phosphorylated into ATP by dint of energy derived from the oxidation of nutrients.

Four protein complexes and ATP synthase, all bound to the IMM, as well as two shuttles are the known players of one of the trickiest mechanisms resolved in biochemistry. The first of these complexes is the NADH:ubiquinone oxidoreductase (complex I) which removes electrons from NADH (produced in the citric acid cycle) and passes them on to the first shuttle, ubiquinone, a liposoluble cofactor located within the phospholipid bilayer of the IMM. Succinate dehydrogenase (or complex II) is another entrance site for electrons into the respiratory chain. In this case, electrons derived from the oxidation of succinate are passed through FAD to ubiquinone. Once ubiquinone is reduced to ubiquinol, it is able to pass electrons to the third complex, ubiquinone:cytochrome *c* oxidoreductase. Here, electrons are moved through several heme groups from the liposoluble shuttle ubiquinone to the water soluble shuttle cytochrome *c*. Cytochrome *c* is a small protein (about 12.5 kDa), located in the intermembrane space (IMS), which can accommodate one electron in its heme group. Despite its water solubility, cytochrome *c* is usually bound to the external surface of the IMM due to the interaction with the cardiolipin (17). This interaction (crucial in the determination of the cell fate) helps the shuttle to reach its electron acceptor, complex IV. Cytochrome *c* oxidase is the last complex of the electron transport. Electrons from cytochrome *c* are accumulated in copper centres and passed to oxygen through heme groups. Oxygen is then reduced to water. This constitutes the bulk of oxygen consumption in all aerobic life.

Electron transport through complexes I, III and IV induces the pumping of protons from the matrix to the IMS. Specifically, for every two electrons coming from one molecule of NADH, four H^+ are moved by complex I, four by complex III, and two by complex IV. The second respiratory complex does not generate any proton movement (18). The respiratory chain in active mitochondria generates a large difference in $[H^+]$ across the IMM, resulting in the generation of an electrical potential (about -180 to -200 mV) and variation in the pH of about 0.75. A constant proton motive force drives the ATP synthesis trough the last step of OXPHOS, the ATP synthase. Understanding the activity and organization of this enzyme won researchers more than one Nobel Prize. First, Peter Mitchell in 1978 received his prize for the formulation of the chemiosmotic theory. Initially he

hypothesized how an enzymatic activity could at the same time involve ion transport (proton transport through the IMM) and a chemical reaction (ATP phosphorylation). Almost two decades later, in 1997, the Nobel Prize was awarded to Paul Boyer and John Walker who elucidated the mechanism of action of ATP synthase, here briefly reviewed. ATP synthase could be divided in two main components: F_0 that allows the channelling of protons, and F_1 that catalyses ATP phosphorylation. The F_0 is embedded in the IMM, while the F_1 resides in the mitochondrial matrix and is bound to the F_0 through a γ subunit (which drives conformational changes) and a b2δ dimer (that holds F_0 and F_1 together). The protons flow from the intermembrane space to the matrix through the F_0 inducing its rotation; the movement is transmitted from the γ subunit to the F_1 causing conformational rearrangements. The F_1 has a trimeric structure consisting of αβ dimers. The sequential changes are linked to the binding of substrates, phosphorylation and release of ATP. The three available dimers are never in the same conformational state and, what is more, the conformational changes in one dimer drive rearrangements in the other (for a more detailed explanation refer to (19)). It has been calculated that for the synthesis of one ATP molecule, 4 protons are required (3 for the ATP synthase rearrangements and 1 for ATP, ADP and Pi transport, (20)). Once synthetized, ATP can locate inside mitochondrial matrix or be transported into the IMS by the nucleotide exchanger adenine nucleotide translocase (ANT) that passively exchanges ATP with ADP. Once in the IMS, ATP can freely pass the OMM through the voltage dependent anion channel (VDAC).

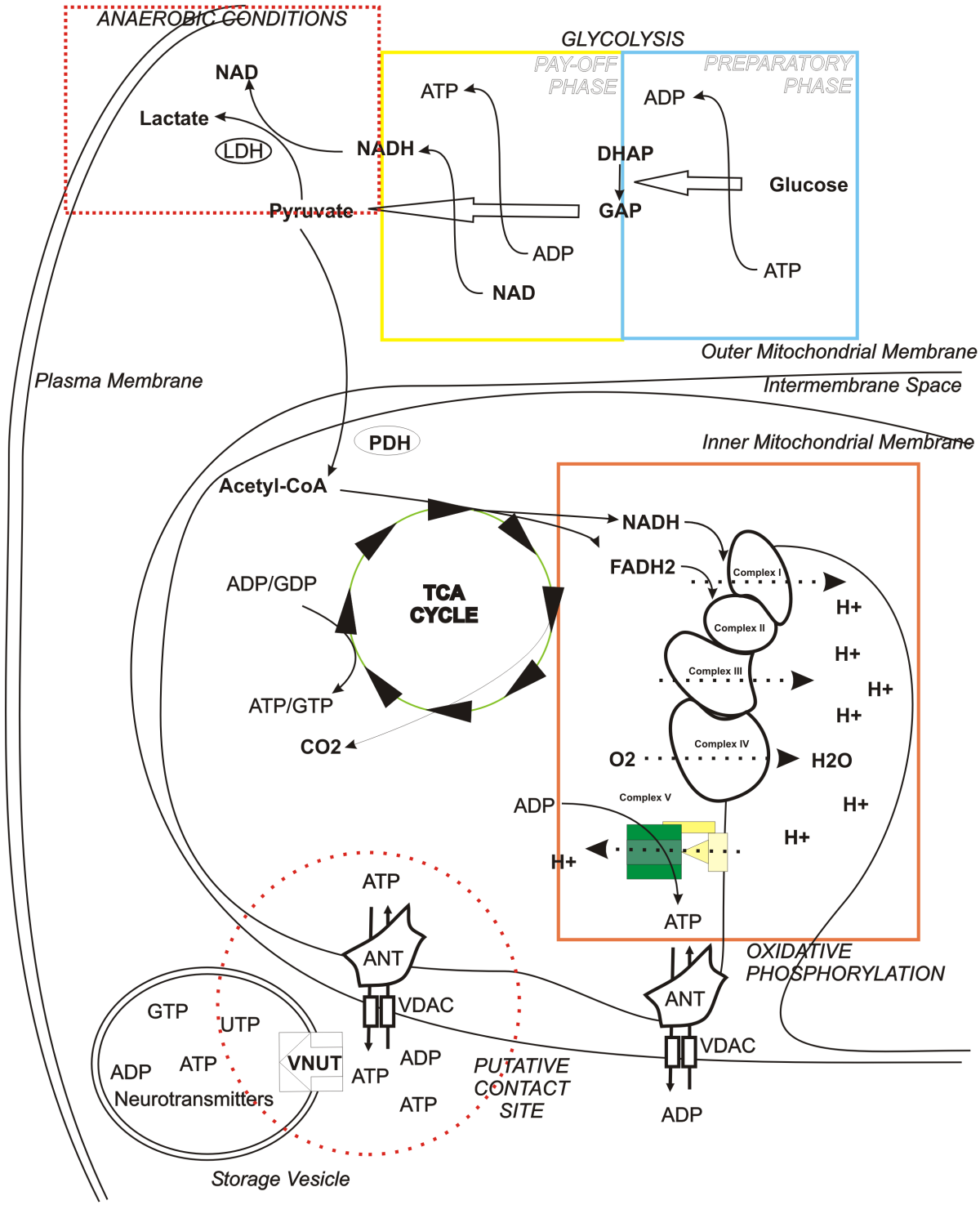

Fig2. A schematic representation of principal metabolic reactions occurring within mitochondria. Glycolysis is represented in the yellow and blue boxes, the TCA cycle by the green circle, and oxidative phosphorylation in the orange box. Reduction of pyruvate to lactate is represented inside the red dotted rectangle. Hypothetical contacts between ATP storage vesicles and mitochondria, with preferential ATP transfer, are shown within the red dotted circle.

Mitochondria: versatile players between cell proliferation and death

At the same time, mitochondria are also important checkpoints of the apoptotic process, as they may release caspase cofactors (21). Indeed, the apoptotic intrinsic pathway is activated by the release of several mitochondrial proteins into the cytosol. The main player in the finely tuned apoptotic activation process is undoubtedly cytochrome c. The majority of cytochrome c is tightly bound to mitochondrial inner membrane, thanks to its electrostatic interactions with acidic phospholipids, but a small fraction probably exists loosely attached to inner mitochondrial membrane and available for mobilization.

This protein is an irreplaceable component of the mitochondrial electron transport chain, shuttling electrons from complexes III to IV, and is thus essential to life: the disruption of its only gene is embryonic lethal (22). Once released in the cytoplasm, this protein drives the assembly of a caspases activating complex together with Apaf-1 (apoptosis–protease activating factor 1) and caspase 9, the so-called 'apoptosome'. Cytochrome c, once in the cytosol, induces the rearrangement and heptaoligomerization of Apaf-1: each of these complexes can recruit up to seven caspase molecules, leading to their proteolytic self-processing and consequent activation (23).

Mitochondria contain several other proapoptotic, intermembrane space-resident proteins, such as Smac/ DIABLO, HtrA2/Omi, AIF and EndoG. DIABLO (direct inhibitor of apoptosis-binding protein with a low isoelectric point) and HtrA2 (high temperature requirement protein A2) both have an N-terminal domain that can interact and inhibit IAPs (inhibitor of apoptosis proteins). IAPs, such as XIAP, cIAP-1 and cIAP-2, are cytosolic soluble peptides that normally associate and stabilize procaspases, thus preventing their activation. Conversely, apoptosis-inducing factor and EndoG (endonuclease G) translocate from intermembrane space to the nucleus upon treatment with several apoptotic stimuli where they seem to mediate chromatin condensation and DNA fragmentation (24).

In HeLa cells upon ceramide treatment, we observed Ca^{2+} release from the ER and loading into mitochondria. As a consequence, organelle swelling and fragmentation were detected that were paralleled by the release of cytochrome c. These changes were prevented by Bcl-2 expression as well as experimental conditions that lowered $[Ca^{2+}]_{er}$ (25). Mitochondrial permeability transition pore (PTP: a large conductance channel that opens through a conformational change of its still debated protein components) opening in ceramide-dependent apoptosis was directly demonstrated by Hajnoczky and colleagues (26) who could demonstrate that the lipid mediator facilitates PTP opening. In this case, ceramide acts as a 'mitochondrial sensitizer' that transforms physiological IP3-mediated Ca^{2+} signals into inducers of apoptosis.

The Bcl-2 protein family controls the above-described intrinsic pathway of apoptosis. Proapoptotic Bax and Bak proteins exist as inactive monomers in viable cells with Bax localizing in the cytosol, loosely attached to membranes, and Bak residing in mitochondrial fraction. Upon apoptosis induction, Bax translocate to mitochondria where it homo-oligomerizes and inserts in the outer membrane; similarly, also Bak undergoes a conformational change, which induces its oligomerization at the outer mitochondrial membrane. Together, these events trigger mitochondrial outer membrane permeabilization, the crucial process mediating the release of intermembrane space-resident caspase cofactors into the cytoplasm (27).

Mitochondria also undergo a more 'macroscopic' remodelling of their shape during the programed cell death. Indeed, after apoptosis induction, mitochondria become largely fragmented, resulting in small, rounded and numerous organelles. This process occurs quite early in apoptotic cell death, soon after Bax/Bak oligomerization, but before caspase activation. Interestingly, the perturbation of the equilibrium between fusion and fission rates seems to correlate with cell death sensitivity. In particular, conditions in which mitochondrial fission is inhibited, such as DRP1 (dynamin-like protein 1) downregulation or mitofusins overexpression, strongly delay caspase activation and cell death induced by numerous stimuli. Similarly, stimulation of organelle fission (by DRP1 overexpression or Mfn1/2 and OPA1 inhibition) promotes apoptosis by facilitating cytochrome c release and apoptosome assembly (28). However, the relationship between mitochondrial fusion/fission and apoptosis is complex and mitochondrial fragmentation is not necessarily related to apoptosis. Indeed, mitochondrial fission per se does not increase cell death and DRP1 overexpression has been reported to protect cells from some apoptotic challenges, such those dependent on mitochondrial Ca^{2+} overload (29).

Another hallmark of apoptosis is the loss of mitochondrial membrane potential, secondary to the opening of mPTP triggered by different pathological conditions (e.g., Ca^{2+} overload, ATP depletion, oxidative stress, high inorganic phosphate or fatty acid). The molecular structure of this pore is currently highly debated, but the main players in mPTP assembly seem to include the adenine nucleotide transporter (ANT) in the inner membrane, the voltage-dependent anion channel (VDAC), the peripheral benzodiazepine receptor in the outer membrane and cyclophilin D, a matrix protein (30). The availability of chemical mPTP inhibitors such as cyclosporine A and related compounds lacking the cytosolic inhibitory effect on calcineurin, as well as the development of cyclophilin D knockout mouse will help to clarify the role of mPTP in physiological and pathological condition and identify areas of pharmacological intervention in common disorders such as ischemia-reperfusion injury, liver diseases, neurodegenerative and muscle disorders (31-33).

Interestingly, some of the proposed components of the mPTP participate in Ca^{2+} homeostasis. Indeed, transient expression of VDAC enhanced the amplitude of the agonist-dependent increases in mitochondrial matrix Ca^{2+} concentration by allowing the fast diffusion of Ca^{2+} from ER release sites to the inner mitochondrial membrane. As to the functional consequences, VDAC overexpressing cells are more susceptible to ceramide-induced cell death, thus confirming that mitochondrial Ca^{2+} uptake has a key function in the process of apoptosis (34). ANT overexpression instead reduced the amplitude of the $[Ca^{2+}]_m$ peak following ER Ca^{2+} release, and this effect was partially reversed by treating the cells with cyclosporine A, suggesting the involvement of mPTP in ER-mitochondria Ca^{2+} transfer (35). Moreover, mitochondria are quantitatively the most important source of intracellular reactive oxygen species and leak from the electron transfer chain is supposed to be the main route (36). Recently, a totally new, unexpected pathway has emerged that involves p66Shc in mitochondrial reactive oxygen species production. Intriguingly, upon phosphorylation by PKCb and peptidyl–prolyl cis/trans isomerase (Pin1) recognition, p66shc translocates to mitochondria (37) where it exerts its own oxidoreductase activity (38). As a consequence, p66shc directly oxidizes cytochrome c (thus allowing electron to escape mitochondrial electron transport chain) and generates H_2O_2, leading to mPTP opening and in turn cell death. The existence of a protein that 'steals' electrons from the mitochondrial electron transport chain and produces reactive oxygen species provides direct evidence for the role of reactive oxygen species in signal transduction, that may represent the biochemical basis of the free radical theory of ageing (39).

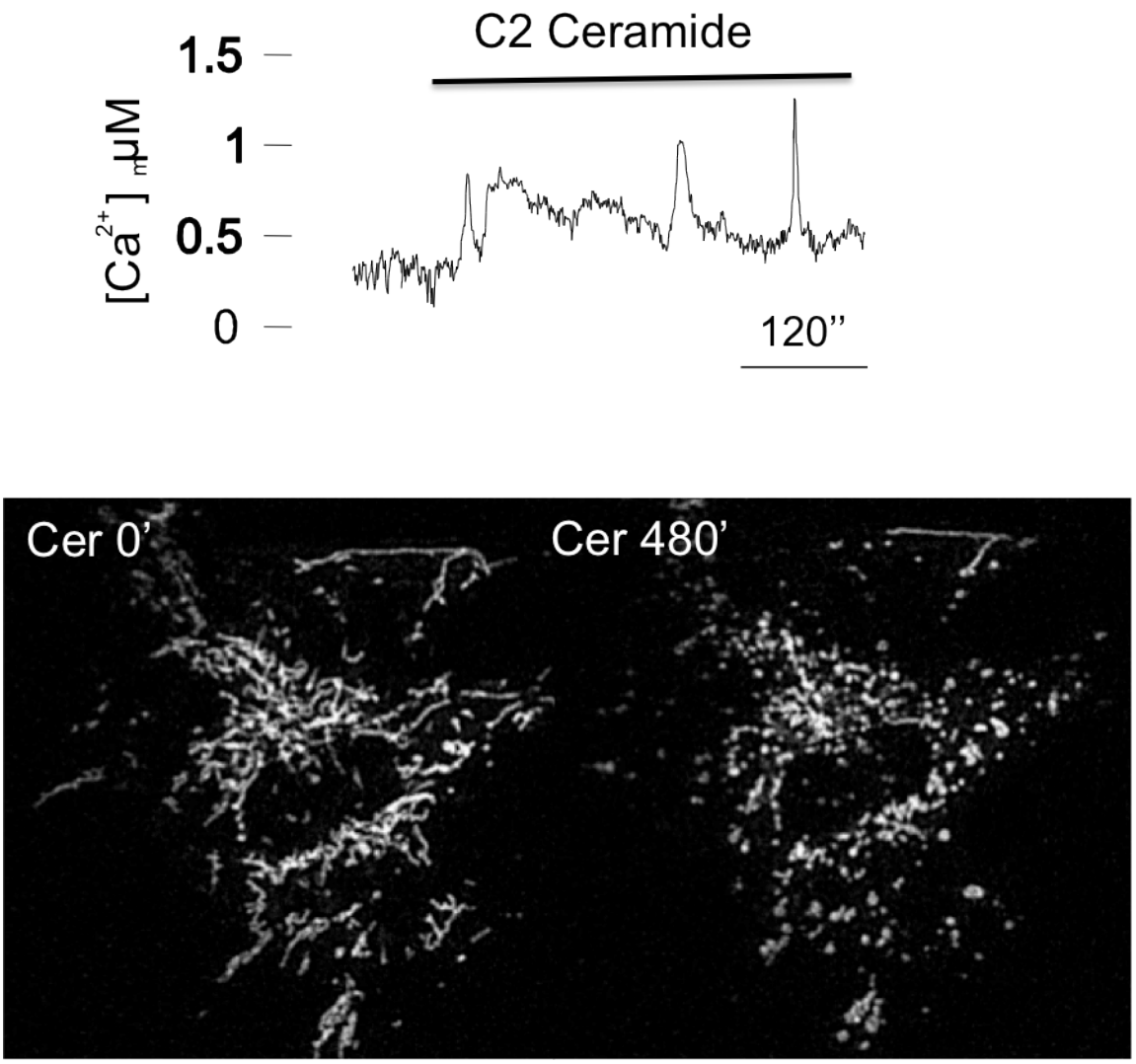

Fig3. The prolonged Ca^{2+} uptake by mitochondria during apoptotic stimulation. In upper panel a representative kinetic of Ca^{2+} accumulation within mitochondria during the proapoptotic stimulus C2-ceramide measured with aequorin. In the lower panel confocal images of mitochondria stained with mtGFP and exposed to the same stimulation

Mitochondria associated Membranes MAM

Mitochondrial and ER networks are fundamental for the maintenance of cellular homeostasis and for the determination of cell fate under stress conditions (40). Recent structural and functional studies revealed the interaction of these networks. These zones of close contact between ER and mitochondria, called MAM (41), support the communication between the two organelles involved in bioenergetics and cell survival.

Close appositions between the ER (or sarcoplasmic reticulum, SR) and mitochondria have long been known to exist and have been observed by electron microscopy (EM) in fixed samples of several cell types. These regions have long been considered to represent the sites of phospholipid exchange between the two organelles. Although such close appositions between ER and mitochondria may, at least in part, represent fixation artefacts, an EM picture taken from quickly

frozen samples, which prevents most artefacts of chemical fixation, reveals that such close appositions are not only visible, but are actually more frequent than in traditionally fixed samples. Experiments in living cells with the two organelles labelled by GFP (4) and electron micrograph images of quickly frozen samples (42) have demonstrated conclusively that such physical interactions between the two organelles indeed exist. Recently, it has also been shown by electron tomography that ER and mitochondria are adjoined by tethers (43) (10 nm at the smooth ER and 25 nm at the rough ER) (Fig.4) and that coupling between these two organelles can be weakened (or strengthened) by rupture (or enforcement) of this inter-organelle protein linkage (44). Some evidence supports the hypothesis that the movement of mitochondria might occur concomitantly and in synchrony with that of specific ER regions. The mechanism of this reciprocal organelle-docking remains unresolved but it has been proposed that it depends on the expression on both membranes, of complementary proteins that link the two organelles together, possibly at specific sites (45).

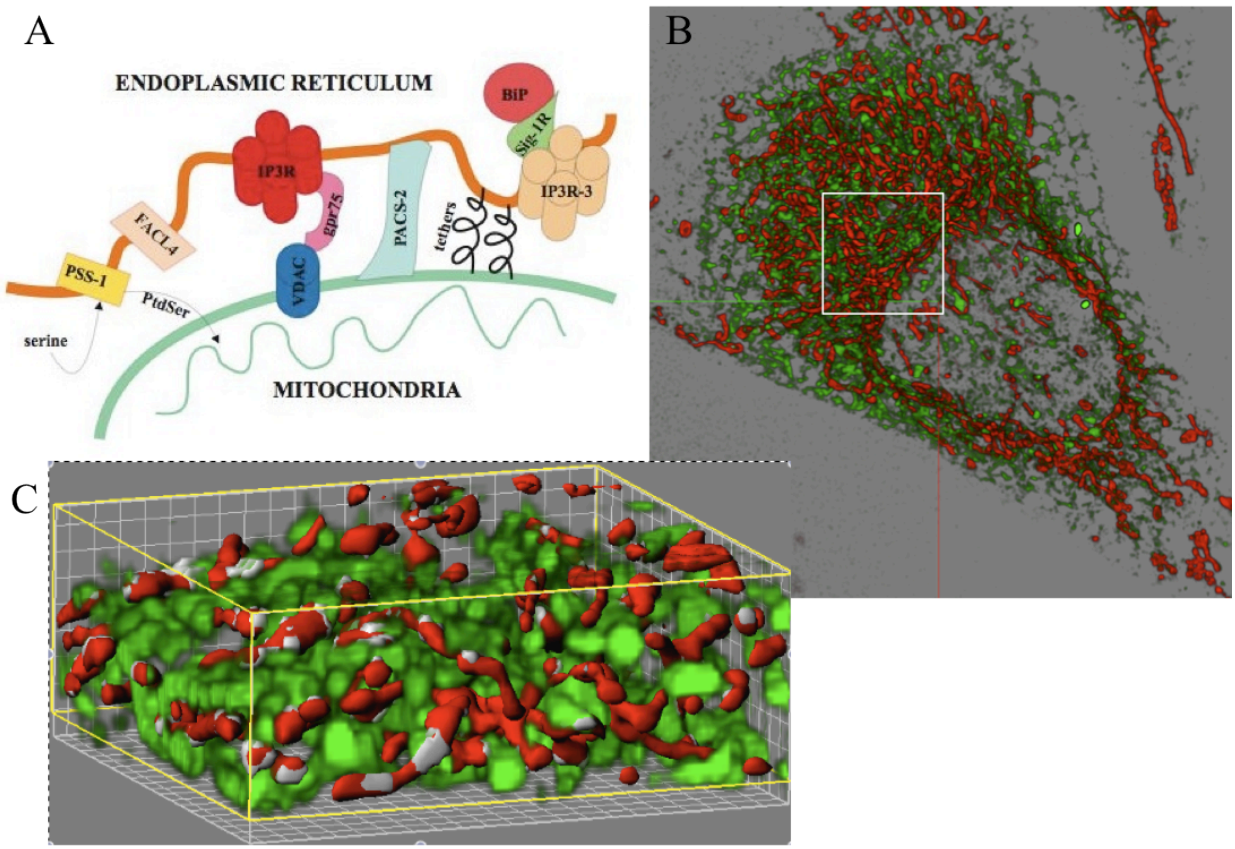

Fig4. A schematic representation of the organization of MAM. The model MAM include key players of lipid metabolism, Ca^{2+} signalling elements (receptor of inositol 4,5-trisphosphate (IP3R), voltage dependent anion channel (VDAC), chaperones (PACS-2: phosphofurin acidic cluster sorting protein 2, grp75: glucose-regulated protein 75, Sig-1R: Sigma-1 receptor) and peptidic tethers keeping mitochondria and ER in close contact. (B) Rapresentative volume rendering fro HaLa cell stained with er-GFP and mtDsRed. (C) Region selected from image (B) was zoomed and rendered with isosurface for mitochondria (Red) and volume for ER (green). Contact sited are shown in white.

In particular it has been identify a tethering complex, composed of proteins resident of both ER and mitochondria, Mmm1/Mdm10/Mdm12/Mdm34, that was functionally connected to Ca^{2+} and phospholipids exchange between the two organelles (43).

MAM contain multiple phospholipid- and glycosphingolipid-synthesizing enzymes, including long-chain fatty acid-CoA ligase type 4 (FACL4) and phosphatidylserine synthase-1 (PSS-1) (Fig.4), and support direct transfer of lipids between the ER and mitochondria (46, 47). In addition, MAM also exchange Ca^{2+} ions which regulate processes ranging from ER chaperone-assisted folding of newly synthesized proteins to the regulation of mitochondria-localized dehydrogenases involved in ATP-producing Krebs cycle reactions, and the activation of Ca^{2+}-dependent enzymes that execute cell death programs (48). Recently, several proteins bound to mitochondria or ER have been shown to be important for maintaining the spatial relationship between the two organelles (49).

The interactions between the two organelles seem to be modulated by a family of "mitochondria-shaping proteins" and by a family of chaperone proteins. In mammals, the best characterized of the "mitochondria-shaping proteins" are DRP-1 (9) and Mitofusin 1 and 2, that regulate mitochondria fission and fusion (50).

MAM are also enriched in key chaperones that may play a role in regulating Ca^{2+} signalling between ER and mitochondria. Moreover they noted that in physiological conditions Sig-1R is retained in the MAM. Upon ER stress, redistribution of Sig-1Rs occurs, from MAM to the periphery of the ER.

Interestingly, Sig-1Rs and the 3 isoform of IP3R co-localize and associate with each other at MAM, Sig-1Rs form a Ca^{2+}-sensitive chaperone machinery with BiP (immunoglobulin binding protein also known as 78-kDa glucose-regulated protein GRP78) and prolong Ca^{2+} signalling from the ER to mitochondria by stabilizing IP3R-3 at MAM. (51).

In addition, Simmen et al. demonstrated that PACS-2 is a multifunctional sorting protein that controls the ER–mitochondria axis and the role of this axis in cellular homeostasis and apoptosis. They showed that PACS-2 is required for the intimate association of mitochondria with the ER. PACS-2 depletion induces mitochondria fragmentation and uncouples this organelle from the ER, raising the possibility that, in addition to mediating MAM formation, PACS-2 might also influence ER folding and Ca^{2+} homeostasis.

The requirement of PACS-2 for the apposition of rod-like mitochondria to the ER suggests that PACS-2 has an essential role in ER-mitochondria communication, and influences the dynamic mitochondria fusion/fission events that are coupled with mitochondria homeostasis and inter-mitochondria communication (52).

In addition to mediating the ER-mitochondria axis, PACS-2 was found to have a profound role on ER homeostasis. Indeed, both IP3Rs and RyRs possess potential PACS-2-binding sites (53) and may be associated with MAM (54). Thus, disruption of PACS-2 may cause mislocalization of IP3Rs, resulting in reduced Ca^{2+} transfer from the ER to mitochondria.

Finally, in a recent study, it has been demonstrated that the IP3R-mediated mitochondrial Ca^{2+} signalling is regulated by the mitochondrial chaperone grp75 (55). In particular, isoform 1 of VDAC is physically linked to the ER Ca^{2+}-release channel IP3R through grp75, highlighting chaperone-mediated conformational coupling between the IP3R and the mitochondrial Ca^{2+} uptake machinery (Fig.4).

These findings together support a new emerging picture whereby chaperone machineries at both ER and mitochondrion orchestrate the coordinate regulation of Ca^{2+} signalling between these two organelles.

The concept of Ca^{2+} as a cellular signal

In the past two decades, our understanding of how extracellular signals are conveyed to eukaryotic cells via an increase in intracellular Ca^{2+} concentration has widely expanded. It is today common knowledge that a variety of extracellular stimuli (ranging from the binding of hormones, neurotransmitters, growth factors to phenomena such as cell-cell interactions), through diverse mechanisms (e.g. receptors that are themselves ion channels, or have an intrinsic enzymatic activity or are coupled to enzymatic effectors via G proteins) induce a rise in cytoplasmic Ca^{2+} concentration ($[Ca^{2+}]_c$) with defined amplitude and kinetics (56); (57).

In most eukaryotic cells, a large electrochemical gradient for Ca^{2+} exists across the plasma membrane. The transmembrane potential across the membrane is 70 to 90 mV. The interior of the cell is the more negative, yet the cytoplasmic concentration of Ca^{2+} ($[Ca^{2+}]_c$) is less than one-ten thousandth of that in the extracellular milieu. There are also intracellular organelles, such as the endoplasmic reticulum (ER) and secretory granules, that contain one to ten thousand fold greater concentrations of Ca^{2+} than the cytoplasm.

Moreover, the technological advancements in probe design and imaging systems, by allowing the accurate measurement $[Ca^{2+}]$ at the single cell level, has revealed a marked asynchronicity in cell response and a high spatio-temporal complexity of the intracellular Ca^{2+} signal. We now know that the Ca^{2+} signal can be conveyed as repetitive $[Ca^{2+}]_c$ spikes (commonly referred to as Ca^{2+} oscillations) (58) as well as localised $[Ca^{2+}]_c$ increases that may either be confined or gradually propagate to the rest of the cell ("Ca^{2+} waves") (59),(60).

An extensive Ca^{2+}-signalling toolkit is used to assemble signalling systems with very different spatial and temporal dynamics. Rapid highly localized Ca^{2+} spikes regulate fast responses, whereas slower responses are controlled by repetitive global Ca^{2+} transients or intracellular Ca^{2+} waves. The Ca^{2+} has a direct role in controlling the expression patterns of its signalling systems that are constantly being remodelled in both health and disease. During the *on reaction*, stimuli induce both the entry of external Ca^{2+} and the formation of second messengers that release internal Ca^{2+} that is stored within the endoplasmic reticulum or Golgi apparatus. Most of this calcium is bound to buffers, whereas a small proportion binds to the effectors that activate various cellular processes. During the *off reactions*, Ca^{2+} leaves the effectors and buffers and is removed from the cell by various exchangers and pumps. The Na^{+}/Ca^{2+} exchanger (NCX) and the plasma membrane Ca^{2+}-ATPase (PMCA) extrude Ca^{2+} to the outside, whereas the sarco/endoplasmic reticulum Ca^{2+}-ATPase (SERCA) pumps Ca^{2+} back into the ER.

Mitochondria also have an active function during the recovery process in that they sequester Ca^{2+} rapidly trough a uniporter, and release more slowly back into the cytosol to be dealt with by the SERCA and the PMCA. Cell survival is dependent on Ca^{2+} homeostasis, whereby the Ca^{2+} fluxes during the off reactions exactly match those during the on reaction.

Aequorin

In the last decade the study of Ca^{2+} homeostasis within organelles in living cells has been greatly enhanced by the utilisation of a recombinant Ca^{2+}-sensitive photoprotein, aequorin. aequorin is a Ca^{2+} sensitive photoprotein of a coelenterate that, in the past, was widely employed to measure Ca^{2+} concentration in living cells. In fact the purified protein was widely used to monitor cytoplasmic $[Ca^{2+}]$ changes in invertebrate muscle cells after microinjection. However, due to the time-consuming and traumatic procedure of microinjection, the role of aequorin in the study of Ca^{2+} homeostasis remained confined to a limited number of cells (giant cells) susceptible to microinjection. Thus in most instances, it was replaced by the fluorescent indicators developed by Roger Tsien and co-workers. The cloning of aequorin cDNA (61) and the explosive development of molecular biology offered new possibilities in the use of aequorin, as microinjection has been replaced by the simpler technique of cDNA transfection. As a polypeptide, aequorin allows the endogenous production of the photoprotein in cell systems as diverse as bacteria, yeast, plants and mammalian cells. Moreover, it is possible to specifically localise it within the cell by including defined targeting signals in the amino acid sequence. Targeted recombinant aequorins represent to date the most specific means of monitoring $[Ca^{2+}]$ in subcellular organelles.

General properties of aequorin.

aequorin is a 21 KDa protein isolated from jellyfish of the genus Aequorea that emits blue light in the presence of calcium. The aequorin originally purified from the jellyfish is a mixture of different isoforms called "heterogeneous aequorin" (62). In its active form the photoprotein includes an apoprotein and a covalently bound prosthetic group, coelenterazine. As schematically shown in Fig.5 when calcium ions bind to the three high affinity E-F hand sites, coelenterazine is oxidized to coelenteramide, with a concomitant release of carbon dioxide and emission of light.

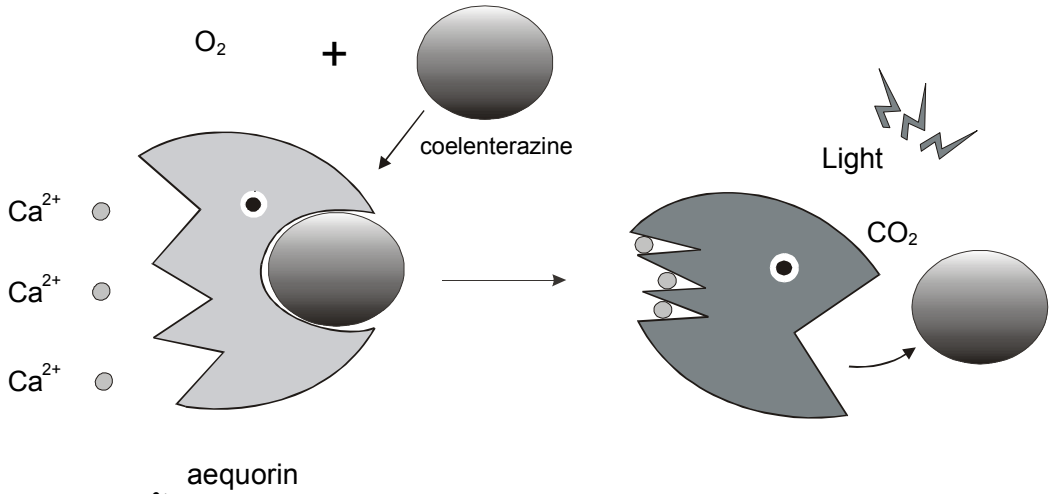

Fig.5: Scheme of the Ca^{2+} induced photon emission process.

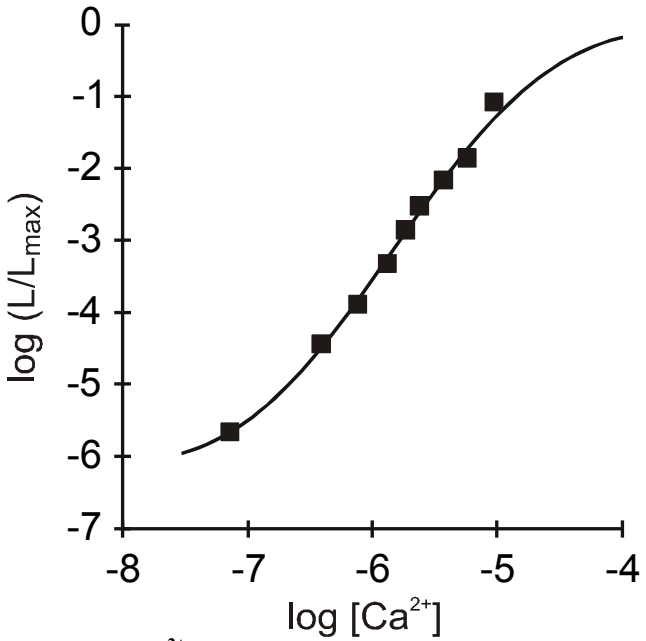

Fig.6: Relationship between the free Ca^{2+} concentration and the rate of aequorin photon emission. The fractional rate of aequorin consumption is expressed as the ratio between the emission of light at defined [Ca^{2+}] (L) and the maximal rate of the light emission at saturating [Ca^{2+}] (L max).

Although this reaction is irreversible, in vitro an active aequorin can be obtained by incubating the apoprotein with coelenterazine in the presence of oxygen and 2-mercaptoethanol. Reconstitution of an active aequorin (expressed recombinantly) can be obtained also in living cells by simple addition of coelenterazine to the medium. Coelenterazine is highly hydrophobic and has been shown to permeate cell membranes of various cell types, ranging from the slime mold Dictyostelium discoideum to mammalian cells and plants (63).

Different coelenterazine analogues have been synthesized that confer to the reconstituted protein specific luminescence properties (64). A few synthetic analogues of coelenterazine are now commercially available from Molecular Probes.

The possibility of using aequorin as a calcium indicator is based on the existence of a well-characterized relationship between the rate of photon emission and the free Ca^{2+} concentration. For physiological conditions of pH, temperature and ionic strength, this relationship is more than quadratic in the range of $[Ca^{2+}]$ 10^{-5}-10^{-7} M. The presence of 3 Ca^{2+} binding sites in aequorin is responsible for the high degree of cooperativity, and thus for the steep relationship between photon emission rate and $[Ca^{2+}]$ (Fig.6). The $[Ca^{2+}]$ can be calculated from the formula L/L_{max} where L is the rate of photon emission at any instant during the experiment and L_{max} is the maximal rate of photon emission at saturating $[Ca^{2+}]$. The rate of aequorin luminescence is independent of $[Ca^{2+}]$ at very high (>10^{-4} M) and very low $[Ca^{2+}]$ (< 10^{-7} M). However, as described below in more details, it is possible to expand the range of $[Ca^{2+}]$ that can be monitored with aequorin. Although aequorin luminescence is not influenced either by K^+ or Mg^{2+} (which are the most abundant cations in the intracellular environment and thus the most likely source of interference in physiological experiments) both ions are competitive inhibitors of Ca^{2+} activated luminescence. Sr2+ can also trigger aequorin photon emission but its affinity is about 100 fold lower than that of Ca^{2+}, while lanthanides have high affinity for the photoprotein (e.g. are a potential source of artefacts in experiments where they are used to block Ca^{2+} channels). pH was also shown to affect aequorin luminescence but at values below 7. Due to the characteristics described above, experiments with aequorin need to be done in well-controlled conditions of pH and ionic concentrations, notably of Mg^{2+}.

Recombinant aequorins

The cloning of the aequorin gene has opened the way to recombinant expression and thus has largely expanded the applications of this tool for investigating Ca^{2+} handling in living cells. In particular, recombinant aequorin can be expressed not only in the cytoplasm, but also in specific cellular locations by including specific targeting sequencing in the engineered cDNAs.

Extensive manipulations of the N-terminal of aequorin have been shown not to alter the chemiluminescence properties of the photoprotein and its Ca^{2+} affinity. On the other hand, even marginal alterations of the C-terminal either abolish luminescence altogether or drastically increase Ca^{2+} independent photon emission (65). As demonstrated by Watkins and Campbell, (66) the C-terminal proline residue of aequorin is essential for the long-term stability of the bound coelenterazine. For these reasons, all targeted aequorins synthesized in our laboratory include modifications of the photoprotein N-terminal. Three targeting strategies have been adopted:

1.Inclusion of a minimal targeting signal sequence to the photoprotein cDNA.

2. Fusion of the cDNA encoding aequorin to that of a resident protein of the compartments of interest.

3. Addition to the aequorin cDNA of sequences that code for polypeptides that bind to endogenous proteins.

Chimeric Aequorin cDNAs

Below I briefly describe the constructs that were present in our laboratory and used in this thesis

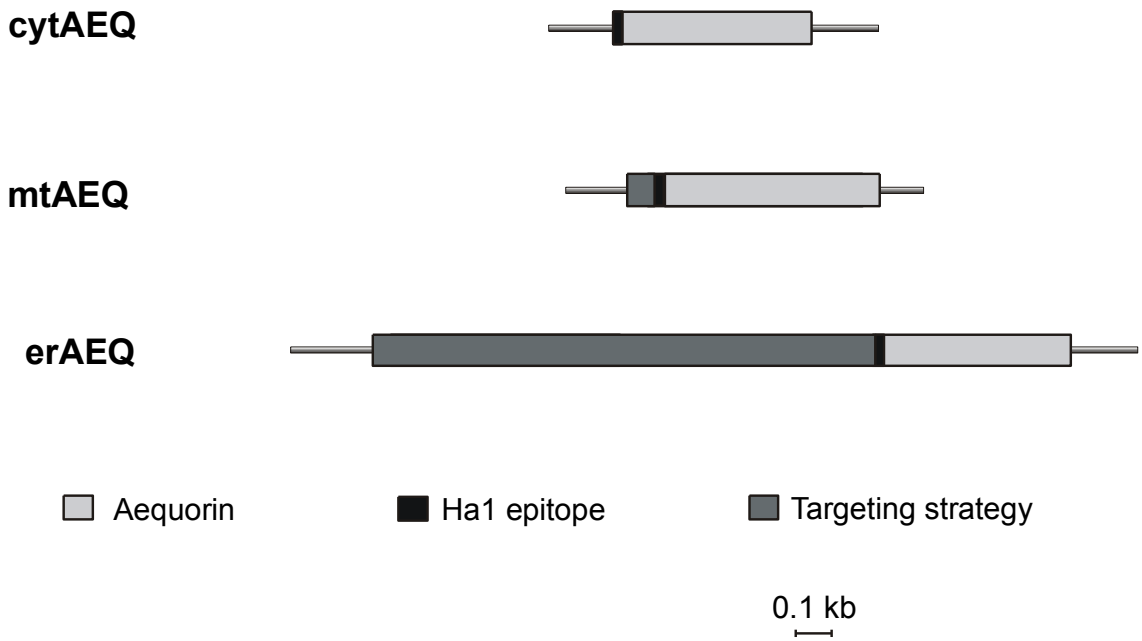

Fig.7 : Schematic representation of aequorin chimeras.

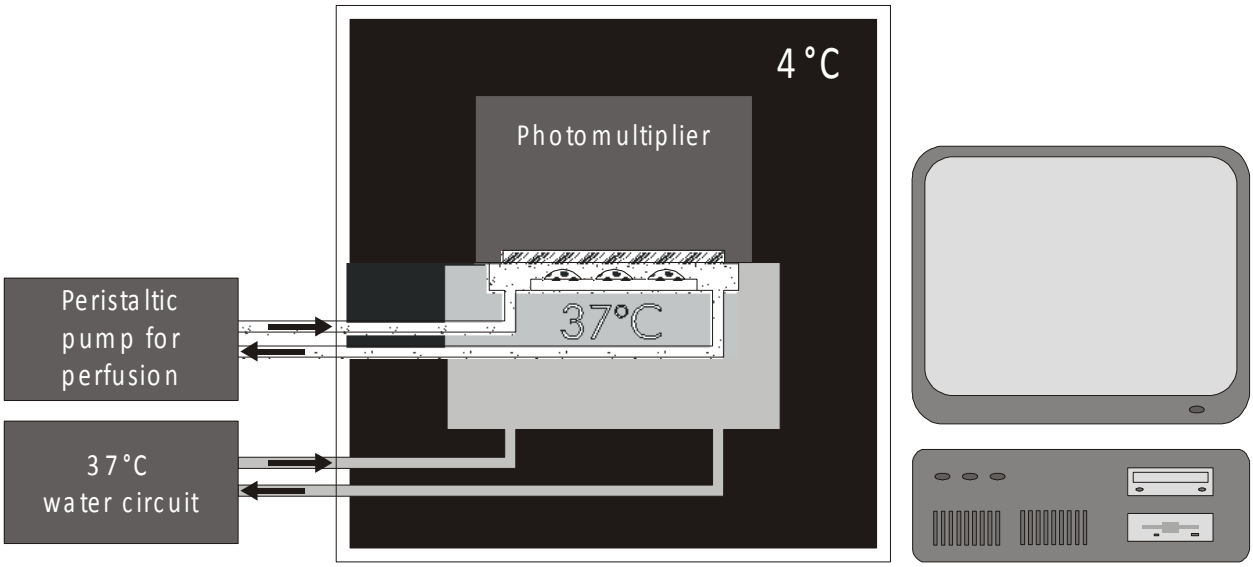

Fig.8. Schematic representation of a custom-built luminometer. Cells loaded with functional aequorin probe are incubated in a perfusion chamber, at 37°C, in close proximity to a photon-counting tube. The complete assemblage is kept at 4°C, in the dark, to minimize extraneous signals. Acquisition of the data and subsequent calculations to transform light emission into $[Ca^{2+}]$ are performed by a dedicated computer algorithm.

Cytoplasm (cytAEQ)

An unmodified aequorin cDNA encodes a protein that, in mammalian cells is located in the cytoplasm and, given its small size, also diffuses into the nucleus. An alternative construct was also available that is located on the outer surface of the ER and of the Golgi apparatus. This construct was intended to drive the localization of aequorin to the inner surface of the plasma membrane given that it derives from the fusion of the aequorin cDNA with that encoding a truncated metabotropic glutamate receptor (mgluR1). The encoded chimeric protein, however, remains trapped on the surface of the ER and Golgi apparatus, with the aequorin polypeptide facing the cytoplasmic surface of these organelles. The cytoplasmic signal revealed by this chimeric aequorin is indistinguishable from that of a cytoplasmic aequorin, but it has the advantage of being membrane bound and excluded from the nucleus.

- Mitochondria (mtAEQ)

All mitochondrial proteins, but the 13 encoded by the organellar genome, are synthesized on cytoplasmic ribosomes and then imported into the organelle. In most cases, import depends on the presence of a cleavable signal at the N-terminus of a precursor protein. This signal (rich in basic and hydroxylated residues, and devoid of acidic ones) usually referred to as mitochondrial presequence, is removed after import by matrix proteases (67). When added to a heterologous protein, a mitochondrial presequence is sufficient to drive its import into mitochondria. MtAEQ was the first

targeted aequorin generated in the laboratory, which has been successfully employed to measure the [Ca^{2+}] of the mitochondrial matrix of various cell types. This construct includes the targeting presequence of subunit VIII of human cytochrome c oxidase fused to the aequorin cDNA (68).

- Endoplasmic Reticulum (erAEQ)

The erAEQ includes the leader (L), the VDJ and Ch1 domains of an IgG heavy chain fused at the N-terminus of aequorin. Retention in the ER depends on the presence of the Ch1 domain that is known to interact with high affinity with the luminal ER protein BiP (69).

Luminescence detection

The aequorin detection system is derived from that described by Cobbold and Lee (70) and is based on the use of a low noise photomultiplier placed in close proximity (2-3 mm) of aequorin expressing cells. The cell chamber, which is on the top of a hollow cylinder, is adapted to fit 13-mm diameter coverslip. The volume of the perfusing chamber is kept to a minimum (about 200 µl). The chamber is sealed on the top with a coverslip, held in place with a thin layer of silicon. Cells are continuously perfused via a peristaltic pump with medium thermostated via a water jacket at 37°C. The photomultiplier (EMI 9789 with amplifier-discriminator) is kept in a dark box and cooled at 4°C. During manipulations on the cell chamber, the photomultiplier is protected from light by a shutter. During aequorin experiments, the shutter is opened and the chamber with cells is placed in close proximity of the photomultiplier. The output of the amplifier-discriminator is captured by an EMIC600 photon-counting board in an IBM compatible microcomputer and stored for further analysis.

Advantages and disadvantages of aequorin compared to other Ca^{2+} indicators.

Today numerous indicators are available to measure [Ca^{2+}]. In this section, I will briefly describe some advantages and disadvantages of the photoprotein over the most widely used fluorescent indicators, the tetracarboxilate dyes such as fura-2, indo-1, fluo-3 etc.

Advantages:

1) Selective intracellular distribution. Whereas recombinant expressed wild-type aequorin is exclusively cytosolic, adding specific targeting sequences can modify the intracellular fate of the photoprotein.

2) High signal-to-noise ratio. Due to the low luminescence background of cells and the steepness of the Ca^{2+} response curve of aequorin, minor variations in the amplitude of the agonist-induced [Ca^{2+}] changes can be easily appreciated with aequorin.

3) Low Ca^{2+} buffering effect. Although the binding of Ca^{2+} by aequorin may, in principle, affect intracellular Ca^{2+} homeostasis, this undesired effect is less relevant than with fluorescent indicators. In fact, thank to the excellent signal to noise ratio, aequorin is loaded at a concentration which is 2-3 orders of magnitude lower than dyes, i.e. usually from <0.1 μM (for the recombinant expressed photoprotein) to ~1 μM (in the case of microinjection of the purified photoprotein for single cell studies).

4) Wide dynamic range. It is clearly evident from Fig.6 that aequorin can accurately measure $[Ca^{2+}]$ ranging from 0.5 μM to 10 μM, i.e. reaching concentrations at which most fluorescent indicators are saturated. Indeed, thank to these properties and to the low buffering effect, it is possible to estimate the large $[Ca^{2+}]_c$ rises that occur, for example, in neurons (71). Moreover, by introducing point-mutations in the Ca^{2+}-binding sites (72), using surrogate cations, such as Sr^{2+}, and/or modified prosthetic groups, the sensitivity of the recombinant photoprotein can be further reduced, and thus the $[Ca^{2+}]$ can be monitored also in intracellular compartments endowed with high $[Ca^{2+}]$ (e.g. the lumen of the ER).

5) Possibility of co-expression with proteins of interest. A powerful approach for investigating the role, and the properties, of the various molecular components of the Ca^{2+} signalling apparatus is either the overexpression of the heterologous protein, followed by the study of the molecularly modified cell. This can be accomplished in two ways, either by generating stably transfected cell clones, or by transiently expressing the protein of interest in a cell type. While the former is associated with various problems (the clone may substantially differ from the parental line, the approach cannot be employed with primary cultures, etc.), in transient transfections a major problem is the selective analysis of the transfected sub-population. For this purpose, the single-cell imaging of positive cells, identified via a co-transfected reporter (e.g. GFP), is effective, but time-consuming, as a large number of cells must be analyzed to minimize cell-to-cell variability. Conversely, with co-transfected aequorin, as the luminescence signal is contributed only by the positive cells, the data will average the behaviour of the whole transfected subpopulation.

Disadvantages:

1) Overestimation of the average rise in cells (or compartments) with inhomogeneous behaviour. The steepness of the Ca^{2+} -response curve of aequorin while accounting for the excellent signal to noise ratio is also the cause of a major pitfall in the use of the photoprotein: a small fraction of the photoprotein pool exposed to very high $[Ca^{2+}]$, by undergoing a massive light discharge, significantly increases the calibrated mean value. Indeed, by using targeted aequorin to monitor subplasmalemmal Ca^{2+} concentration, we measured a mean resting $[Ca^{2+}]$ of 1-2 μM, which most

likely does not reflect the real average $[Ca^{2+}]_{pm}$ value, but, rather, the contribution of microdomains in the proximity of flickering Ca^{2+} channels (73).

2) Low light emission. In distinction to the fluorescent dyes (where up to 10^4 photons can be emitted by a single molecule, before photobleaching occurs), only 1 photon can be emitted by an aequorin molecule. Moreover, the principle of the use of aequorin for Ca^{2+} measurements is that only a small fraction of the total pool (varying, in a typical physiological experiment, from 10^{-7} to 10^{-2}) emits its photon every second. This means that, out of the 10^4-10^5 molecules/cell of a typical aequorin transfection, light emission will vary from nil to 1000 photons at most. The consequences are quite obvious. While in all cases an appropriate apparatus must be used (see below), this is not a major limitation in population studies, as averaging over 10^3-10^4 cells, the light signals vary from 20-30 photons (at resting $[Ca^{2+}]$) to $>10^5$ photons/sec. Conversely, single cell imaging requires very high expression and special apparatuses (73) and is endowed with lower spatial and temporal resolution than that obtained with fluorescent indicators.

3) Loading procedure. As a polypeptide, aequorin needs either to be microinjected (in the case of the native protein) or transfected in living cells. The well-established procedure of aequorin microinjection is obviously limited to a small number of cell models. In the case of recombinant aequorin, transfection is the simplest loading procedure. In this respect it should be remembered that i) some cell lines may be quite resistant to transfection (although a wide range of procedures is now available, ranging from calcium phosphate to liposomes, electroporation and particle gun); in many cases, time is required to find the appropriate transfection protocol and ii) time for protein expression must be waited before carrying out the Ca^{2+} measurements; although we detected reasonable aequorin expression also 4 hours after transfection, this can be a problem with primary cultures with limited time span.

In summary, aequorins, and in particular targeted recombinant aequorins, may represent for some applications a useful, and sometime superior, tool (compared to fluorescent Ca^{2+} indicators) to investigate Ca^{2+} signalling in living cells. Quite recently the group of Tsien (74) has introduced the Ca^{2+} indicators named “cameleons”, molecularly engineered proteins capable of coupling the advantages of aequorins in terms of selective targeting to the high signal characteristics of fluorescent molecules. This technique is presently in its infancy, but its potential in this field is enormous.

GREEN FLUORESCENT PROTEIN

GFP is in nature the legitimate partner of aequorin, produced by the same jellyfish (*Aequorea victoria*) and packed in close association to the photoprotein. GFP acts as a natural fluorophore that

absorbs the blue light emitted by the photoprotein and re-emits photons of a longer wavelength. This accounts for its name and for the greenish blue colour of the jellyfish luminescence (75-77). In research applications, GFP retains its fluorescence properties, and thus can be added to the long list of probes of the cell biologist's toolbox (78). Some of its unique properties account for its explosive success. In relatively few years (the first report of GFP expression in heterologous systems dates back to 1994) (79) GFP has become a powerful and versatile tool for investigating virtually all fields of cell biology, ranging from gene expression to protein sorting, organelle structure, measurement of physiological parameters in living cells and so on (80, 81).

The main reason for the success of GFP is its own nature: the fluorescent moiety is a gene product, with no need for cofactors, that is open to molecular engineering, transiently or stably expressed upon transfection in virtually any cell types. Moreover, its mutagenesis has allowed the adaptation of its fluorescence properties to different experimental needs [for a detailed description see reviews (78, 82)]. GFP mutants can be grouped in two major classes: the first are the "optimising" mutations, i.e. those that increase light emission by either altering the intrinsic properties of the fluorescent protein (83, 84) or increasing its production in mammalian cells (85). The latter are the so called "humanised" versions of the cDNA, in which silent mutations are introduced that convert some of the codons into forms most common and efficient for translation in mammalian cells. As a consequence, with equal amounts of mRNA, more fluorescent protein is produced. This property is very useful at low mRNA levels (e.g. for the prompt detection of promoter activity). As to the modifications of GFP properties, mutations have been described that alter the stability of the protein and/or the quantum efficiency upon illumination with visible light. Native GFP has in fact a bimodal excitation peak, larger with UV than with blue light, while all currently employed green variants of GFP are best excited with blue light, a change that minimizes cytotoxicity and photobleaching. Among these mutations, the most useful appears to be the substitution of Ser^{65} with Thr (S65T) that causes the chromophore to be entirely in the anionic form. When compared to wild-type GFP the quantum efficiency of this mutant upon excitation with blue light is increased 6-fold, the rate of fluorophore formation is 4-fold faster and photobleaching is markedly reduced. The second class is represented by GFPs emitting light of a wavelength that can be clearly distinguished from the green colour of native GFP. This class includes a few popular mutants commonly referred to as blue (Y66H, Y145F), cyan (Y66W) and yellow (T203Y) GFPs.

The search, by mutagenesis, of a truly "red" GFP mutant has been extensive, but unsuccessful. Recently, however, a red companion of GFP, RFP, has been isolated from a coral, and is currently utilized in numerous labs. Finally, with the notable exception of the blue mutant, all GFPs are strongly resistant to photobleaching. This permits the prolonged visualizations of these proteins

under the laser illumination of confocal microscopes. For this reason, GFP has often replaced already available probes in a variety of applications.

Another green fluorescent protein, found in the sea pansy *Renilla*, has been biochemically characterized (86) while the cDNA has not been isolated yet. Although the chromophore of *Renilla* is similar to that of *Aequorea*, some of their biochemical properties differ. *Renilla* GFP has a much higher extinction coefficient, is an obligate dimer and is more resistant to pH-induced conformational changes. This could make it useful for specific cell physiology studies.

Nowadays the most frequent application of the GFPs is that of a tag. In frame fusion of the GFP cDNA to the cDNA coding for a protein of interest makes possible the study of the function(s) and of the fate of the resulting chimera in living cells. Moreover, chimeras with different spectral properties can be employed for visualising simultaneously two proteins of interest (e.g. two isoforms of a signalling molecule) or to investigate the morphology and spatial relationship between two intracellular compartments.

GFPs can also be used as a tool for analysing transfection efficiency. In 1994 Chalfie and co-workers (79) demonstrated the possibility of using GFPs to monitor gene expression in prokaryotic (*Escherichia coli*) and eukaryotic (*Caernorhabiditis elegans*) living cells. However, some of GFP properties (long life-time, time required for fluorophore formation, background fluorescence) are not ideally suited for the analysis of promoter activity. In fact Rutter and co-workers (87) imaged gene transcription at the single cell level using both GFP and luciferase and showed that the latter appears preferable, given that GFP analysis is hampered by the lack of linearity between protein concentration and fluorescence intensity and by the interference of cellular autofluorescence.

GFPs can also be used as sensors for physiological parameters. This approach stems from an interesting phenomenon, called fluorescence resonance energy transfer (FRET), occurring between two GFPs with different colours. FRET may occur only if the fluorescence emission spectrum of the "donor" GFP overlaps with the excitation spectrum of the "acceptor" GFP and if the two fluorophores are located within few nanometers in a favourable orientation. Any alterations of these parameters can drastically alter the efficiency of FRET. Indeed, the rate of energy transfer is proportional to the sixth power of the distance $E=[1+(R\backslash R_0)^6]^{-1}$ and thus becomes negligible when the two fluorophores are >5-6 nm apart. The earliest use of FRET between GFP mutants was reported by Heim and Tsien (88), who linked two fluorophores via a sequence of 25 aminoacid including a trypsin cleavage site. After addition of trypsin, the short peptide was cleaved and FRET drastically reduced. Many other similar studies have later yielded consistent results (see for example (89-91)).

FRET was also used by different labs to monitor intracellular Ca^{2+} changes. Romoser and co-workers (92) fused BFP and GFP via a linker that included a calmodulin binding site derived from smooth muscle myosin light chain kinase. Addition of Ca^{2+}-calmodulin to this construct disrupted FRET probably influencing the correct orientation of the fluorophores. Miyawaki et al. (92) developed a chimera called Cameleons, in which appropriate GFP variants were linked by a peptide including the N-terminal part of calmodulin and the M13 peptide that associates to calmodulin in a Ca^{2+} dependent manner. Moreover, by targeting this chimera to the ER the authors were able to measure the luminal [Ca^{2+}] of this organelle. Finally, FRET between GFP mutants can be employed for monitoring protein-protein interactions, such as, for example, Bcl2-Bax (91) and epidermal growth factor receptor-Grb2.

A new biophysical approach, known as bioluminescence resonance energy transfer (BRET), has recently been developed. BRET is a phenomenon resulting from radiation-less energy transfer between luminescent donor (i.e. with no need of external illumination) and fluorescent acceptor proteins. Using this approach and taking advantage of emission spectral overlap between the bioluminescent *Renilla* luciferase and YFP, Xu and colleagues (93) demonstrated homodimerization of the cyanobacteria clock protein KaiB in *Escherichia coli*. Among the same lines, Angers et al. (94) used BRET to reveal dimerization of β2-adrenergic receptors in HEK-293 living cells.

Experimental set-up: collecting and analysing the GFP images.

The fluorophore of GFP is formed by the cyclization of three amino-acid residues of the primary sequence. This process directly follows, with few constraints (a relatively brief time lag), the synthesis of the protein, and thus GFP proved brightly fluorescent when expressed in a wide variety of cell types (mammalian cells, plants, fungi, bacteria, etc.) and intracellular locations (cytoplasm and virtually every organelle). Thus, also in our experiments the various GFP chimeras are transfected with the appropriate procedure (calcium phosphate, liposomes or particle gun, depending on the cell type), and directly visualised in living cells after allowing sufficient time for expression and chromophore formation (usually 24-36 hours). For this purpose, the coverslip with the transfected cells is fitted at the base of a thermostated chamber, which is placed on the microscope stage.

The microscope set up is presented in figure 8. In brief, a traditional wide-field, epifluorescence microscope is equipped with filter-wheels located both in

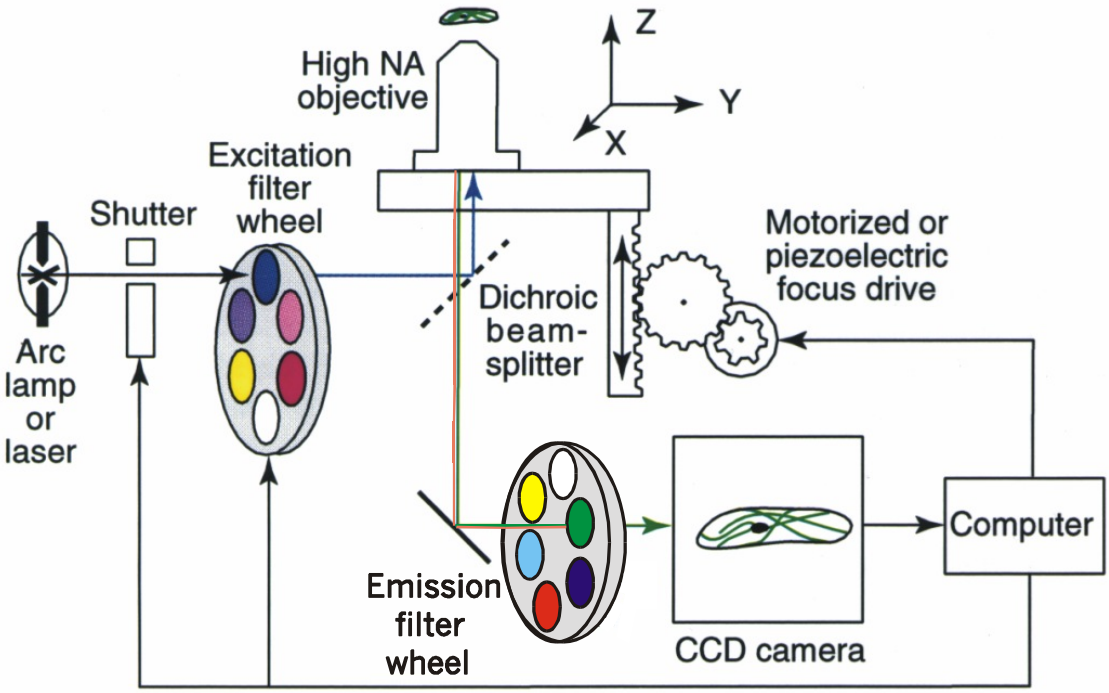

Fig.9. A digital imaging system, built on an epifluorescence microscope, is equipped with filter-wheels placed on the excitation and emission light paths, a piezoelectric motor and a CCD camera. The system is operated by software that also permits to analyse and computationally deblur the images.

The incoming and in the out-coming light paths (thus allowing to rapidly alternate excitation and/or emission wavelength) and a piezoelectric transducer (or motor drive) for rapid focussing in the z plane. The fluorescence image is collected by a back-illuminated and cooled (-40°C), charge coupled device (CCD) camera having high quantum efficiency (>70% at 500nm) and low noise (<10e^- RMS at 1MHz) characteristics, and the image is stored as a digital file using the Metamorph/Metafluor program (Universal Imaging). This allows the direct monitoring of fluorescence intensity, important for some applications (e.g. the monitoring of FRET, or the pH measurements using the pH-sensitive GFP mutants, a topic that for reasons of brevity will not be discussed in this thesis).

A high-resolution, 3-D reconstruction of the distribution of a GFP chimera can be obtained with the technique of digital image restoration, also called deconvolution or deblurring. (95).

A high-speed version of this microscopy has been developed (4) that can acquire an entire through-focus image series of a GFP labelled cell in less than 1 second. This microscope system can be used to follow spatial and temporal intracellular dynamics (e.g. motor-protein based transport, signal transduction) too rapid for conventional fluorescence microscopy (4); (96). Conversely, if only the time course rather than the 3-D distribution of a fast process (e.g. Ca^{2+} signalling) needs to

be assessed, single fluorescent images of the microscope field of interest can be acquired every 10-20 ms with no further image processing (97).

Finally, the filter-wheels allow the alternate imaging of two different fluorophores at different excitation and emission wavelengths, and thus the simultaneous visualisation of two different proteins of interest in the same cell, or the measurement of donor and acceptor fluorescence in FRET applications. When compared to laser scanning confocal microscopy, digital imaging is characterised by higher flexibility in the selection of excitation wavelengths, lower illumination intensity (thus reducing photobleaching and photodamage) and lower cost. Conversely, its disadvantages are the need for time-consuming off-line image processing and the unsuitability for the analysis of thick specimen (e. g. tissue slices).

p53 interaction with the Sarco/Endoplasmic Reticulum Ca^{2+} ATPase sensitizes mitochondria to apoptosis

Introduction.

p53 is a master regulator of cell fate

In 1979 six different research groups, independently, reported the discovery of a 53KDa protein, present in both human and murine cells, five of this shows how the protein was able to bound the T large antigen from SV40, while the sixth that the protein was present in several murine tumour cell types (98), (99), (100), (101),(102).

Initially believed as an oncogene, because of its correlation to the SV40 antigen, in 1989, the TP53 gene was found mutant in tumour cells compared to the one of neighbouring sane tissues. Definitely TP53 was labelled as an oncosuppressor gene, and the p53 used to that date to show its oncogenetic activity was effectively a mutant (103)

Later TP53 has been found as one of the most mutant genes in human tumours and, to date, more then 25000 mutations have been reported, most of that as missense mutations. These natural occurring mutations has been reported also to be often dominant negative or gain of function for oncogenic activities.

Mutations in p53 alleles are found in more then 50% of human tumours, most of it are concentrated within the DBD, in just a few position knowed as Hot Spot. These mutations are able to impair proper p53 transcription regulation, but recently several other roles has been proposed (see later).

The p53 protein is composed of at least 4 domains:

- N-terminal trans-activational domain,
- A proline-rich domain, for protein interactions (such as for Mdm2),
- A DNA binding domain (DBD),
- An oligomerization domain (OD), principal target for post-transactional modifications such as phosphorylation, acetylation, methylation, ubiquitinilation, sumoilation, neddylation, which can influence protein stability or its interactions.
-

The presence of a DBD and a trans-activational domain make p53 a transcription factor involved in processes like cell cycle block, control of proliferation, apoptosis induction and others all equally important in tumour suppression.

Fig.10. representation of domains of p53. Domains are represented in different colours; yellow labels indicate phosphorylation sites while black bars on upper panel indicate Hot Spot mutation found in human tumours.

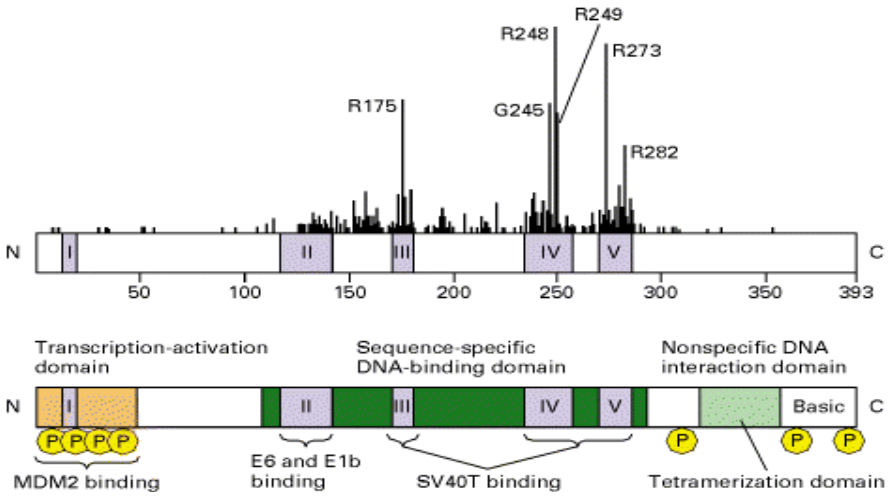

In normal conditions p53 is present at very low levels, due to its interaction with the E3-ubiquitin ligase Mdm2. This interaction allows constant ubiquitinilation of p53 and its consequent degradation via proteasome. During several stress conditions different proteins can phosphorylate the binding site for Mdm2 on p53 proline-rich domain inhibiting p53 degradation, allowing a rapid accumulation of the protein and engage of its activities (104)

This peculiarity of p53 response to stress, bid researchers to usually not describe p53 activation event (in order of lacking an enzymatically activity), but of p53 stabilization.

P53 stabilization is induced by a plethora of stimuli, not only of genotoxic nature, but also:

- telomeres erosion,
- serum starvation,
- hypoxic damage,
- ribosomal stress,
- oncogene activation.

With the ultimate fate to induce cell cycle arrest or apoptosis, but also favouring DNA repair and genomic stability, senescence, survival, regulation of metabolism (specially inhibition of glycolysis and promotion of respiration), regulation of autophagy, oxidative stress regulation, cell motility and cell differentiation.

Fig.11 the many routes of p53. Blue boxes indicates the activating signals induced in different stress conditions, while pink boxes display several induced answers by p53 accumulation. Figure source (105)

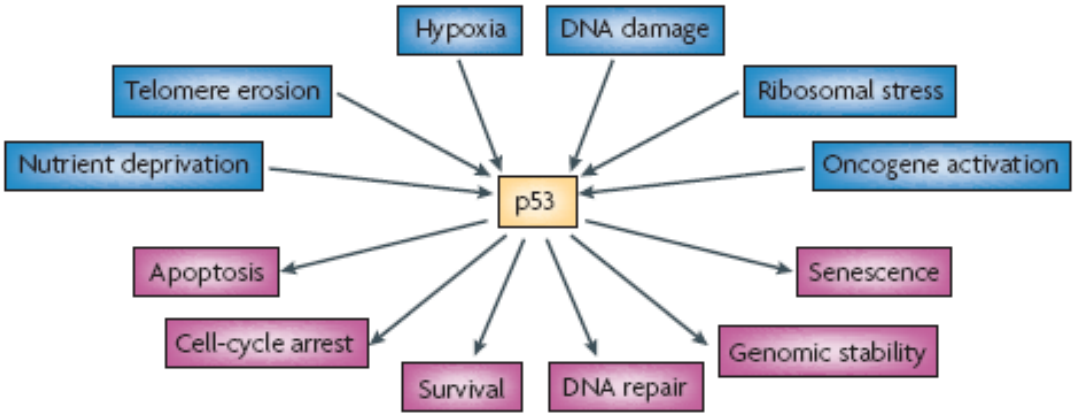

All these aspects evidence p53 as an overall regulator of cell fate and tissutal homeostasis, requiring, within the cell, the presence of a huge amount of regulators of p53 that could act directly (i.e. Mdm2), but specially by post-translational regulation and subcellular localization.

Ability of p53 to regulate gene expression is in turn fundamental to orchestrate all the response describe above and to date hundreds of genes has been found directly regulated p53 because of the presence of one or more of its consensus sequence i.e.

$p53^{AIP1}$, Apaf-1, BAX, Caspase-1 and Caspase 6, cathepsin D, DINP1, DR4, DR5, Fas, IGF-BP3, NOXA, p85, PERP, PIDD, PIG3, PTEN, PUMA, Scotin, p21, E124/PIG8.

Signals stabilizings p53 are not acting all through the same participants or mechanism, i.e. ARF protein that bound and inhibits Mdm2 is activated by oncogenes, but is not involved during DNA damage stress *(106)*. Similarly the ribosomal protein L11allow p53 stabilization after ribosomal stress *(107)*.

Interestingly the genotoxic activation pathway (induced by radiotherapy and many chemioterapic agents) recently has been suggested as the most primitive, but not as the most relevant in order of tumour suppression *(108)*, while the most efficient from this point of view appears to be exactly the once activated by oncogene activated and mediated by ARF (109).

P53 stabilization has been recently linked to metabolism, even during non-genotoxic conditions. During glucose deprivation p53 activate the AMP kinase (AMPK) that in turn allow cell survival (110) moreover Matoba and co-workers in 2006 shown how p53 (111) in basal condition favour the expression and assembly of Respiratory Complex IV favouring cell respiration. Loss of p53 in turn would favour cell growth and tumour formation even in presence of low nutrient conditions and appearance of Warburg effect.

Moreover p53 has been implicated also in metabolism of reactive oxygen specie as both antioxidant and pro-oxidant. Link between p53 and ROS start with observation that p53 could induce genes able to promote ROS production (112) as PIG3 and Proline Oxidase (113) as well as it is able to

inhibit expression of antioxidant genes *(114)*. This would increase sensitivity to p53 dependent apoptosis and, through DNA damage, to induce a feedback loop for p53 activation.
Nonetheless p53 is also able to induce genes like sestrines (115), glutathione peroxidase (116), aldehyde dehydrogenase (117), allowing reduction of levels of ROS.

The mitochondrial route of p53.

In presence of apoptotic stimulations a distinct fraction of p53 has been shown to translocate to mitochondria, where it does interact with pro and anti-apoptotic members of Bcl-2 family in order to activate the first and inhibit the latter. This event, occurring even previously of p53 translocation to the nucleus would induce a mitochondrial permeability state that induce Cyt C release and apoptosis initiation.
First evidence of p53 translocation to mitochondria arrive from Marchenko et al (118) that show how, after its stabilization, a fraction of the protein translocate to mitochondria, preceding perturbations of $\Delta\Psi m$, Cyt C release and caspase activation.
At this site p53 interact with Bcl-2 and Bcl-XL, neutralizing their inhibitor activity on the proapototic members and Bax and Bak (119) allowing MOMP, moreover, by interaction with Bcl-Xl, it also able to allow activation of tBid or Bad (120). Apparently this interaction occurs only in the central domain of p53, through an electrostatically interaction mediated by positive charges on p53 DBD and negative acidic charges of lower domain of Bcl-2/Xl (121). Similarly, trough it's DBD, p53 interacts with Bak, removing the negative regulation mediated by Mcl-1 (122).
Nonetheless affinity for Bcl-2/Xl is apparently 10 times higher compared to binding with Bak/Bax that displays a lower acidic surface neither a BH4 domain, suggesting that p53 preferentially binds to Bcl-2/Xl.
A different explanation for non-nuclear p53 has been proposed involving PUMA. In physiological condition cytolasmic p53 would be sequestered in an inhibitory complex with Bcl-Xl. In response to stress p53 would translocate to the nucleus where promote transcription of its target PUMA. PUMA, in turn, disrupt this complex by binding Bcl-Xl and allowing p53 to activate Bak monomer within cytosol (123, 124).

Mitochondrial translocation to p53 has been shown to be PUMA and Bax indipendent and would allow not only Bak/Bax oligomerization on the OMM, but involved also VDAC, inducing a complex formation with cyclophillin D.

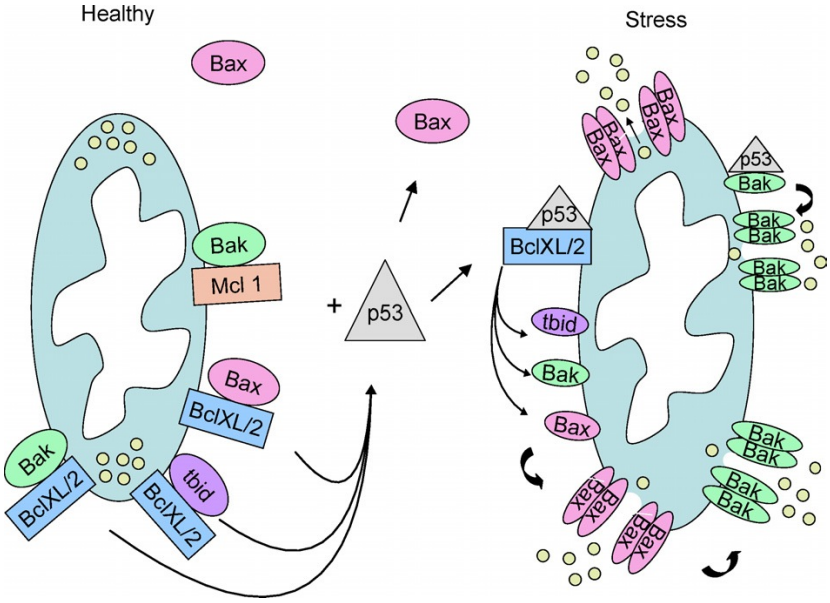

Fig.12 The Bcl-2 model for mitochondrial p53. In normal condition on OMM Bcl-2/XL and Mcl-1 maintain Bax and Bak inhibited, p53 by removal of Bcl-2/Xl/Mcl-1 allow the generation of a permeability transition state. Figure source (125).

Studies on negative dominant heterozyogusity for p53 with naturally occurring mutants shows how the gene transcription is impaired in this condition, while the mitochondrial route appear completely normal (126). Should be noticed that, while nuclear p53 act as a tetramer (or dimer of dimers), the mitochondrial path appear exerted by monomeric p53, explaining why this route appear not affected by tumour derived missense mutants. This phenomen has been explained as a security mechanism versus dominant negative mutation.

Recently also has been show how p53 interact with Mdm4, allowing translocation to mitochondria and binding to Bcl-2 (127). Moreover, while interaction between p53 and Bcl-2 occurs even in physiological conditions, interaction between Mdm4 and Bcl-2 is dependent by apoptotic stimulation.

This evidences counteract the idea that Mdm4 would be a negative regulator of p53, while propose a more fine regulation of p53 levels during transition between physiological state and stressed conditions (128, 129).

Despite these interesting evidences collected about physiology of p53 still is not clear neither which are all the cytoplasmic functions of p53 nor which are he pathways allowing p53 to choose its path

and specially P53 do not show any translocation sequence (at least within the plethora of the knowed once).

The most relevant post-translational modification linked to this route for p53 is a monoubiquitinilation actually (130). Monoubiquitinilation are known as regulatory events linked to protein compartmentalization (131, 132), despite the role for ubiquitin in proteasomal degradation, where at least 4 copy of the protein has to be linked to the target to induce is removal (133). P53 monoubiquitinilation is apparently driven by Mdm2 (as the poliubiquitinilation that mediate its degradation), but still is not clear what determine the "stop" after the first labelling step. Once to mitochondria p53 is rapidly deubiquitinilated by HAUSP, impeding a further ubiquitinilation and allowing engagement of apoptosis initiation.

The mitochondrial p53 induction of apoptosis has been addressed to radiotoxicity in organs like thymus and spleen where appear to translocate faster compared to the nuclear translocation. Nonetheless this pathway has been also linked to cerebral ischemia and reperfusion damage in kidney (134), to such a big extent that inhibiting this mitochondrial route, with a drug called pifithrin can allow tissue survival reducing the toxicity due to chiemioterapy (135)

Oncosuppressors as regulators of apoptotic Ca^{2+} transfer

Important evidence pointing to a key role of Ca^{2+} in apoptotic cell death comes from the demonstration that oncogenes that protect from cell death perturb intracellular Ca^{2+} homeostasis. A critical link between Ca^{2+} and apoptosis was established while studying the oncoprotein B cell lymphomas 2 (Bcl-2) and its mechanism of action. Bcl-2 is a central regulator of apoptosis, able to block or delay apoptosis in different cell types, from hematopoietic to neural (136). The immediate interest generated around this protein's functions led to the discovery of several other proteins displaying sequence homology. These are also active in the control of apoptosis and have given rise to a whole family of Bcl-2 proteins.

To date, this family comprises at least thirteen members that can be easily classified, regarding their control of apoptosis, as proapoptotic and antiapoptotic (137). The antiapoptotic members conserve the higher sequence homology with Bcl-2 and especially within four highly conserved Bcl-2 Homology domains (BH1-4), like the Bcl-2-related gene A1, BCL-XL, BCL-w, and MCL-1.

Our group demonstrated how Bcl-2 over-expression was able to reduce the steady state of Ca^{2+} levels within the ER, with resulting reduced Ca^{2+} transfer to mitochondria during apoptotic stimulation and reduced triggering of mitochondrial fragmentation and apoptosis initiation (138, 139). Other groups have reported similar data, confirming how Bcl-2 could mediate an augmented leak from the compartment without affecting activity of ER Ca^{2+} ATPase (140, 141). Our group

also addressed the hypothesis that its putative pore forming activity could mediate regulation of ER Ca^{2+} release, see Fig.13B (142). Some controversy still remains, however, regarding the mechanism through which Bcl-2 reduces the Ca^{2+} transfer from ER to mitochondria. Bassik et al. showed how Bcl-2 alters the phosphorylation of IP3R, promoting its basal leaking (143). A few years later, the group of Distelhorst proposed the direct interaction between the BH4 domain of Bcl-2 and the IP3R, reducing its opening probability and conferring resistance to apoptosis during prolonged exposure to the TCR (144). These data was recently confirmed in glioma cell lines. In this elegant work, it was shown how the interaction between Bcl-2 and IP3R is able not only to inhibit apoptosis, but also to inhibit its propagation through several cells in a Ca^{2+}- and IP3-dependent manner (145).

Observation obtained during part of my phD, indicates as also the PML protein, encoded by a tumor suppressor gene implicated in the pathogenesis of leukemia and cancer, plays a critical role in the Ca^{2+} cross talk between ER and mitochondria during apoptotic stimulation. Within the cell PML isoforms display both nuclear and cytosolic distribution. At the nucleus PML epitomizes a multiprotein nuclear structure, the PML-nuclear bodies (PML-NBs), which depends on PML for its formation and function (146, 147) Interestingly, in the cytosol PML is now found to localize at the ER and the MAMs (146). MAMs are the specialized domains selectively enriched of mitochondrial Ca^{2+} signaling elements, where Ca^{2+} transfer between ER and mitochondria takes place. In particular, on the ER side MAMs are enriched in IP3R. Pml-/- mice and cells are protected from apoptosis triggered by a number of stimuli such as Fas ligand, tumor necrosis factor α and type I and II interferons. These effects depend in part on the PML modulation of nuclear transcriptional pro-apoptotic pathways (148). However, PML regulates apoptosis also induced by Ca^{2+} dependent stimuli in a transcription-independent way through its ER/MAMs localization. Indeed, in these hot signaling sites, PML is shown to regulate the phosphorylation of IP3R by controlling the activity of Akt through the recruitment of the PP2A phosphatase at the ER/MAMs. Was in fact demonstrated from my group how Akt is able to modulate Ca^{2+} release from IP3R mediating is antiapoptotic effect(149). In so doing, PML is able to regulate Ca^{2+} mobilization into the mitochondrion, which then triggers the cell death program. Conversely, in the absence of PML, PP2A does not accumulate in the complexes with IP3R and Akt, and this results in an accumulation of activated Akt (phospho-Akt).

These observation are just opening a completely new perspective in which, not only contact sites between mitochondria and ER act as a preferential gateway for signals transmission, but where components of cytoplasmic and nuclear routes acts to modulate sensitivity to apoptosis, as by manipulating a rheostat represented by calcium transmission (fig. 12).

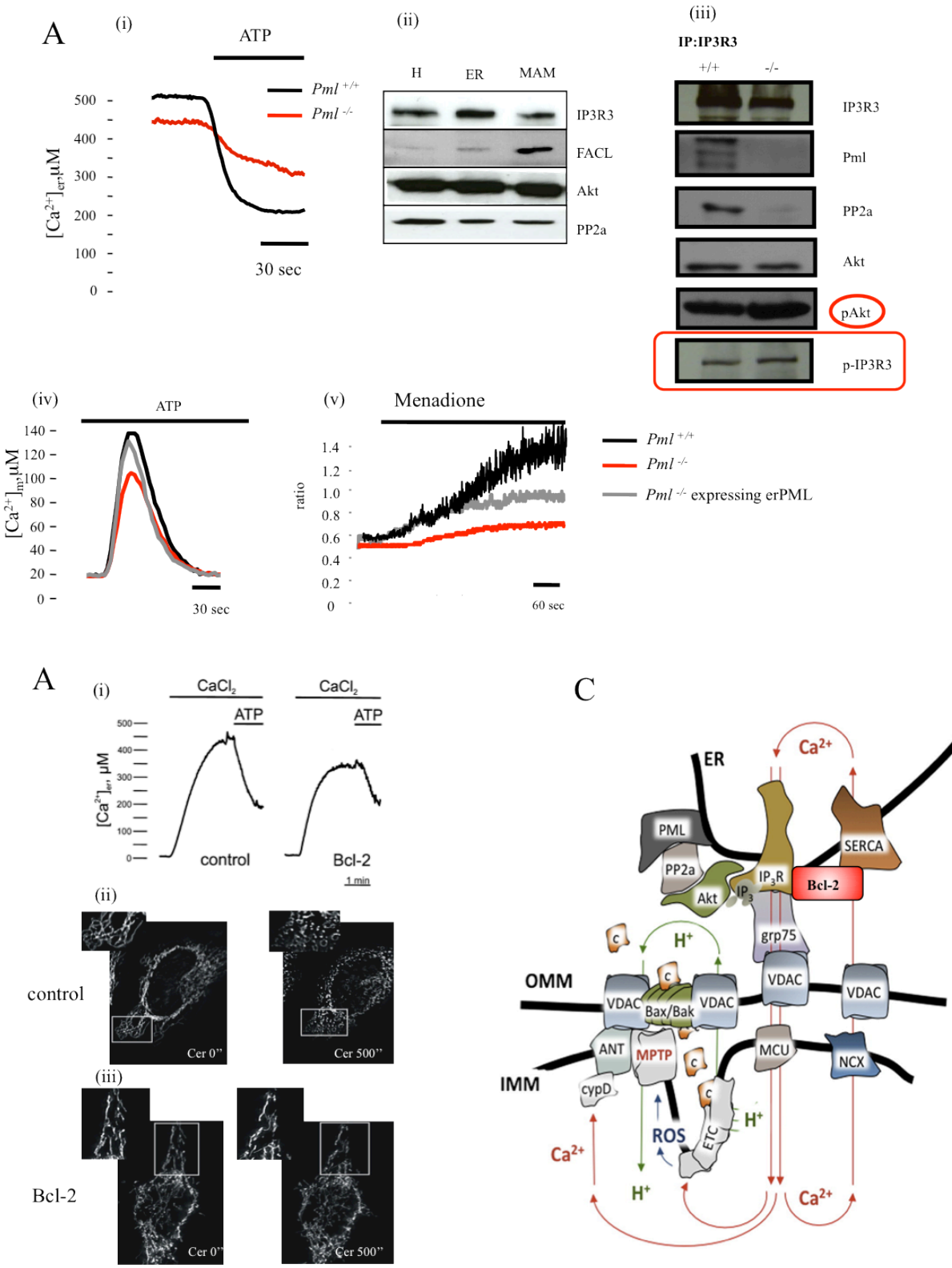

Fig.13. different regulation of apoptotic Ca^{2+} transmission by oncosuppressors. (Ai) kinetics of Ca^{2+} release from ER in MEF PML+/+ and -/- and in HeLa controls compared to HeLa overexpressing Bcl-2 **(Bi).** The first show reduced calcium release, while the latter cause steady state levels PML localize to MAM together with AKT and IP3R3 **(Aii),** its interaction with these components cause alteration of phosphorylation state in IP3R3 mediated by AKT **(Aiii)**. Reintroduction of PML localized to ER cause recovery of calcium released during agonist or apoptotic stimulation in PML KO. The reduced calcium loaded in Bcl-2 overexpressing HeLa cause mitochondrial protection during stimulation with the apoptotic inducer C2-Ceramide **(Bii and iii). (C)** Schematic rappresentation of the role of oncosuppressors PML and Bcl-2 at MAM sites. Adapted from (150)

Results

p53 localizes to ER and MAM during stressing condition

We recently demonstrated the unexpected localization of the promyelocytic leukemia protein (PML) at the Endoplasmic Reticulum (ER) and at the Mitochondria-Associated Membranes **(**MAMs) (146), a specialized domains of close contacts between ER and mitochondria, involved in maintaining a dynamic cross-talk between the two organelles (151). PML is a tumor suppressor that physically interacts and synergizes with p53 in apoptosis induction (152). On the other hand, ER-mitochondrial cross-talk is fundamental for up-regulating mitochondrial metabolism in stimulated cells (153) and plays a key role also in decoding Ca^{2+}-mediated apoptotic signals (44, 51, 154, 155). Down-regulation of ER-mitochondrial Ca^{2+} transfer caused by Bcl-2 over-expression or PML impairment is important for the anti-apoptotic effect of these proteins (156).

On the light of these observations, we verified the intracellular localization of p53 by subcellular fractionation, both in primary mouse embryonic fibroblasts (MEFs) and in the human colon cancer HCT-116 $p53^{+/+}$ cell line (157). Similarly to PML, p53 is localized in the nucleus, in the cytosol and, interestingly, both in the ER and in the MAMs, but not in the "pure" mitochondrial fraction (Fig.14, A and B).

Since it was previously shown that in the absence of p53 MEF cells were resistant to apoptosis induced by thapsigargin (TG) (158) and being p53 localized at ER/MAMs compartments, we investigated whether p53 could be a fundamental component of the ER stress-induced apoptotic pathway. To address this question we investigated its role in the ER stress induced by H_2O_2 and menadione (MEN), two oxidizing agents that induce ER Ca^{2+} release. 16 h after applying the stress inducers, the percentage of apoptotic cells, determined by flow cytometry analysis, was shown to be markedly lower in $p53^{-/-}$ MEFs as compared to wt cells (Fig.14C). The importance of p53 at ER/MAMs was further strengthened by the observation of an increase in p53 levels in these regions after pharmacological treatment by the potent p53 inducer, adriamycin (Fig.14, D and E).

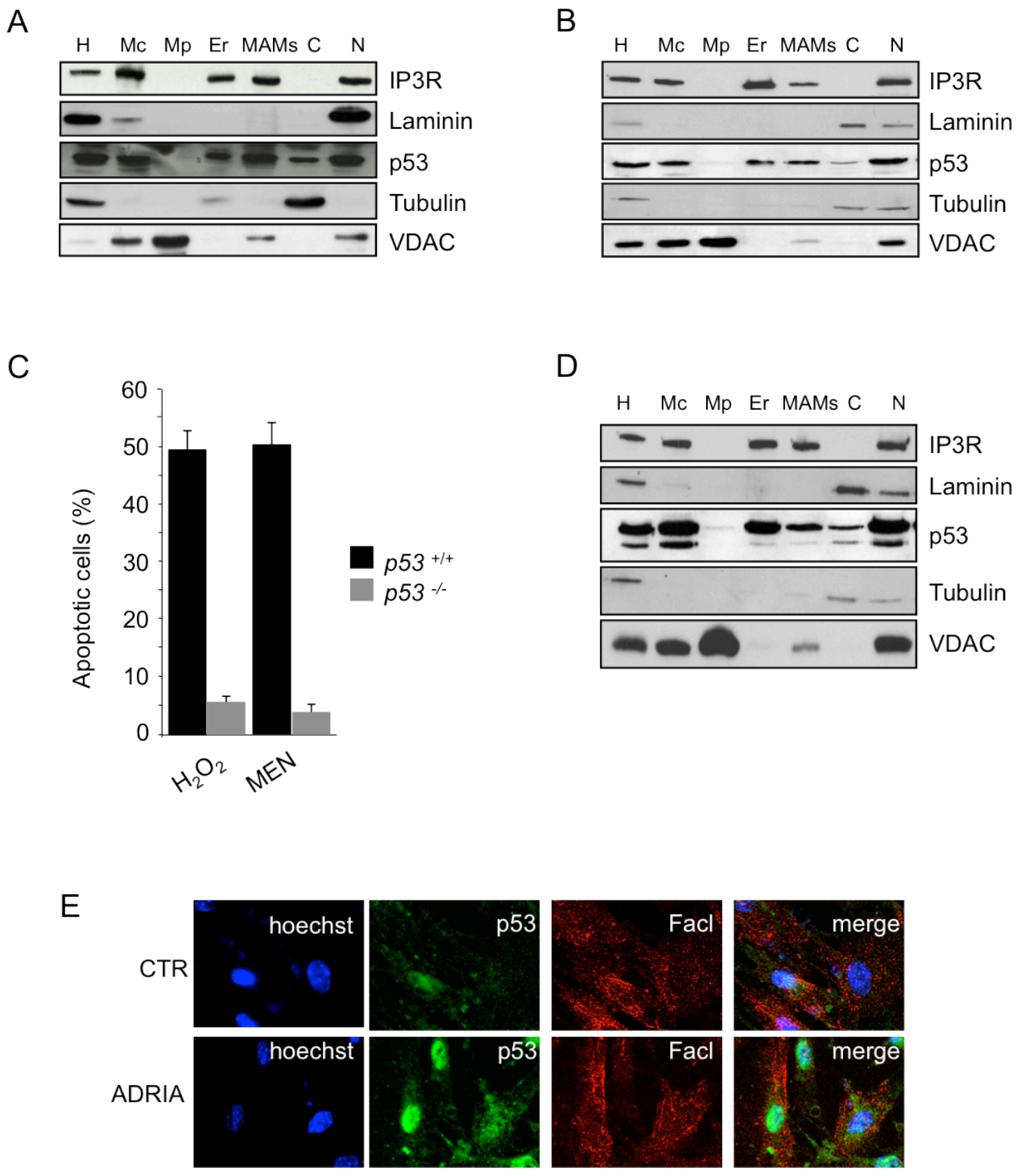

Fig.14 p53 localization at ER and MAM regions is fundamental for its apoptotic activity. Detection of p53 by immunoblotting in *p53*$^{+/+}$ MEFs **(A)** and HCT-116 *p53*$^{+/+}$ **(B)** fractionations. IP3R, Laminin, tubulin and voltage dependent anion channel (VDAC) are used as markers. H: homogenate; Mc: crude mitochondria; Mp: pure mitochondria; ER: Endoplasmic Reticulum; MAMs: mitochondria associated membranes; C: cytosol; N: nucleus. **(C)** Apoptosis induced by 1 mM H_2O_2 or 15 µM menadione (MEN) in *p53*$^{+/+}$ or *p53*$^{-/-}$ MEFs treated for 16 h. Mean of six independent experiments. **(D)** Accumulation of p53 at ER and MAMs regions after Adriamycin induction in HCT-116 *p53*$^{+/+}$ cells. **(E)** Co-localization of p53 (green) and FACL (long-chain fatty acid-CoA ligase type 4, used as MAM marker, red) in *p53*$^{+/+}$ MEFs in control condition (CTR) and after Adriamycin induction (ADRIA), analyzed by immunofluorescence.

Calcium homeostasis alterations induced by p53

The key process connecting apoptosis to ER-mitochondria interaction is an alteration in Ca^{2+} homeostatic mechanisms (159) that results in massive and/or a prolonged mitochondrial Ca^{2+} overload (160). We thus examined the effect on Ca^{2+} homeostasis of p53 down-regulation and induction, respectively. Using recombinant aequorin probes (161), $[Ca^{2+}]$ was measured selectively in the cytosol and in organelles acting as source (ER) or target (mitochondria) of cellular Ca^{2+} signals. A striking difference was evident in $[Ca^{2+}]_{er}$ steady state levels (Fig.15A). After p53 induction by adriamycin, the degree of ER filling was higher, whereas the loss of p53 caused a reduction of ER Ca^{2+} content compared to wt. Conversely, the kinetics of Ca^{2+} release from ER were comparable in all conditions thus suggesting a selective impairment in the Ca^{2+}-import mechanisms from the cytosol to the lumen of ER (Fig.15A) (*p53*$^{+/+}$: $[Ca^{2+}]_{ER}$ peak 360 ± 21 μM; *p53*$^{-/-}$: $[Ca^{2+}]_{ER}$ peak 282 ± 32.4 μM; *p53*$^{+/+}$+ ADRIA: $[Ca^{2+}]_{ER}$ peak 431 ± 28 μM. n=15 from five independent experiments and $p<0.01$).

In agreement with the $[Ca^{2+}]_{er}$ data, the $[Ca^{2+}]$ increases evoked by stimulation with ATP in the mitochondria and in the cytosol were significantly larger after adriamycin treatment and smaller in p53$^{-/-}$ than in wt MEFs (Fig.15, B and C) (*p53*$^{+/+}$: $[Ca^{2+}]_m$ peak 80 ± 16 μM; $[Ca^{2+}]_c$ peak 2.5 ± 0.18 μM. *p53*$^{-/-}$: $[Ca^{2+}]_m$ peak 43 ± 9.3 μM; $[Ca^{2+}]_c$ peak 1.85 ± 0.31 μM. *p53*$^{+/+}$+ ADRIA: $[Ca^{2+}]_m$ peak 105 ± 14 μM; $[Ca^{2+}]_c$ peak 2.9 ± 0.22 μM. n=15 from five independent experiments and $p<0.01$). Similarly, increased Ca^{2+} traffic from ER to mitochondria was observed both in HeLa cells over-expressing a p53 wt construct (130) (Fig.16 A, B, C) and in HCT-116 *p53*$^{+/+}$ upon Adriamycin treatment. (Fig.16D) (HeLa control: $[Ca^{2+}]_{ER}$ peak 228 ± 35 μM; $[Ca^{2+}]_m$ peak 42 ± 21 μM; $[Ca^{2+}]_c$ peak 3.1 ± 0.2 μM. HeLa expressing p53 wt: $[Ca^{2+}]_{ER}$ peak 355 ± 29 μM; $[Ca^{2+}]_m$ peak 53 ± 11 μM; $[Ca^{2+}]_c$ peak 3.7 ± 0.25 μM. n=10 from five independent experiments and $p<0.01$. HCT-116 *p53*$^{+/+}$: control peak 1.36 ± 0.5 μM, ADRIA peak 1.7 ± 0.6 μM).

On the contrary, Adriamycin treatment in MDA-MD 468 breast cancer cells, which are hemizygous for p53 mutation, had no effects on Ca^{2+} homeostasis (Fig.16E) (MDA-MD 468: control peak 6.53 ± 1.3 μM, ADRIA peak 6.47 ± 1.2 μM) as well as in p53$^{-/-}$ MEFs and HCT *p53*$^{-/-}$ (data not shown).

To assess if the observed ER Ca^{2+} overload is a pro-apoptotic condition, we analyzed mitochondrial morphology after apoptotic stress induction. Mitochondria of wt MEFs were labelled with targeted GFP and mitochondrial volume was evaluated by confocal microscopy. Treatment with H_2O_2 for 3 hours caused a strong reduction of the average mitochondrial volume, as expected, upon network breakage (Fig.15D). Induction of p53 alone did not significantly affect mitochondrial volume but Adriamycin treatment followed by H_2O_2 exposure induced a greater reduction in mitochondrial volume compared to H_2O_2 alone. As for the volume, Adriamycin alone did not alter the

mitochondrial morphology while the combination of Adriamycin and H_2O_2 caused a strong increase of fragmentation (Fig.15D).

The same experiments were performed in MEF p53 KO to exclude any non-specific effect of Adriamycin on mitochondria. As expected H_2O_2 exposure caused a low reduction on mitochondrial volume and increase in fragmentation, but this effect was not significantly influenced by Adriamycin pre-treatment (Fig.15D).

As mentioned above, there is a general literature agreement linking Ca^{2+} transfer from the ER to mitochondria and the effect of apoptotic stimuli. We thus investigated whether the absence or the induction of p53 could alter the increases in $[Ca^{2+}]_m$ after apoptotic stimuli. We observed that the reduction mediated by the oxidative apoptotic stimuli H_2O_2 of agonist-dependent mitochondrial Ca^{2+} response, was proportional to p53 expression (Fig.15E). Similarly, the increases in $[Ca^{2+}]_m$, evoked by H_2O_2, triggering a progressive release of Ca^{2+} from the ER and an activation of the capacitative Ca^{2+} influx (139), were higher after adriamycin p53 induction compared to wt and null conditions (Fig.15F). As consequence, the activation and accumulation of p53 to ER/MAMs compartments render cells more prone to die after apoptotic stress (Figs. 15, G-H).

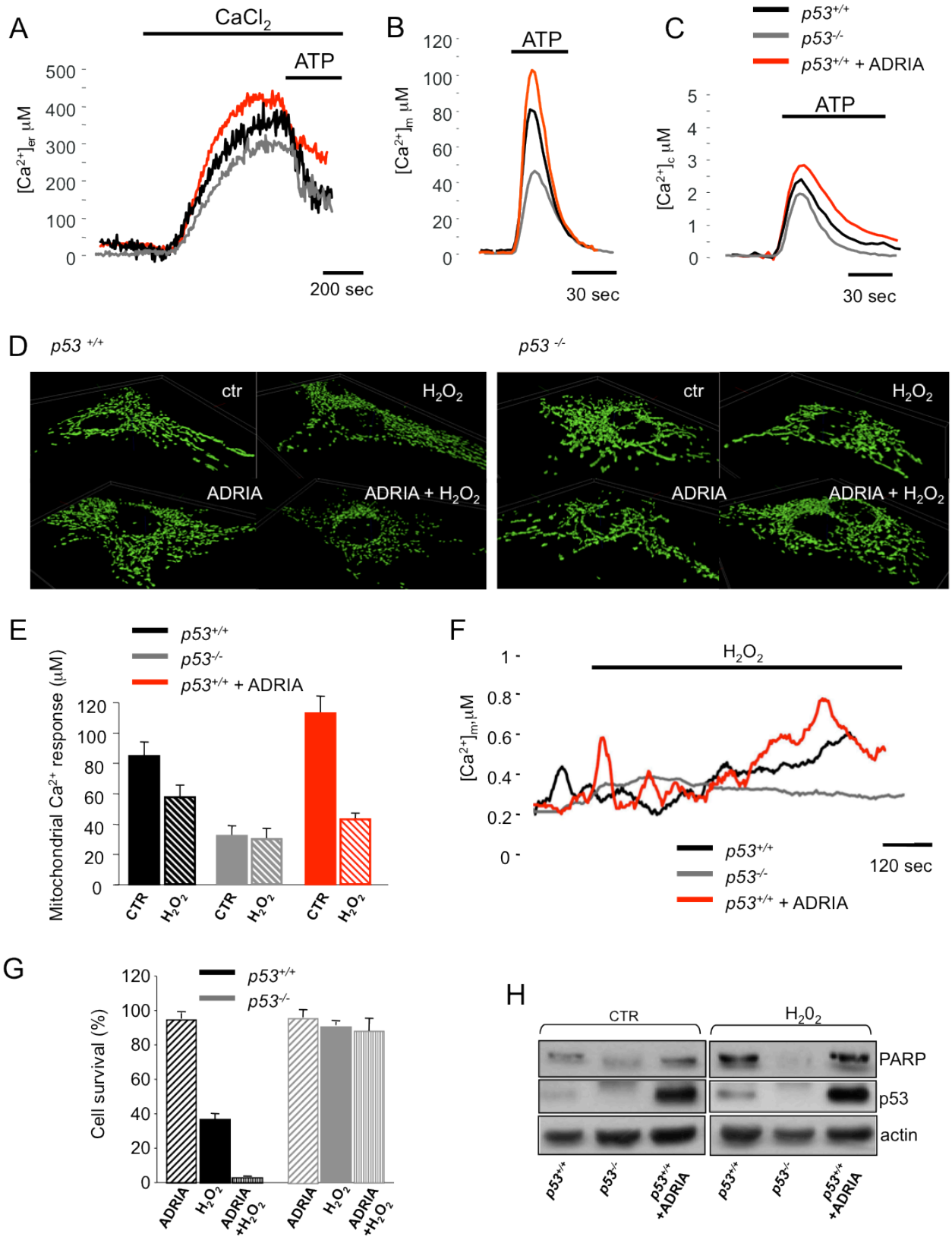

Fig.15 Alterations of Ca^{2+} homeostasis after p53 induction is Human Tumour cell lines (A-C) Measurements of $[Ca^{2+}]$ using aequorin upon agonist (100 mM ATP) stimulation in ER (A), mitochondria (B) and cytosol (C). **(D)** Isosurface rendering of $p53^{+/+}$ and $p53^{-/-}$ MEFs expressing mtGFP in basal conditions, after ADRIA and/or H_2O_2 exposure. **(E)** Mitochondrial Ca^{2+} response ATP dependent in $p53^{+/+}$ **(F)** Analysis of $[Ca^{2+}]_m$ during oxidative stress upon H_2O_2 stimulation (2 mM).

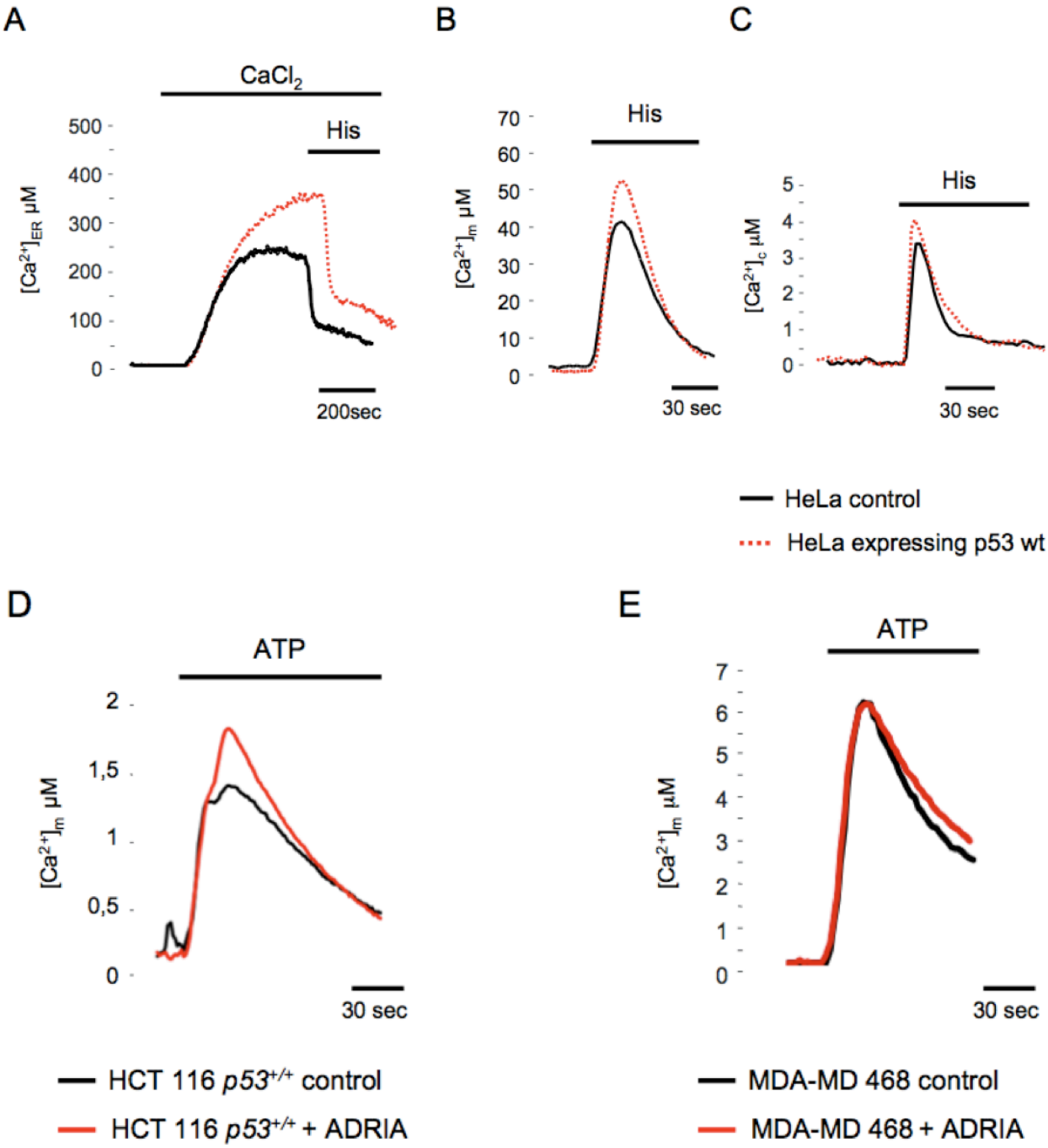

Fig 16 Analysis of Ca^{2+} homeostasis in ER (A), mitochondria (B) and cytosol (C) in HeLa cells in control condition and after expression of the p53 wt construct. Measurements were obtained with aequorin targeted chimeras after agonist stimulation (100 mM Histamine). Mitochondrial [Ca^{2+}] after ATP stimulation measured in HCT-116 $p53^{+/+}$ (D) and MDA-MD 468 (E) cells in control condition and after ADRIA treatment (1 µM, 6 h)

Perturbations of Ca^{2+} homeostasis are not linked to p53 transcriptional activity

In order to exclude that a transcriptional-dependent pathway of p53 accounts for its effect on Ca^{2+} homeostasis (and in turn to the sensitivity of ER-stress apoptotic stimuli) we used both specific

drugs blocking the transcriptional arm of p53 and a nuclear import-deficient p53 mutant (p53-NLS). We used α-amanitin, a highly specific and potent inhibitor of the RNA polymerase II transcription, or a combination of pifithrin α, a specific inhibitor, which selectively blocks p53-mediated transcription and Adriamycin to activate the remaining p53 pathways. As expected, in both conditions we observed increased mitochondrial Ca^{2+} responses (Fig 17A), reflecting an increased ER Ca^{2+} release (*p53*$^{+/+}$: peak 79.6 ± 13.8 μM, *p53*$^{+/+}$+ α-amanitin: peak 110.3 ± 12.1 μM and *p53*$^{+/+}$+ pifithrin α + ADRIA: peak 99.6 ± 5.8 μM).

Moreover, over-expression of the p53-NLS chimera in *p53*$^{-/-}$ MEFs (Fig.17C) as well as in HeLa (Fig.17D), H1299 non-small lung carcinoma cells (Fig.17E) and HCT-116 *p53*$^{-/-}$ (Fig.17F), was able to enhance mitochondrial Ca^{2+} signaling, similarly to the effect of p53 induction by Adriamycin (Fig 15B). On the contrary, naturally occurring mutants of p53 over-expressed in those cell lines lost their ability to increase ER Ca^{2+} loading (Fig.17 D, E, F blue and grey dotted lines) (MEFs peak 35 ± 6.8 μM in *p53*$^{-/-}$ vs 65.5 ± 10.6 μM in *p53*$^{-/-}$ + p53-NLS; HeLa control: 40.1 ± 14 μM, p53-NLS peak: 60.5 ± 10.3, p53 R175H peak: 37.7 ± 11.2 μM, p53 R273H peak: 36.8 ± 6.2 μM; HCT116 ko control peak: 2.1 ± 0.2 μM, p53-NLS peak: 4.81 ± 0.3, p53 R175H peak: 2.4 ± 0.45 μM, p53 R273H peak: 2.7 ± 0.41 μM; H1299 control peak: 0.43 ± 0.06 μM, p53-NLS peak: 0.67 ± 0.07, p53 R175H peak: 0.5 ± 0.17 μM, p53 R273H peak: 0.5 ± 0.23 μM. n=12 from three independent experiments and $p<0.05$).

To verify if the regulation of Ca^{2+} homeostasis by p53 depends on its localization to the ER/MAMs, we generated a chimera containing the p53-NLS protein targeted to the outer surface of the ER by the addition of the short hydrophobic C-terminal ER-targeting sequence cloned from the yeast UBC6 protein (162) (Fig.18A).

The introduction of ER-p53 in *p53*$^{-/-}$ MEFs (Fig.18B) and in H1299 cells (Fig.18D) restored Ca^{2+} signals evoked by agonists to values comparable to those obtained after over-expression of the p53-NLS chimera (MEFs, $[Ca^{2+}]_m$ peak 40.6 ± 8.7 μM in *p53*$^{-/-}$ vs 81.5 ± 15.6 μM in *p53*$^{-/-}$ + ER-p53; H1299, ER-p53 chimera: 0.75 ± 0.08 μM; control: 0.41 ± 0.08 μM, as well as in wt MEFs after adriamycin induction (Fig.17C and 15B). This effect was moreover associated with a re-established sensitivity to apoptosis induced by ER stress, as determined by cell count analysis (Fig.18E) and PARP cleavage (Fig.18F).

A mechanism proposed for p53-dependent cell death is through a transcription-independent pathway involving the Bcl-2 family (163) and in particular Bax/Bak proteins (122, 164) that localize also at ER (165). To evaluate whether the role of p53 at ER/MAMs in ER stress-dependent cell death stimuli requires Bax/Bak proteins, we analyzed the effects of p53 induction in cells deficient of Bax and Bak (DKO cells). In these cells, Adriamycin still raised $[Ca^{2+}]_m$ (Fig.18C) thus

suggesting a mechanism independent from the Bax/Bak proteins.

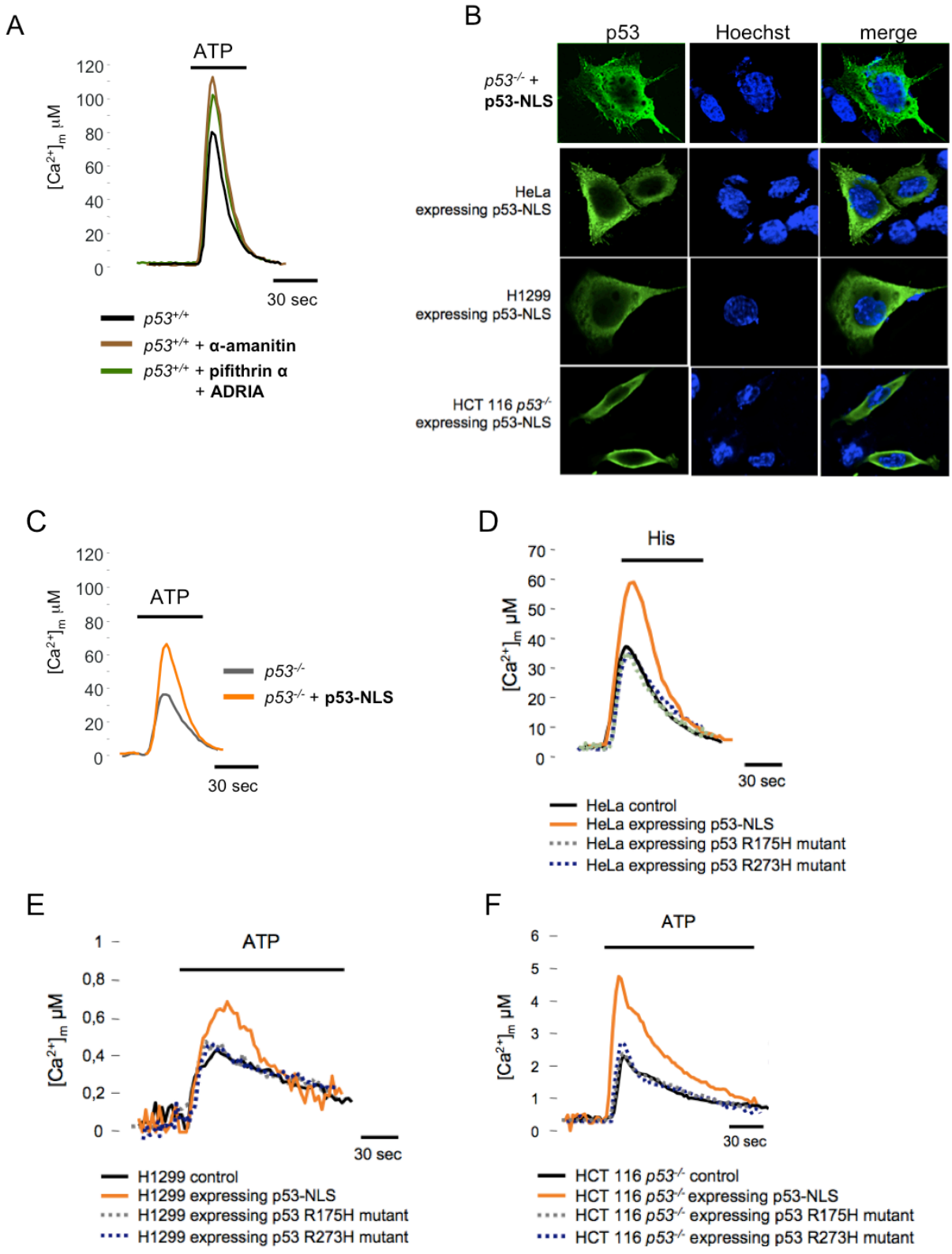

Fig.17 Alteration of Ca^{2+} homeostasis after p53 induction is Human Tumour cell lines (A-C) Measurements of $[Ca^{2+}]$ using recombinant aequorin upon agonist (100 mM ATP) stimulation in ER (A), mitochondria (B) and cytosol (C). **(D)** Isosurface rendering of representative *p53*$^{+/+}$ and *p53*$^{-/-}$ MEFs expressing mitochondrial GFP in basal conditions, after ADRIA and/or H_2O_2 exposure. **(E)** Mitochondrial Ca^{2+} response ATP dependent in *p53*$^{+/+}$ **(F)** Analysis of $[Ca^{2+}]_m$ during oxidative stress upon H_2O_2 stimulation (2 mM).

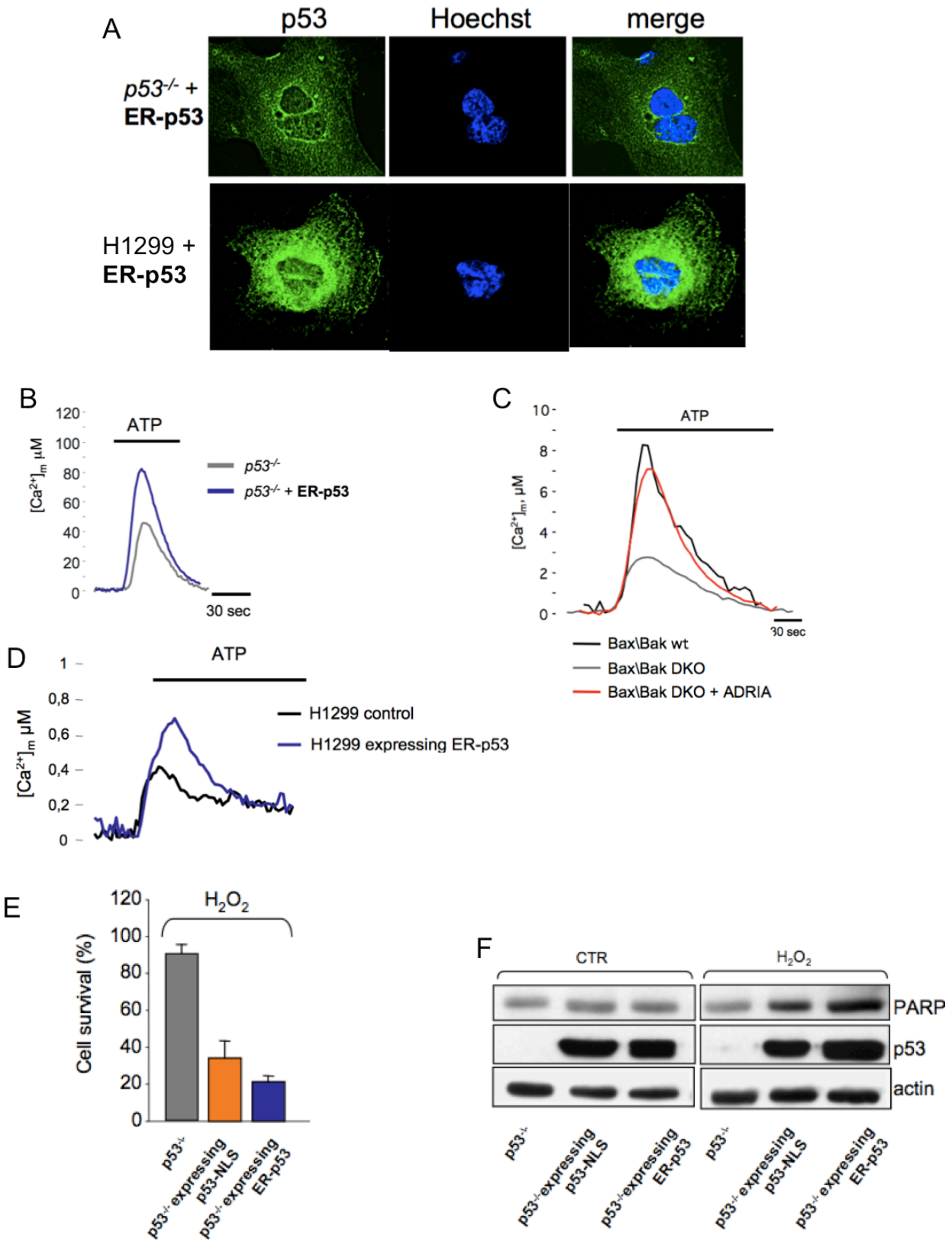

Fig 18 Transcriptional path of p53 is not required for perturbation of Ca^{2+} homeostasis. (A) Agonist-dependent $[Ca^{2+}]_m$ response in $p53^{+/+}$ MEFs after pharmacological block of transcriptional arm of p53. N=12 from three independent experiments and p<0.05. **(B)** Immunofluorescence of $p53^{-/-}$ cells expressing p53-NLS stained with the anti-p53 antibody and Hoechst (as nuclear marker). $[Ca^{2+}]_m$ in $p53^{-/-}$ MEFs **(C)** after over-expression of p53-NLS**,** and during overexpression of naturally occurring mutants in HeLa **(D)** HCT116 $p53^{-/-}$ **(E)** and H1299 **(F)** compared with p53-NLS.

p53 promotes SERCA activity

The above findings clearly suggest that the localization of p53 at ER/MAMs compartments is important for a Ca^{2+}-mediated, transcription-independent apoptotic pathway and that it exerts its major impact on ER Ca^{2+} uptake, a process mediated by the SERCA, i.e. Sarco-Endoplasmic Reticulum Ca^{2+}-ATPase. Thus, we tested whether p53 functionally and physically interacts with SERCA. As shown in Fig.18A, the *in vitro* interaction between p53 and endogenous SERCA2b was first detected by MBP pull down assay in H1299 cell line lacking of p53, after over-expression of a p53 wt construct and then confirmed by the co-precipitation in MEFs wt (Fig.19E)

Next we mapped the region of p53 involved in the interaction with SERCA 2b. To this end, we took advantage of HA-tagged p53 deletion constructs: HAp53 1-175, HAp53 175-393, HAp53 294-393 and the full-length HA-p53. In immunoprecipitation experiments performed in H1299 cells transfected with various HA-p53 constructs, SERCA2b selectively bound to the C-ter regulatory domain of p53, i.e. a region where post-translational modifications can modify the interaction of p53 with partner proteins (Fig.19B).

Finally, we investigated whether p53 has a direct effect on the activity of SERCA pump. For this purpose, the kinetics of ER Ca^{2+} accumulation were studied in MEF wt and p53 null as well as after p53 induction by adriamycin in a time-dependent manner. The rate of Ca^{2+} accumulation in the ER increased proportionally to the induction of p53, indicating a stimulatory role of p53 on SERCA activity (Fig.19C) (MEFs. $p53^{-/-}$: $\mu M[Ca^{2+}]/s$ 3.73 ± 0.11, n = 7; $p53^{+/+}$: $\mu M[Ca^{2+}]/s$ 6.71 ± 0.6, n = 14; $p53^{+/+}$ ADRIA 30min: $\mu M[Ca^{2+}]/s$ 7.76 ± 0.82, n = 13; $p53^{+/+}$ ADRIA 3h: $\mu M[Ca^{2+}]/s$ 8,81 ± 0.45, n = 21; $p53^{+/+}$ ADRIA 6h: $\mu M[Ca^{2+}]/s$ 9,31 ± 1.15, n = 15; from at least three independent). SERCA expression levels were unmodified, further excluding a transcriptional mechanism (Fig.19F). This data was confirmed also in HeLa cells over-expressing p53 wt and p53-NLS chimera (Fig.19D)(control, $\mu M[Ca^{2+}]/s$ 4.15 ± 0.23, n = 8; over-expression of p53 wt $\mu M[Ca^{2+}]/s$ 8.05 ± 2.1, n = 8; and p53-NLS $\mu M[Ca^{2+}]/s$ 9.4 ± 3.1, n = 8).

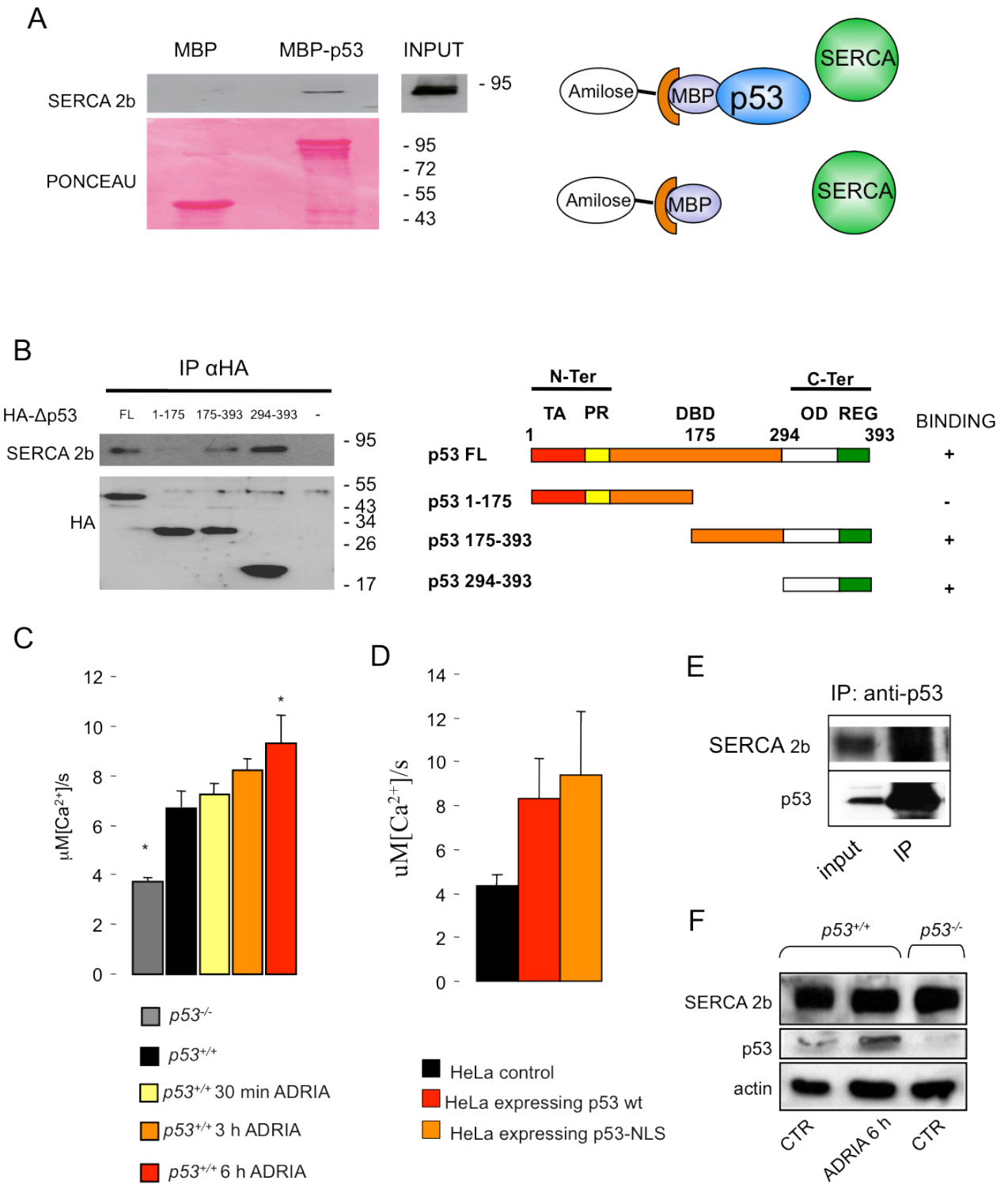

Fig.19. p53 modulates Ca^{2+} signals interacting with SERCA 2b pump. (A) *In vitro* binding of endogenous SERCA 2b to MBP-p53. Lysates of H1299 cells were incubated with bacterially expressed MBP-p53 protein or MBP as control. Ponceau staining shows the amount of MBP proteins used in the experiments. **(B)** Full length and HA-tagged p53 deletion mutants transiently expressed in H1299 cells were immunoprecipitated by anti-HA 12CA5 antibody and analysed by western blots with anti-HA 12CA5. Co-immunoprecipitated SERCA 2b proteins were analyzed with SERCA 2b antibody. **(C)** Rate analysis of Ca^{2+} refilling in the ER at different time of ADRIA treatment (1µM) in MEFs. *P53*$^{-/-}$ and in HeLa Cells during overexpression of wt-p53 and p53-NLS **(D). (E)** immunoprecipitation assay revealing interaction between p53 and SERCA2b in MEFs. **(F)** Analysis of SERCA 2b levels in MEFs by western blot in presence or absence of activated p53.

Discussion

From the early years after its discovering p53 has been always linked to molecular oncology. Initially described as a transcription factor has been addressed as a master gene involved in control of several processes that goes from promotion of apoptosis, regulation of autophagy, block of cell cycle, DNA damage repair, regulation of metabolism with final aim to inhibit tumour appearance and progression. Just recently has been proposed that p53 has important cytoplasmic activity, specially has been demonstrated how p53 could undergoes through monoubiquitinilation that drives its localization to mitochondria in order to induce MOMP and release of Cyt C, with subsequent activation of caspase 9 and apoptosis induction (166). Even more interesting this event appear to occur before of its nuclear translocation (167). After these initial reports several others appears, indicating how mitochondrial p53 localization could be mediated by a huge amount of cell stressing events (168).

Nonetheless, most of these reports are based on biochemical protocols that allow obtainment of mitochondria enriched fractions that are prone to artefacts, allowing enrichment of other membranes, especially from endoplasmic reticulum. Known the close association between mitochondria and ER we investigated in this study if p53 could also localize to ER and especially to its contact sites with mitochondria, also known as MAM.

We start the investigation by isolating mitochondria pure fraction, ER pure and MAM with subcellular fractionation in two different cell types Mouse Embryonic Fibroblast (MEF) and Human colon cancer cells (HCT116). Interestingly we found p53 able to localized to the ER and MAM fractions in both cell types, and specially, in $HCT116^{+/+}$ the p53 stabilization promoted by a genotoxic stress, Adriamycin, induce a further accumulation of the protein. On opposite we almost not detected p53 in the mitochondrial fraction.

Known the relevance for p53 in the apoptotic process we tested if, from this site, the same relevance could be maintained. Endoplasmic Reticulum participates in the apoptotic process by a special communication between mitochondria and ER. Several apoptotic stimuli in fact are able to induce a slow and sustained Ca^{2+} release from the ER that is capted by mitochondria allowing mitochondrial swelling and Cyt C release. Was though relevant to investigate if p53 could participate in such kind of processes. Wt and p53 ko cells were then challenged with two oxidizing factors (Menadione and H_2O_2) that allow the previously described calcium transmission and observed that ko cells appear strongly resistant compared to wt indicating p53 as a possible participant in the Ca^{2+} dependent apoptotic process.

To provide a causal link we start monitoring general Ca^{2+} homeostasis taking advantage of the calcium sensitive luminescent reporter aequorin targeted to the different cell compartments involved in this transmission, cytoplasm, mitochondria and ER. MEF wt in which p53 was induced by Adriamycin display a higher concentration of both $[Ca^{2+}]_m$ and $[Ca^{2+}]_c$ when Ca^{2+} waves were induced by extracellular ATP. Contemporary $[Ca^{2+}]_{er}$ display a significant increase during the steady state, suggesting that alterations of Ca^{2+} waves where due to an increased amount of calcium within the ER. As expected ko cells display a reduced steady state within ER as also reduced calcium waves within cytoplasm and mitochondrial uptake.

Moreover an increase in mitochondrial uptake was observed in HeLa cells expressing wt p53 as also in HCT116 exposed to Adriamycin. These data strongly indicates that Ca^{2+} content within ER is linked to the presence of p53 and that this event is reproducible not only in primary cultures but also in tumor derived cell lines. Interestingly MDA-MD 468 cells, derived from breast cancer, do not show significant alterations in $[Ca^{2+}]_m$ after exposure to Adriamycin. Peculiarity of this cell line is the fact that they carry a mutant allele for p53, the R273H that is considered one of the hot spot mutations for p53. This mutation has been mapped within the DNA-binding domain of p53 and one of the most frequent in tumours associated with p53, enforcing the link between the p53 proapoptotic activity and a transcription independent activity.

Then was monitored the direct impact of p53 on mitochondrial calcium overloading and fragmentation. It is assumed from literature that mitochondria can undergoes through Ca^{2+} overload during Ca^{2+} dependent apoptotic stimuli that induce fragmentation of the mitochondrial network before to induce Cyt C release, even if it still under debate which are the molecular participant involved. In MEF wt pretreatment with Adriamycin do not significantly alter mitochondrial network interconnectivity without induction of apoptosis, on opposite it strongly promote appearance of round mitochondria, in spite to elongated, during H_2O_2 exposure. Contemporary, calcium accumulation within mitochondria (monitored with aequorin), elicited by H_2O_2 appear, longer and with higher amplitude in cells pre-treated with Adriamycin, reflecting an increased amount of Ca^{2+} released from ER.

A direct link between p53 localization to ER and MAM was anyway still missing. To address this question $[Ca^{2+}]_m$ was monitored during conditions non-permissive for transcriptional activity of p53. Administration of α-amanitin, an inhibitor of RNA polymerase II induce blockage of mRNA transcription and an indirect activation of cytoplasmic p53 (169). In wt MEFs a-amanitin was able to promote mitochondrial Ca^{2+} accumulation, and stabilization of p53 with Adriamycin still produce the same effect in presence of pifitrin-α, a well known inhibitor only of the transcriptional activity of p53. Similarly the overexpression of p53-ΔNLS, a chimeric p53 in which the nuclear export

sequences were mutated or deleted promote the same effect as wt p53 in cells ko for p53 both from primary cultures, MEF p53 -/-, as derived from human tumours, H1299, HeLa, HCT116$^{-/-}$. Clearly suggesting that the transcriptional arm of p53 activity is not required for alteration of Ca^{2+} homeostasis.

These data resemble what observed in MDA-MD 468, for long time p53 has been reported only as transcription factor, due to this the hot spot mutations naturally occurring in tumours, mapped in the DBD, has been addressed to the loss of transcriptional activity. Here we report a new non-transcriptional role for p53 in the regulation for apoptosis. Nonetheless overexpression of p53-R175H and p53-R273H, both carrying natural occurring mutants, were again able to elicit increase in mitochondrial calcium uptake in cells derived from tumour and KO for p53. Should be noticed that recently the same mutation has been mapped in newly defined interaction sites for Bcl-2 (170).

The Bcl-2 route of p53 activity has been taken into consideration in literature to explain the mitochondrial activity of p53. Bcl-2 at the OMM bound to BAX and BAK impeding their oligomerization and the formation of permeability transition state that should allow Cyt C release. Current opinion is that p53 interacting with Bcl-2 sequesters it from OMM allowing oligomerization of BAX/BAK the Cyt C release.

Here we provide that what observed to now be not linked to this mechanism. First of all should be considered that Bcl-2 also localize to ER, thus its interaction with p53 would promote its localization to the ER, second, we performed experiments of $[Ca^{2+}]_m$ measurement in MEF BAX/BAK ko and observed that in such cells Adriamycin was still able to promote calcium uptake, third, we generated an ER targeted p53 chimera fusing p53-ΔNLS to an ER localization sequence from the yeast ubiquitin ligase UBC6. Overexpression of this chimera in MEF$^{-/-}$ as well as in H1299 was able to both induces the expected alteration of Ca^{2+} homeostasis as well as on sensitivity to cell death.

Last point was investigation of the molecular mechanism by which p53 is able to alter Ca^{2+} homeostasis at the ER. Measurements of Ca^{2+} homeostasis shows a difference in the kinetic of Ca^{2+} uptake within the ER, in the initial part of the experiment, when extracellular calcium where added. Usually this event is regulated by activity of SERCA protein, a Ca^{2+} ATPase located to the ER membrane that constantly pump Ca^{2+} within the ER lumen. Calcium uptake rate was increased in HeLa cells Expressing both p53 wt and p53-ΔNLS, moreover in MEF wt correlate directly with the time of exposure to Adriamycin.

Through co-immunoprecipitation assay we observed that p53 is able to interact with isoform 2b of SERCA in MEF wt. We next generated p53 fragment to isolate the domain of interaction. GST pulldown assay revealed, in H1299 that the p53 is able to interact with SERCA2b through a region

out of its DBD, between its oligomerization domain and the regulative domain. Apparently the interaction domain is outside from its DBD, far from the hot spot sites, indicating that these sites are not directly involved in interaction with SERCA. This suggests that interaction between SERCA and p53 is mediated by other proteins. A second possible explanation is that several hot spot mutation, even if occurring within the DBD, are reported to induce a deformation in p53 structure (171). That in turn could induce a loss of interaction with SERCA-2b even if located far from the DBD.

Overall these data reveal a novel mechanism through which p53 exerts its potent pro-apoptotic role. We demonstrate that the non-nuclear fraction of p53 is present in the ER/MAMs fraction and physically interacts with SERCA, thus potentiating Ca^{2+} accumulation in the ER lumen. This allows apoptotic stimuli and ER stress conditions, to rapidly and efficiently load mitochondria with Ca^{2+}, a priming step for the release of caspase cofactors and induction of apoptosis via the intrinsic pathway. In cancer cells this pro-apoptotic mechanism could be impaired due to functional inactivation of p53 and contribute to the disease progression. The identification of the critical signalling steps activating this new function of p53 may provide new targets to restore sensitivity to cell death and develop new therapeutic approaches.

Tumour necrosis factor alpha inhibits oligodendrocytes differentiation by inhibiting mitochondrial functions

Introduction

Multiple sclerosis (MS) is a neurological disorder of the central nervous system characterized by demyelination and neurodegeneration. MS is characterized by its relapsing-remitting course and neuro-pathologically manifests with multifocal areas of perivascular leukocyte infiltration associated with demyelination of the CNS. Early clinical symptoms result from oligodendrocytic damage and/or demyelination. The regression of symptoms is attributed to resolution of immune-based attack, associated edema and to partial remyelination or redistribution of sodium channels along demyelinated segments of axons (171). Although the pathogenesis of MS is not completely understood, various studies suggest that immune-mediated losses of myelin and mitochondrial dysfunction are associated with the disease (172). In particular, mitochondrial functions might be required for proper oligodendrocyte differentiation and myelination. Specifically, it has been demonstrated that i) mitochondrial transcripts and copy number are induced by oligodendroglia differentiation, ii) slight mitochondrial inhibition inhibits differentiation, and iii) stronger mitochondrial inhibition selectively decreases viability of differentiating oligodendroglia but not undifferentiated cells (173).

It is now well established that mitochondria play a pivotal role in cell survival in large part because of their participation in the dynamic regulation of cellular Ca^{2+}. Under normal conditions, the accumulation of Ca^{2+} in mitochondria stimulates oxidative metabolism. However, overload of mitochondria with Ca^{2+}, as a consequence of pathological stimuli, results in dramatic alterations in mitochondrial functions, including decreased ATP production and increased generation of reactive oxygen. For example, compounds generated in response to inflammation (e.g., reactive oxygen and nitrogen species) inhibit mitochondrial electron transport, resulting in axonal energy deficits (174, 175). Recent reports have documented impaired activity of several mitochondrial respiratory complexes in MS plaques (176).

Oligodendrocytes are particularly susceptible to oxidative injury. Having a low concentration of the antioxidant glutathione predisposes these cells to the accumulation of intracellular hydrogen peroxide. Contributing factors include their high metabolic rate and ATP requirement for the synthesis of large amounts of myelin membrane, the high production of hydrogen peroxide in

peroxisomes, and the large intracellular stores of iron. Whereas iron is critical for myelin production (177), this metal can also trigger free radical formation and lipid peroxidation, via conversion of hydrogen peroxide into hydroxyl radicals (178). Microglia present at the sites of injury play an important role in triggering or potentiating oligodendrocyte injury by several mechanisms. Both resting and activated microglia may release glutamate via a cystine-glutamate antiporter (179) as well as proinflammatory cytokines, such as tumour necrosis factor (TNFα), which impair expression or function of glutamate transporters in astrocytes and oligodendrocytes. TNFα can also trigger oligodendrocyte apoptosis both via death receptors and by activation of sphingomyelinase, with consequent release of ceramide (180). There is in vitro evidence that cytokine-induced oligodendrocyte injury may be mediated by iron and involves mitochondrial dysfunction (178)

Evidence that implicates TNFα in the underlying pathology of MS includes: i) the observation that, at autopsy, MS patients have elevated TNFα levels at the site of active MS lesions (181); ii) reports that CSF and serum TNFα levels in individuals with MS are elevated compared to unaffected individuals and TNFα levels correlate to the severity of the lesions [(182),(183)]; and iii) evidence that peripheral blood mononuclear cells from MS patients just prior to symptom exacerbation have increased TNFα secretion after stimulation compared to cells from the same patients during remission (184). Based on these strong clinical parameters implicating TNFα signalling in contributing to MS disease severity, the effects of manipulation of the TNFα pathway were investigated in mouse models of MS. Specifically, overexpression of TNFα leads to demyelinating disease and neutralization of TNFα with anti- TNFα antibodies or receptor fusion proteins is protective in experimental autoimmune encephalomyelitis (EAE) transgenic mouse models (185).

Oligodendrocyte progenitors upregulate both TNFR1 and TNFR2 in response to inflammatory conditions, indicating that the proliferative effect of TNFα may be directly mediated through these receptors (186). In most reports, the exacerbating effect of TNFα is attributed to TNFR1, whereas TNFR2 is shown to have little or no effect on demyelination (187),(188),(189).

It has been shown that TNFα signalling through TNFR2 promotes the accumulation of proliferating oligodendrocyte progenitors, which then develop into mature oligodendrocytes required for remyelination. These results have a significant effect on the promotion of oligodendrocyte precursor growth and remyelination *in vivo* and *in vitro*, and the treatment of demyelinating diseases.

TNFα may promote early pathology, but its actions appear to be more complex than just induction of cell death. In fact, using mice lacking TNFα and its associated receptors, an unexpected role for TNFα and TNFR2 in repair of the CNS has been reported. This role of TNFα expands its known function in proper organogenesis and indicates a critical involvement in the timely production of oligodendrocyte precursors and mature oligodendrocytes in the CNS. Indeed, the lack of TNFα and

TNFR2 leads to a significant reduction in oligodendrocytes due to a delay in the generation of these cells (190).

To date it is widely reported how TNFα is able to impair oligodendrocytes differentiation. At low concentration TNFα has been shown to induce retardation in appearance of adult oligodendrocytes in vitro, while at higher concentration it appear to be able to induce also cell death (191).

Moreover, in leukemic cell lines, TNFα induced cell death requires the impaired activity of Complex I of the mitochondrial respiratory chain, NADH dehydrogenase, strategic for the regulation of ATP synthesis, as well as being one of the most important sources of ROS within cells.

In this study we address the possibility that TNFα a impairs oligodendrocytes differentiation by impairing mitochondrial physiology and further we evaluate the possibility that this impairment involve mitochondrial calcium signalling.

Results

TNFα at distinct concentrations impair oligodendrocyte differentiation or cell death

The first point considered was the ability of TNFa to impair oligodendrocytes differentiation in our in vitro system, set up following the protocol published by Chen et al (192). Oligodendrocyte progenitor cells (OPCs) were obtained by overnight shaking of mixed glial cultures generated from rat cortex. Isolated OPCs were then cultured for 7 days in presence of a selective chemically defined DMEM (OPC medium). Immunostaining with marker for total oligodendrocytes population (OSP), oligodendrocyte precursors (NG2), marker of fully differentiated oligodendrocytes (MBP) and marker of astrocytes (GFAP) were performed to verify the purity of the culture, assessed at about 95% of OPCs (data not shown). After 7 days of culture OPCs where treated for 24h with sublethal concentration of TNFa, 10ng/ml, as suggested by literature (193). Subsequently the growth factors present within the medium (fundamentals for OPCs replication) were substituted with T3 thyroid hormone to stimulate cell differentiation. After 5 days cells where fixed and immunostained for antigens able to mark different stages of oligodendrocytes maturation. According to the literature three different antigens were selected for three stages of differentiation: NG2 chondroitin sulphate proteoglycan for precursor, O4 for immature oligodendrocytes and MBP for fully differentiated (194). All the cells were contemporary stained for the oligodendrocytes specific antigen OSP to restrict the analysis only to the oligodendrocytes population and avoid artefacts coming from any contaminants. Cells were then acquired through an image based high content throughput system and classified by antigen positivity and nuclear features. During differentiation process in fact oligodendrocytes undergoes through deep rearrangement of cell and nuclear shape, specially nuclei increase their volume while reaching adulthood (Fig.20A).

Assay reveal that low TNFα concentration induce a reproducible reduction in MBP+ and O4+ cells %, with concomitant slight increase in NG2+ %, suggesting that an early block in the differentiation process was occurring. (control NG2+:34.2% ± 3.67, O4+:51.85% ± 2.01, MBP+:16.75% ± 5.58; TNF 10ng/ml: NG2+:39.05 % ± 1.06, O4+:42.7 % ± 2.35, MBP+:8.75 % ± 0.49. n:4 $p<0.05$.) Unexpectedly at high concentration no significant variation were observed (Fig.20B). (TNF50ng/ml NG2+:33.8% ± 5.06, O4+:43.73% ± 2.85, MBP+:13.83% ± 5.84; TNF 100ng/ml: NG2+:35.45% ±2.47, O4+:48.23% ± 0.87, MBP+:17.63% ± 0.94. n:4 $p<0.05$.)

Further we tested the ability of TNFα to induce cell death. Cells were growth, exposed to TNFα and induced to differentiate as described previously. After fixation, cells were stained for a TUNEL assay. This technique is based on an enzymatical incorporation of fluorescence labelled deoxynucleotide in DNA breaks in nuclei (195) making it very sensitive for identification of

apoptotic nuclei. TUNEL assay reveal that only at high concentration TNFα was able to promote apoptosis, moreover the effect appear generalized in all the populations, explaining why no relative enrichment of some populations were observed (Fig 20C). (control 6.28% ± 3.69; TNF10ng/ml 7.43%±1.85, TNF50ng/ml 11.14%±3.89, $p<0.1$; TNF100ng 13.51±3.36, $p<0.05$ $n>6$).

Taken toghether these data support the hypothesis that at low concentrations TNFα is more able to affect oligodendrocytes differentiation, causing a block in very early stages with a consequent accumulation mostly of NG2+ oligodendrocytes. On opposite, higher TNFα concentration cause an increase of apoptosis induction.

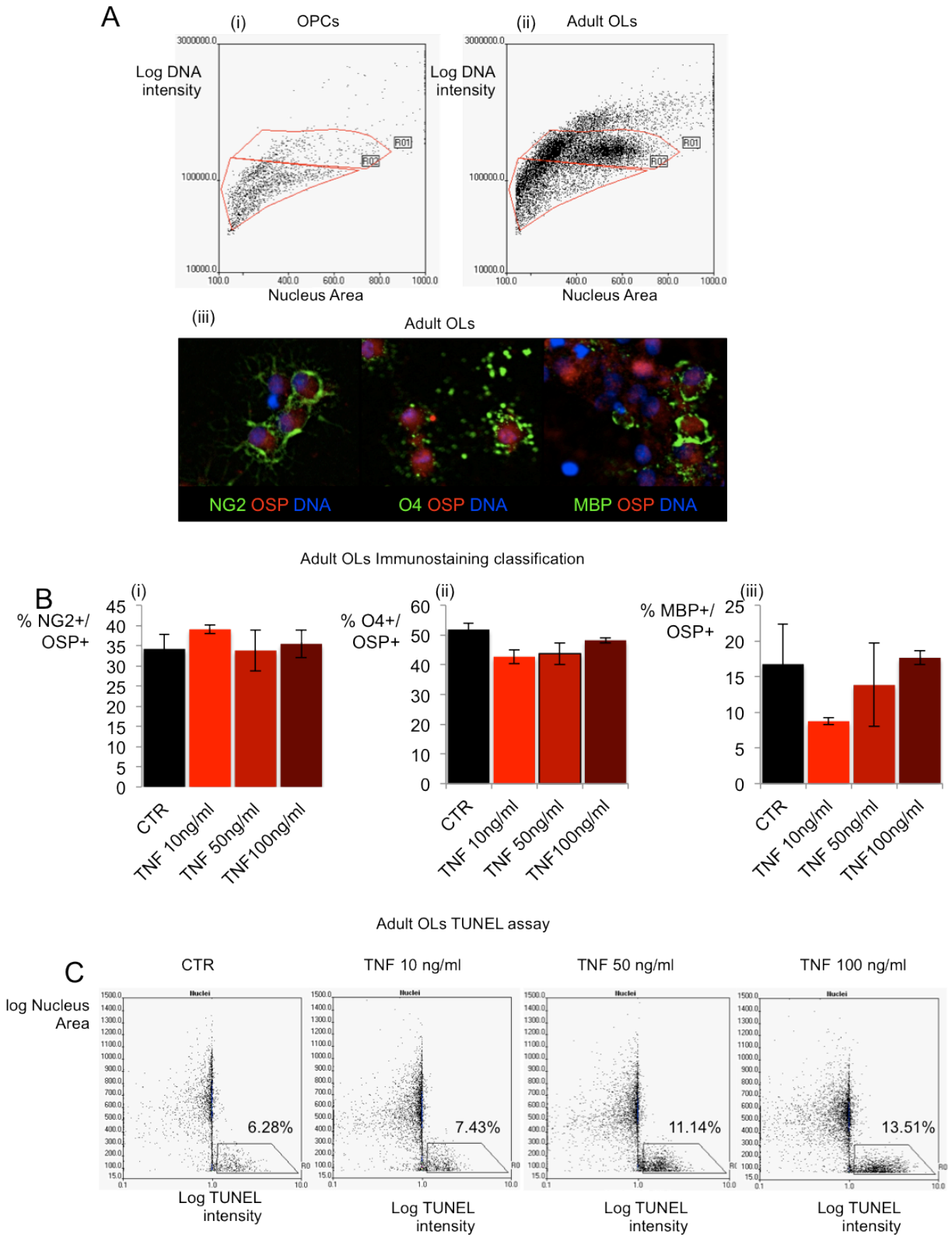

Fig.20. Distinct cell response initiated by TNFα. Nuclear pattern for scoring OPCs (Ai) or Adult Oligodendrocytes (Aii) and typical immunostaining for antigens used to score oligodendrocytes populations. **(B)** Oligodendrocytes enrichment for precursor (i), immature (ii) and adult cells (iii) during different concentration of TNFα. **(C)** Tunel assay in Oligodendrocytes populations during exposure to TNFα

Low concentration of TNFα selectively impair mitochondrial Ca^{2+} uptake

Second part was to consider mitochondrial physiology under TNFα exposure. As previously discussed mitochondrial calcium uptake could be considered as an affordable readout for monitor mitochondrial physiology. It is infact true that calcium is uptaken by mitochondria through the driving force provided by ΔΨm at the site in which mitochondria take contact with the ER. Once entered into mitochondria, calcium flow within the entire network because of the high amount of dynamic interconnections existing between mitochondria into the same cell. Noteworthy both ΔΨm and mitochondrial interconnectivity (or fragmentation) could be considered readout of mitochondria energy status, as well as exposure to stress or apoptosis induction.

Thus to monitor mitochondrial physiology under TNFα exposure we tested their ability to uptake calcium following agonist exposure. To this attempt OPCs where infected with an adenoviral vector carrying cDNA for mitochondrial targeted mutant aequorin, 24h post infection cells were exposed to different TNFα concentrations (as previously described) and at 24h of TNFα exposure aequorin measurements were performed.

We elicited Ca^{2+} waves by stimulation with Carbachol (CCH) that after binding on its muscarinic receptor expressed on OPCs surface (196) was able to induce IP3 generation and Ca^{2+} release from ER stores.

CCH stimulation induce a rapid increase in $[Ca^{2+}]_m$ in OPC, measured at 53.64 μM (n:6, ± 6.73) that recover to basal levels within one minute (Fig.21A). On opposite TNFα exposure was able to reduce mitochondrial calcium accumulation showing stronger effect at low concentration, $[Ca^{2+}]_m$ values are reported as follow:

TNFα concentration (ng/ml)	**Measured $[Ca^{2+}]_m$ (μM)**	**SD**	**P value**	**% variation VS control**
10	29.35	10.35	0.00035	-45.27
50	37.53	11.39	0.00904	-30.03
100	48.62	13.30	0.07449	-9.46

The most interesting observation is linked to the complete absence of a proportional dose response dependency.

Nonetheless what has been considered more interesting for prosecution of investigation is the observation that when TNFα is already able to impair differentiation without sensibly affecting apoptosis, is also able to induce a strong effect on mitochondrial physiology, while with instauration of clear apoptosis induction the effect on mitochondrial physiology become

progressively attenuated. Based on this observation is the choice to further investigate only the effects elicited by TNFα 10ng/ml.

To further address the events linking altered mitochondrial physiology to calcium uptake we investigated whether TNFα was able to affect global Ca^{2+} signalling homeostasis. We tested this hypothesis by performing the previous experiments but measuring cytosolic Ca^{2+} responses using aequorin located in the cytosol (cytAEQ). As shown in Fig.21B, in control cells carbachol rapidly and transiently increases cytosolic Ca^{2+} concentration ($[Ca^{2+}]c$) reaching maximum values (1.82 ± 0.08 uM, n=25) similar to those detected in OPC pretreated with 10 ng/ml for 24h (1.72 ± 0.09 uM, n=25, p>0.05), indicating that the observed effects were restricted to mitochondrial physiology.

We then investigated the effects of IFNgamma (INFγ) on mitochondrial Ca^{2+} homeostasis. It is in fact well know how this cytokine, as for TNFα, is able to mediate inflammation execution during Multiple Sclerosis and other demyelinating disorders. OPC were treated with IFNγ 20 ng/ml for 24h, then mitochondrial Ca^{2+} variations elicited by agonist stimulation were investigated. As shown in Fig.21C, no significant difference in $[Ca^{2+}]mt$ was observed between IFNγ treated and control cells (peak amplitude 79.7 ± 5.14 uM vs 89.4 ± 5.74 uM, n = 16; p > 0.05). Suggesting that a special binomial exist between TNFα and mitochondrial physiology.

We then investigated whether TNFα affects mitochondrial Ca^{2+} homeostasis in other glia cell types, such as astrocytes.

To address this issue, we analyzed $[Ca^{2+}]_{mt}$ in astrocytes obtained from the same cortex culture used for the growth of oligodendrocytes. As described in the protocol of Chen, a dissectioned rat cortex is seeded in a 75ml flask and cultured for 10 days permitting oligodendrocytes to growth on an astrocytes layer. This layer could be detached by trypsin exposure and seeded onto a coverglass for aequorin measurements. The elevated abundance of astrocytes from this mixed glia culture yields a culture almost pure in astrocytes. Interestingly, contrary to our previous observations in OPC, in astrocytes (Fig.21D) treatment with TNFα caused a significant increase in $[Ca^{2+}]_{mt}$ transients evoked by agonist stimulation (peak amplitude 52.6 ± 3.1 mM treated vs 42 ± 3 mM control, p<0.05, n=26).

In summary we observed that TNFα is able to perturb $[Ca^{2+}]_m$ in OPCs only at concentration non-permissive for efficient apoptosis initiation. Contemporary these variations were not reproducible neither by INFγ nor in other glial cells, suggesting a selective and fine regulated link between mitochondria and TNFα in OPCs.

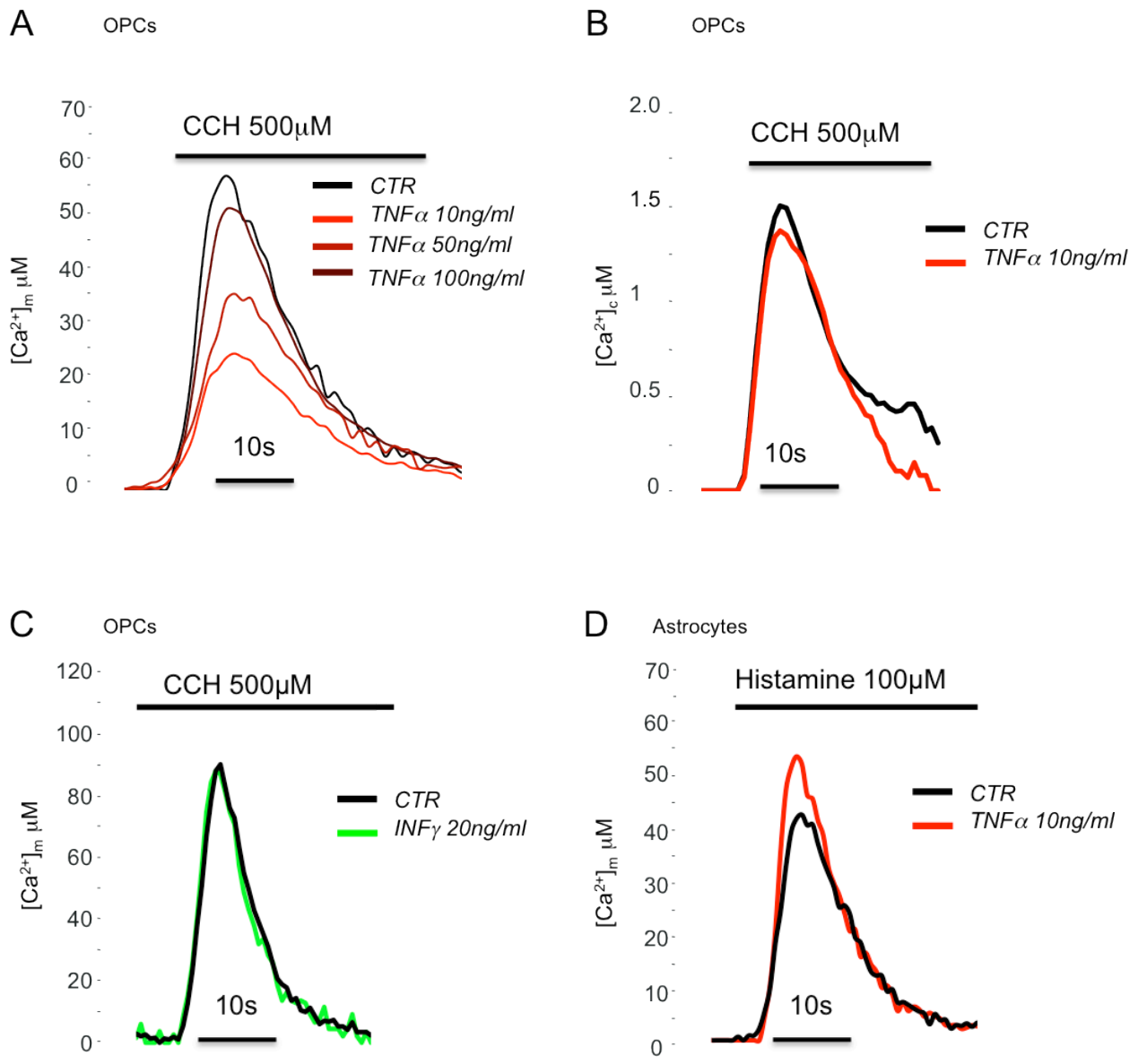

Fig.21. TNFα selectively impair mitochondrial physiology in oligodendrocytes progenitors. Mitochondrial Ca^{2+} measurement in OPCs during agonist stimulation at different TNFα exposure **(A)** or INFγ **(C)**. Cytoplasmic waves in OPCs during low concentration TNFα exposure. Effect of TNFα on Mitochondrial Ca^{2+} response in astrocytes.

TNFα impairs mitochondrial bioenergetics and promote Superoxide production

To clearly define how TNFa was able to promote mitochondrial impairments observed measuring $[Ca^{2+}]_m$ we monitored ΔΨm and network integrity.

Electric potential is generated across inner mitochondrial membrane due to the activity of respiratory chain that consumes oxygen to pump protons to the intermembrane space. This proton gradient will be used by ATP synthase to drive ATP synthesis. ΔΨm could be easily monitored by fluorescence microscopy trough the use of different selective dyes. In our case we performed the measurement through the use of the potential sensitive dye TMRM and laser scanning confocal microscopy. Cells were treated with TNFα 10ng/ml or vehicle for 24h, loaded with TMRM 10nM then acquired before and after FCCP depolarization. The delta value induced by mitochondrial depolarization were considered as index of ΔΨm and compared between TNFα exposed cells and controls. The results evidentiate a strong ΔΨm reduction, of 30.5% (S.E. ±9.76), in cells treated with TNFα, suggesting an important decrease of respiratory chain activity (Fig.22A).

Subsequently we measured alterations of mitochondrial structure through digital deconvolution microscopy. OPCs were infected by adenoviral vector carrying cDNA for mitochondria targeted GFP, then acquired by fluorescence microscopy at high magnification, deconvolved and reconstructed in 3D images. Number and mean volume of mitochondria per cells were obtained and compared between TNFα exposed and control oligodendrocyte. Total network volume per cells is about 40837,4 voxels (S.D. ±12213,18) in control and 43501 voxels (S.D. ±6463,33) in TNFα treated cells (Fig.22Bi), while volume for single mitochondrion was 121,35voxel/object (S.D. ±382,88) in control and 922,69voxel/object (S.E. ±183,17) in TNFα (Fig.22Bii). Nor total network volume neither single particle volume result significantly different between conditions.

These results addressed the previous observed reduced $[Ca^{2+}]_m$ as a consequence of impaired ΔΨm .

It has been reported how impairment of respiratory chain could alter ROS metabolism leading to different ROS generation, nonetheless TNFα itself has been shown to stimulate the same effect.

Electron leak from respiratory chain has been reported mostly to promote generation of superoxide anion, that is mainly reversed to mitochondrial matrix and partly into the inter membrane space (197). Due to effect of Super Oxide Dismutase, $O_2^{-\cdot}$ is rapidly converted to H_2O_2 then detoxified to H2O by catalase. Was in turn considered fundamental to monitor ROS production, three different fluorimetric approaches were used to obtain an overview of general ROS metabolism, based on three different ROS sensitive dyes: dichlorodihydrofluorescein (DCF), Dihydroethidium (DHE) and MitoSOX.

DHE and MitoSOX are well known ethidium based $O_2^{-\cdot}$ Sensitive dyes, with the peculiar difference that could be selectively localized to cytoplasm and mitochondria respectively, while DCF is

generally used as sensor for H_2O_2. To perform this measurments cells where growth for 7 days in multiwells, then exposed to TNFα 10ng/ml for 24h, after treatment cells were stained and measured as further described (see materials and methods). Interestingly within all these three parameters only MitoSOX display significant variations (MitoSOX control 1336.64AFU± 255.06; TNF 10ng/ml: 2397.71AFU± 560.73, n: 3 $p<0.05$; DHE control 7725.72AFU± 543.87; TNF 10ng/ml: 7987.0AFU± 896.15, n: 3; DCF control 55.37AFU/s± 15.41; TNF 10ng/ml: 58.40AFU/s± 9.82, n: 3). Considering that MitoSOX has high selectivity for mitochondrial $O_2^{-\cdot}$ we found this result linear with what previously observed (Fig 22C).

In order to obtain a further comprehension the mechanism by which TNFα was able to produce this effect on ROS production we monitor expression of respiratory complexes by immunoblotting. Immunoreaction was performed with the OxPhos antibody cocktail that allow contemporary to monitor subunits in all the five respiratory complexes, specially the detectable targets are: NDUFB8 for complex I, SDHB for complex II, UQCRC2 for complex III, MTCO1 for complex IV and ATP5A for complex V. As loading marker was choosed mitochondrial HSP60.

The blot display a strong and almost selective reduction in marker for Complex I, even if weak alterations has been displayed for Complex II (Fig.22D).

We consider the alteration of respiratory complex I level as the very basic effect able to induce all the other alterations observed ($[Ca^{2+}]_m$, $\Delta\Psi m$, and $O_2^{-\cdot}$ production). Considering that mitochondria undergoes to continuous processes of degradation and biogenesis, allowing old and damaged organelles recycling, as well as several mitochondrial features are transcriptionally regulated during stress conditions (198, 199) we tested if alterations in Complexes expression and ROS metabolism were maintained during differentiation or if oligodendrocytes undergoes trough adaption.

Experiment were performed as for antigen recognition, briefly cells after 7 days of colture were exposed to TNFα 10ng/ml for 24h then placed in presence of T3 thyroid hormone and let differentiate for 5 days. At the and of this period cells were alternatively used for ROS measurments or immunoblotting. MitoSOX staining resulted yet higher in treated cells compared to control (Fig.21E), but higher variability was measured reducing the significativity of the result (MitoSOX control 644.71AFU± 107.81; TNF 10ng/ml: 2132.15AFU± 2085.7, n: 3).

Interestingly immunoblot result obtained in the same conditions reveal that variations in expression levels of Respiratory Complex I still exist in adult oligodendrocytes as observed in OPCs (Fig.22F).

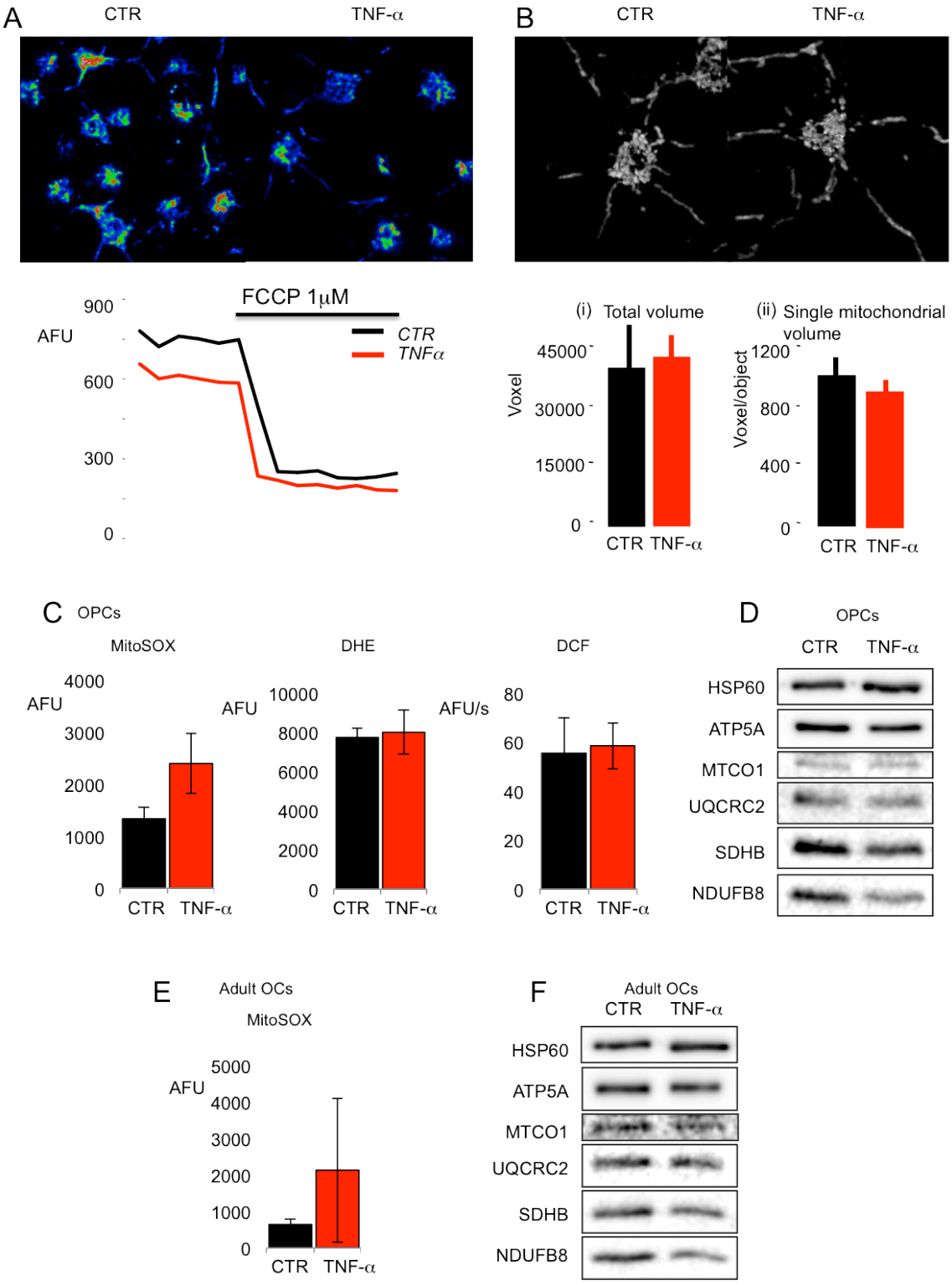

Fig.22. Perturbation of mitochondrial physiology mediated by TNFα in OPCs. (A) Measurements of ΔΨm with potentiometric dye TMRM. **(B)** Representative volume rendering of control OPCs and TNFα treaated cells, (i) voxel quantification of total mitochondrial volume and (ii) single mitochondrial volume. Measurement of Superoxide in OPCs mitochondria (i) cytoplasm (ii) and measurement of H_2O_2 levels (iii). Expression of respiratory complex subunit in OPCs **(D)** and Adult **(F)**, NDUF8B for complex I, SDHB, for complex II, UQCRC2 for complex III, MTCO1 for Complex IV and ATP5A for Complex V. HSP60 has been used as loading marker. Analisis of mitochondrial superoxide in adult cells **(E).**

Mitochondrial dysfunction mediated by TNFα drives impairment of oligodendrocytes differentiation.

The results proposed to now shows a correlation between TNFα induced differentiation blockade and mitochondrial conditioning. Nonetheless a causal link between mitochondrial physiology and OPCs differentiation is still missing on this study.

Initial step was to reproduce in control cells a condition that was able to reproduce the mitochondrial impairment generated by TNFα. To this attempt was choosed carbonylcyanide-p-trifluoromethoxyphenylhydrazone (FCCP), a mitochondrial uncoupler able to induce proton leak trough the inner mitochondrial membrane leading to reduction of ΔΨm . We used FCCP 500nM in substitution to TNFα in OPCs coltures, then we tested its toxicity (by cell count analysis, data not shown) and monitored ΔΨm through the potential sensitive dye TMRM and confocal microscopy. At this concentration FCCP was enough diluited to do not induce toxicity but able to reduce ΔΨm of comparable entity to TNFα (Fig 23A). (control 867AFU ±150.60, FCCP 616 AFU ±83.97, TNF10ng/ml 655.02±68.96 n:3 p Vs control <0.05).

We next test ability of progenitors to differentiate into adult oligodendrocytes during FCCP 500nM exposure. Again the result display high homology with results obtained in presence of TNFα. In fact at 5 days of differentiation we observed FCCP to reduced amount of O4+ and MBP+ oligodendrocytes, while increase the number of NG2 positive cells (control NG2+:57.13% ± 5.9, O4+:26.72% ± 9.36, MBP+:40.65% ± 21.85; TNF 10ng/ml: NG2+:67.9% ± 4.78, O4+:18.46% ± 2.84, MBP+: 23.26% ±20.13. n:4 p<0.05.), suggesting that mitochondrial physiology are fundamental to drive initial phase of differentiation.

Several reports suggested that mitochondrial calcium could be a strategical regulator of oligodendrocytes differentiation, specially different proteins involved in handling of calcium homeostasis and associated to mitochondria or to the mitochondria associated membranes has been reported has regulator of oligodendrocytes differentiation (200, 201), moreover the purinergic signal mediator ATP, that is able to elicit mitochondrial calcium uptake in oligodendrocytes, is also able to promote oligodendrocytes differentiation (194).

We suppose that a possible explanation for FCCP ability in mimicking TNFα effect was due to an impairment of $[Ca^{2+}]_m$ and perform experiments trying to promote mitochondrial calcium accumulation in presence of TNFα with the intention to revert phenotype on differentiation.

We perform two different approach, one based on the MAPK inhibitor SB202190. This is a selective inhibitor of p38 MAPKa/b that display as potent aspecific effect the ability to promote activity of the mitochondrial calcium uniporter (202), with consequent strong promotion to

mitochondrial calcium uptake. In order to avoid inhibition of endogenous MAPK and given that its kd is 38 nM, we start using it at concentration of 1nM.

After 24h of exposure to SB202190 cells display a weak increase in $[Ca^{2+}]_m$, around + 9%, but interestingly it was almost completely able to recover the calcium uptake reduction induced by TNFα (control, peak amplitude 71.48 ± 510.48 uM, TNF 10ng/ml 53.34 ±10.72 uM, SB202190, peak amplitude 74.15 ± 23.64 uM, SB202190 + TNF 10ng/ml 74.33 ±14.59 uM n = 8; p Vs TNF10ng/ml> 0.05).

We next move to verify if SB202190 was contemporary able to recover the differentiation progression. Because the strongest differences were observed with NG2 and MBP markers (probably because are marker of the most extreme stages of differentiation) we perform a differentiation assay with only these two markers.

Interestingly SB202190 alone was strongly able to increase the amount of NG2+ and reduce the amount of MBP+, even more powerful then TNFα itself. Also the contemporary administration of TNFα and SB202190 did not show any synergistic effects, the effect of the cytokine appear to be completely overcomed by SB202190 (Fig.23D). (control NG2+:64.55% ± 4.98, MBP+:38.75% ± 8.12; SB202190 NG2+:77.85% ± 3.88, MBP+:26.075% ± 10.28; TNF 10ng/ml: NG2+:68.5% ± 4.79, MBP+: 15.56% ±8.12; TNF + SB202190: NG2+:71.02% ± 2.32, MBP+: 18.04% ±15.75. n:3).

In summary these results suggest that the mitochondrial impairment induced by TNFα is possibly fundamental for its mechanism, moreover a complex role for $[Ca^{2+}]_m$ appear also to be present unless the present data are to able to unravel it.

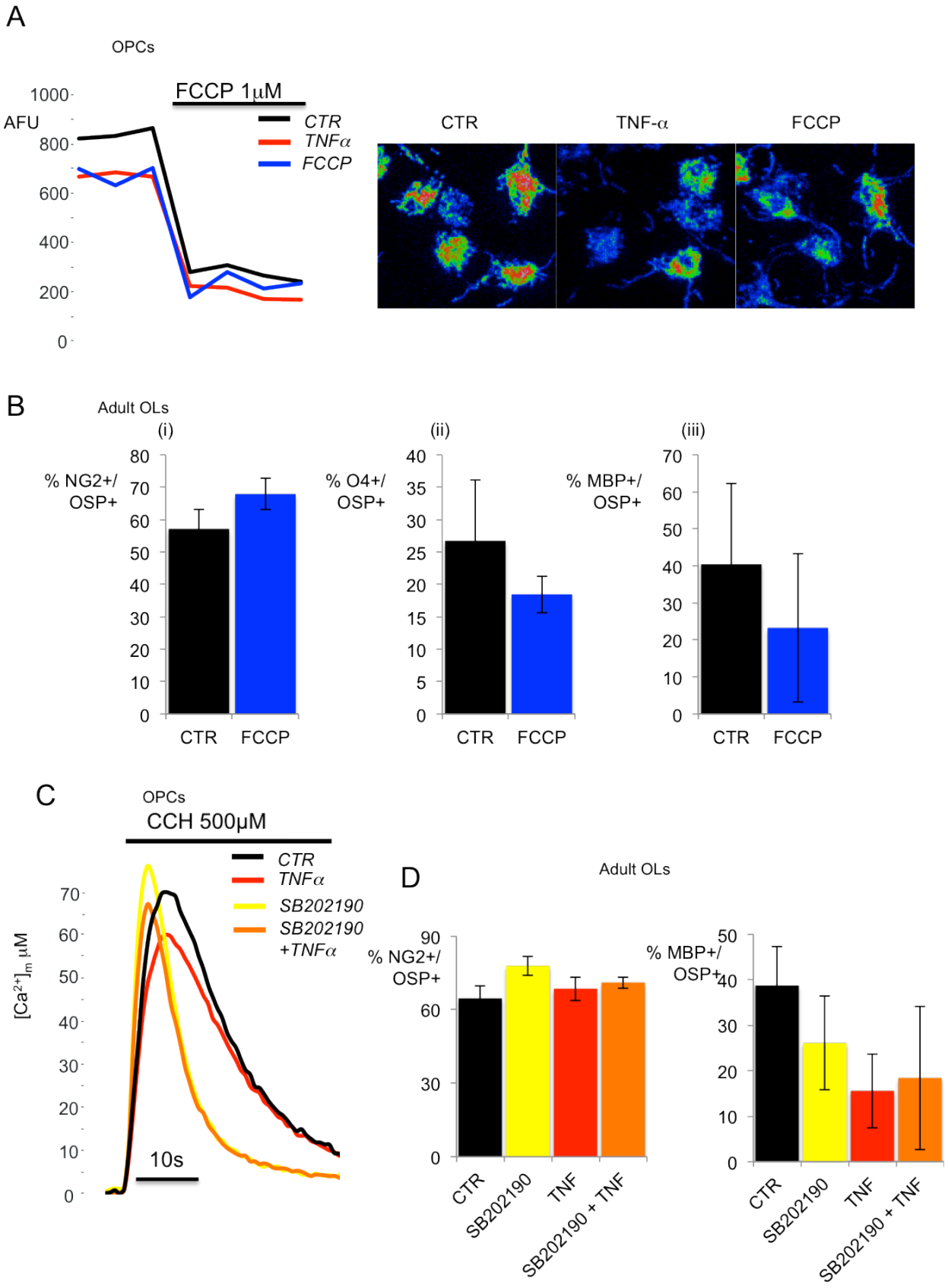

Fig.23. Mitochondria energy state, but not calcium uptake is foundamental for OPCs differentiation. (A) Measurments of ΔΨm with potentiometric dye TMRM in OPCs exposed to FCCP 500nM or TNFα. **(B)** Oligodendrocytes enrichment for precursor (i), immature (ii) and adult cells (iii) during FCCP exposure. **(C)**Mitochondrial Ca^{2+} measurment in OPCs expose to TNFα, to SB202190 or in combination of both drugs. (D) Oligodendrocytes differentiation test in the same conditions.

Discussion

It has been well established that the Tumour Necrosis Factor alpha is one of the most relevant cytokines involved in the pathogenesis of Multiple Sclerosis. In fact, it has been widely reported how the levels of this cytokine correlate with the exacerbation of the pathology as well as how it could affect the physiology of Oligodendrocytes (the principal target of degeneration during aetiology of MS) *in vitro*. This impairment is principaly manifested by the induction of cell death (at high concentrations) as also by blockage of their differentiation process.

In this study we address the hypothesis, that impairment of differentiation due to TNFα exposure is linked to affected mitochondrial physiology.

Initially, we confirmed that exposure to low concentrations of TNFα (10ng/ml) is able to impair OPCs differentiation. We observed an accumulation of NG2+ cells (early progenitors) while reducing the relative amount of O4+ and MBP+ (immature oligodendrocytes and adult oligodendrocytes respectively). This phenomenon was not accompanied by a significant induction of apoptosis. On the other hand, exposure to higher concentrations of TNFα, induced a strong increase in cell death, with no significant accumulation any specific oligodendrocytes population. This led to the hypothesis that TNFα is able to induce an immediate effect in the progenitor population that could generate two distinct outcomes: blockade of differentiation or induction of cell death. These data were in agreement with previously reported results (203).

Basing on this hypothesis we tested whether at this early stage, TNFα was able to affect mitochondrial physiology. As an initial readout we chose to monitor mitochondrial Ca^{2+} uptake as it is often an initial reporter of alterations of mitochondrial physiology.

We took advantage of the Ca^{2+} sensitive luminescent protein Aequorin, (targeted to mitochondria) to measure mitochondrial Ca^{2+} homeostasis in OPCs at an early stage of TNFα exposure. Interestingly we observed a significant reduction in $[Ca^{2+}]_m$ only at a low TNFα concentration. This was in accordance with the "two destinies" hypothesis, suggesting that mitochondrial impairment was a specific event during the differentiation impairment process. The effect on mitochondrial homeostasis was confirmed by measuring cytoplasmic Ca^{2+} waves, with the use of a cytoplasmic aequorin. Cells treated with TNFα [10ng/ml] did not display any differences in cytoplasmic Ca^{2+} compared to controls, indicating that alterations in $[Ca^{2+}]_m$ were not due to a general perturbation of the whole intracellular Ca^{2+} homeostasis.

Next to TNFα, another cytokine, INFγ is well known to participate in the pathogenesis of MS. We have also addressed this cytokine to verify the cytotoxic effects on oligodendrocytes since no relations with the differentiation process have not yet been reported. We used subtoxic

concentrations of IFNγ [20ng/ml] to verify if perturbations of mitochondrial physiology could be considered a general activity of proinflammatory cytokines and we reported no significant variation in $[Ca^{2+}]_m$.

But in order to properly be able to identify a selective relationship between TNFα and OPCs there is a need to test the $[Ca^{2+}]_m$ also in other cell types, known to be sensitive to this cytokine. We found it interesting to monitor $[Ca^{2+}]_m$ in astrocytes cultures, due to the huge amount of reports indicating how astrocytes sense TNFα and also participate to its metabolism (204, 205).

We found that $[Ca^{2+}]_m$ was strongly modified in TNFα-exposed astrocytes. However, instead of being reduced, as measured in OPCs, it was significantly increased. This suggests that a perturbation on mitochondrial physiology was occurring, but in an apposite direction and, presumably, involving different pathways.

It appears clear that a selective cytokine-dependent and cell-dependent relationship exists between mitochondrial physiology and OPCs during TNFα exposure.

To obtain a deeper comprehension about what this mitochondrial perturbation consists of, we measured the $\Delta\Psi_m$ and mitochondrial fragmentation during early TNFα exposure, considering them principal features linked to $[Ca^{2+}]_m$. Mitochondrial Ca^{2+} uptake is driven by the mitochondrial membrane potential, and is it's direct function. Moreover, once in mitochondria, Ca^{2+} flows from the ingress sites (contact sites with endoplasmic reticulum) to the entire network. Due to these features, both, variations of ΔΨm as well as of the mitochondrial network interconnections are reflected in alterations in average Ca^{2+} uptake. Interestingly while mitochondria in treated cells did not significantly change in neither size nor number, they displayed a significantly lower $\Delta\Psi_m$.

Variations of the $\Delta\Psi_m$ are often linked to impaired energy production as also to alterations of ROS metabolism. In particular, a strong elevation of $\Delta\Psi_m$ have been reported to lead to accumulation of different reactive species of oxygen. Moreover TNFα itself is a known ROS inducer in different cellular systems.

To obtain a general overview of ROS metabolism we monitored production of both $O_2^{\cdot -}$ and H_2O_2 with fluorimetric dyes. We were also able to distinguish between mitochondrial and cytoplasmic $O_2^{\cdot -}$ through the use of two different dyes (MitoSOX and DHE respectively), proper recognition of the two different amount of $O_2^{\cdot -}$ was fundamental to properly address the real source. It is well known that mitochondria are the site for the synthesis of a significant amount of $O_2^{\cdot -}$, but it is also generated in large amounts in other organelles (206). What is more, $O_2^{\cdot -}$ has a very short half-life and is usually rapidly dysmutated to H_2O_2 by SODs, making the measurement of $O_2^{\cdot -}$ difficult. Thus, to more precisely assess the overall contribution of ROS, it is crucial to also use other probes, such as DCF (to monitor H_2O_2). Interestingly, we found that only MitoSOX gave a significantly

higher staining in treated cells compared to control, suggesting that mitochondria were stimulated in $O_2^{\cdot-}$ production by TNFα.

To date, the two most important mitochondrial sources for $O_2^{\cdot-}$ are both within the respiratory chain. They are respiratory complexes I and III. Impairment of their activity leads to rapid and robust $O_2^{\cdot-}$ production, with a peculiar difference. Complex I leave the $O_2^{\cdot-}$ produced within the mitochondrial matrix only, whereas complex III is able to generate it both in the matrix and the IMS (207). Since DHE is not able to distinguish between the cytoplasm and the IMS (due to high permeability of the OMM) and due to the different behaviour between MitoSOX and DHE we suggest an impairment of Complex I. Similar suggestions do arrive from the literature. In leukemic cells, TNFα was able to induce death by selectively promoting ROS by complex I (208), while in rat left ventricle TNFα led to a $O_2^{\cdot-}$-dependent reduction in Complex I expression (209).

Through immunoblot we verified that OPCs treated with TNFα for 24h display a strong reduction in respiratory complex I subunit NDUFB8 and even more interestingly, the altered levels were maintained in adult cells during differentiation.

Impairment of the transcript level of this complex could lead to the reduction of $\Delta\Psi_m$ measured in OPCs and gained our particular interest in light of the observed differentiation impairment. It was in fact reported that during differentiation, OPCs undergo to a deep rearrangement of expression of genes involved in metabolism, and that respiratory complex inhibitors like rotenone (for complex I) or azide (for complex IV) (173, 210) strongly impair oligodendrocytes differentiation.

To further link mitochondrial impairment with oligodendrocytes differentiation we observed that exposure to a low concentration of a generic mitochondrial uncoupler, FCCP, was able to reproduce the reduction in $\Delta\Psi_m$ observed for TNFα, as also to reduce the amount of MBP+ and O4+ cells with concomitant accumulation of NG2+ positive cells. This gave strength to the hypothesis that the mitochondrial impairment exerted by TNFα is able to generate a block at an early stage of OPCs differentiation.

The last point that we investigated was the correlation between OPCs differentiation and Ca^{2+}signalling. It has been reported that the Sig-1R, a promoter of the Ca^{2+} transmission between mitochondria and ER, once overexpressed in glial primary cultures is able to induce spontaneous oligodendrocytes differentiation. Moreover, the calcium binding protein S100B is known to be able to interact with the mitochondrial protein ATAD3A and promote oligodendrocytes differentiation. Interestingly, this protein is also found to be located at the contact sites between mitochondria and ER.

It is also well known how the purinergic mediator, ATP, is also able to promote oligodendrocytes differentiation, as also has been reported as and inducer of IP3R receptor opening, leading to

mitochondrial Ca^{2+} accumulation. Interestingly within the central nervous system TNFα is considered as an inhibitor of purinergic signalling (211).

Thus, we found it of great interest to investigate this aspect, given that FCCP while reducing $\Delta\Psi_m$ is also able to block mitochondrial Ca^{2+} uptake it could be possible that in our experimental conditions FCCP was able to mimick TNFα not by exerting a metabolic impairment, but by reducing $[Ca^{2+}]_m$.

To artificially increase $[Ca^{2+}]_m$ we took advantage of the p38 MAPK inhibitor SB202190. This compound, differently from other MAPK inhibitors, is able to promote a rapid potentiation of mitochondrial Ca^{2+} uptake. Whether this effect is dependent on MAPK or not is still under debate. However, it is generally accepted that it could indirectly promote activity of the MCU.

In our cell cultures SB202190 was able to recover $[Ca^{2+}]_m$ in OPCs during TNFα exposure, but surprisingly completely reproduced the effect of TNFα causing an accumulation of NG2+ cells and reducing the amount of MBP+. Moreover, during a co-treatment we did not detect any synergistic effect, but the effect of TNFα appeared to be completely overcome. This suggests that $[Ca^{2+}]_m$ has a special role in the differentiation process, but this role and its cooperation with the path of TNFα still remains unresolved.

Summarizing the present study proposed that the TNFα is able to trigger two distinct cell fates in OPCs. One of blockage of differentiation, the other of induction of cell death. While impairing differentiation, TNFα induces a repression of mitochondrial physiology, through reducing the amount of Respiratory Complex I.

Materials and Methods

Reagents and solutions

ATP, digitonin, H_2O_2, menadione (MEN), Adriamycin, α-Amanitin, Pifithrin were purchased from Sigma, coelenterazine from Molecular Probes, recombinant rat TNFα from Sigma-Aldrich.

KRB contained: 125 mM NaCl, 5 mM KCl, 1 mM $MgSO_4$, 1 mM Na_2HPO_4, 5.5 mM glucose, 20 mM $NaHCO_3$, 2 mM l-glutamine and 20 mM HEPES pH 7.4, and was supplemented with 1 mM $CaCl_2$.

Cells culture, transfection and detection of cell death

Primary $p53^{+/+}$ and $p53^{-/-}$ MEFs were prepared from embryos at day 13.5 of development (E13.5). Early passage (P2–P5) MEFs, grown in DMEM supplemented with 10% FCS, were used in all experiments.

MEFs were transfected with different constructs using the MicroPorator (Digital Bio).

HCT-116 were grown in McCOY supplemented with 10% FBS, 1% P/S and 1% L-Glutammine and

transfected with a standard calcium-phosphate procedure

HeLa and H1299 cells were grown in DMEM supplemented with 10% FCS and transfected with a standard calcium-phosphate procedure.

MDA-MD 468 cells were grown in DMEM supplemented with 10% FCS and infected with adenovirus expressing a mitochondrial targeted aequorin chimera.

Immoratlized MEFs Bax/Bak wt and DKO were grown in DMEM supplemented with 10% FCS and transfected with JetPEI Polyplus transfection kit according to the manufacturer protocol.

MEF, HCT-116 and MDA-MD 468 cells were treated with Adriamycin 1 μM for 6 h, α-amanitin 10 μg/ml for 6 h, pifithrin α 15 μM for 30 min.

For cell death induction, cells were treated as indicated in the text with 1 mM H_2O_2, 15 μM MEN in DMEM supplemented with 10% FCS.

Apoptosis was determined by FACS analysis of cells stained with Annexin-V FITC/Propidium Iodide (BioVision) or by TUNEL assay Click it, according to manufacturer protocol.

Oligodendrocytes Progenitors Cultures generation

Primary oligodendrocytes were prepared following the protocol of Chen et al., 2007. This method contemplates the generation of a population of oligodendrocytes precursor cell on a layer of astrocytes, originated by mixed glia cultures of P1-P2 pup rats. For the separating of the two kind of primary cell cultures, after 10 days of growth in DMEM 20% FBS, the whole preparation is exposed to sheer forces generated by its shaking on an orbital shaker at 190rpm. Collected oligodendrocytes progenitors are separated by residual microglia and astrocytes by incubation of 1h on uncoated petri dish, and then filtered in cell strainers with 40μM holes. Cell where then seeded on coverslip of different dimension, according with the planned experiment and kept in culture for 7 days in chemically defined medium composed by DMEM, 4 mM L-glutamine, 1 mM sodium pyruvate, 0.1% BSA, 50 mg/ml Apo-transferrin, 5 mg/ml insulin, 30 nM sodium selenite, 10 nM D-biotin and 10 nM hydrocortisone, 10 ng/ml PDGF-AA and 10 ng/ml bFGF.

Generation of ER-p53 chimera expression vectors

p53 was addressed to the external surface of ER by fusing sequence from the yeast UBC6 (162) protein to the N-terminal end of the cDNA coding for the human p53-NLS. The chimera obtained, named ER-p53, was cloned in the pcDNA3 vector.

Aequorin measurements

Cells grown on 13 mm round glass coverslips at 50% confluence were transfected with the

appropriate chimera cyt, mt and erAEQ (as previously described (161)) alone or together with expression constructs ER-p53, p53 wt or p53-NLS.

All aequorin measurements were carried out in KRB. Agonists and other drugs were added to the same medium, as specified in the figure legends. The experiments were terminated by lysing the cells with 100 μM digitonin in a hypotonic Ca^{2+}-rich solution (10 mM $CaCl_2$ in H_2O), thus discharging the remaining aequorin pool. The light signal was collected and calibrated into $[Ca^{2+}]$ values, as previously described (161).

Sub-cellular Fractionation

Cells (10^9) were harvested, washed in phosphate- buffered saline medium, pelleted by centrifugation at 500 x g for 5 min, resuspended in homogenization buffer (0.25 M sucrose and 10 mM Hepes pH 7.4) and gently disrupted by dounce homogenization. The homogenate was centrifuged twice at 600 x g for 5 min to remove cellular debris and nuclei, and the supernatant was centrifuged at 10.300 x g for 10 min to pellet crude mitochondria. The resultant supernatant was centrifuged at 100.000 x g for 1 h in a Beckman 70 Ti rotor at 4^0C to pellet microsomes, which were resuspended in homogenization buffer. The mitochondrial pellet, resuspended in isolation medium (250 mM mannitol, 5 mM Hepes (pH7.4), and 0.5 mM EGTA) was, layered on top of 8 ml of Percoll medium (225 mM mannitol, 25 mM Hepes (pH 7.4), 1 mM EGTA, and 30% Percoll (v/v) in a 10-ml polycarbonate ultracentrifuge tube and centrifuged for 30 min at 95.000 x g. A dense band containing purified mitochondria, recovered approximately ¾ down the tube, was removed, diluted with isolation medium, washed twice by centrifugation at 6.300 x g for 10 min to remove the Percoll, and finally resuspended in isolation medium. MAM, removed from the Percoll gradient as a diffuse white band located above the mitochondria, were diluted in isolation medium and centrifuged at 6.300 x g for 10 min. The supernatant containing MAM was centrifuged at 100.000 x g for 1 h in a Beckman 70 Ti rotor, and the resulting pellet was resuspended in the homogenization buffer (41, 212).

The quality of the preparation has been checked by western blot analysis using different markers for the fractions obtained.

- IP3R, as ER marker, should be present at about 20% in MAM fraction of than present in the ER.
- Voltage dependent anion channel (VDAC), as mitochondrial marker, should be present in Mc but must be enriched in Mp fraction. It should be also present in the MAM fraction.
- Tubulin, as cytosolic marker, should be absent in Mp, MAM and ER.

- Laminin B, as nuclear marker, should be absent in Mp and MAM.

Western Blotting

30 μg of protein were separated by SDS-PAGE, transferred onto nitrocellulose membranes and probed using the following antibodies: anti-p53 (1:1000, Cell Signalling) for mouse cells, anti cleaved PARP (1:500 Cell Signalling) anti-IP3R-3 (1:500, BD-Pharmingen), anti-tubulin (1:5000, Santa Cruz), anti-Laminin (1:1000, abcam), anti-panVDAC (1:5000, abcam), anti-actin (1:3000, Santa Cruz), anti SERCA 2b (1:500, abcam), anti-OxPhos (1:1000, Mitoscience), anti-HSP60 (1:1000, Santa Cruz).

Isotype matched, horseradish peroxidase conjugated secondary antibodies were used followed by detection by chemiluminescence (Perkin Elmer).

Immunolocalization

Cells (MEFs, H1299, HCT-116, OPCs, Adult OLs) were fixed with 3.7% formaldehyde in PBS for 20 min, washed three times with PBS and then incubated for 10 min in PBS supplemented with 50 mM NH_4Cl. Permeabilization of cell membranes was obtained with a 5 min incubation with 0.1% Triton X-100 in PBS, followed by a 1 h wash with 2% Non Fat Dry Milk in PBS. The cells were then incubated O/N at 37 °C in a wet chamber with the following antibodies: mouse anti-p53 DO-1 (Santa Cruz), goat anti-ACSL4 (FACL) N-18 (Santa Cruz) dilute 1:50 with 2% Milk in PBS or mouse anti-NG2 (Santa Cruz), mouse anti-O4 (Sigma-Aldrich), mouse anti-MBP (Sigma-Aldrich), mouse anti-OSP (Abcam) dilute 1:100. Staining was then carried out with Alexa 488 goat anti-mouse for p53, NG2, O4 and MBP, with Alexa 633 rabbit anti-goat for FACL, Alexa 594 goat anti-rabbit for OSP secondary antibodies. After each antibody incubation the cells were washed four times with PBS. Fluorescence was then analyzed with a widefield or confocal microscope.

MBP Pull-down Assay

p53 cDNA was cloned in pMAL protein fusion system (Biolabs). MBP-fused protein was expressed in *E.Coli* and was extracted in Column buffer (20 mM Tris-HCl pH7.5, 200 mM NaCl, 1 mM EDTA pH8, and 10 mM β-mercaptoethanol) and purified with amylose resin (NEB) following the manufacturer's instructions. Cells were harvested in the in lysis buffer (20 mM Tris–HCl, pH 8.0, 150 mM NaCl, 1 mM EDTA, 5% glycerol, 0.5% NP-40, 5 mM NaF, 1 mM Na_3VO_4 and a protease inhibitor cocktail). The cell lysate was incubated with 2.5 μg of MBP-p53 or MBP for 2 h then washed 3 times in lysis buffer.

Co-immunoprecipitation

Extracts from MEFs wt were prepared using lysis buffer containing: 50 mM NaCl, 50 mM Tris-HCl pH 7.4, 0.1% NP-40 supplemented with 1 mM PMSF and proteases/phosphatases inhibitors. Protein extracts were pre-cleared with protein G/A beads (Pierce) than precipitated with rabbit anti-p53 FL-393 (Santa Cruz) overnight at 4°C. Protein G beads were added and rocked 5 hours at 4°C. Afterwards, beads were washed with 50 mM NaCl, 50 mM Tris-HCl pH 7.4, 0.1% NP-40 4°C. Samples were proceed by SDS-PAGE and analyzed by standard western blotting technique.
For the HAp53-SERCA 2b co-immunoprecipitation cells were lysed in Co-IP Buffer (50 mM Tris-HCl pH 8, 150 mM NaCl, 1% NP-40, 10% glycerol) with protease inhibitor cocktail (Sigma), 1 mM PMSF, 5 mM NaF, 1 mM Na3VO4, and 2mg of cleared lysates were then incubated for 2h with monoclonal anti-HA 12CA5 antibody covalently bound to protein G–Sepharose (Amersham) using 5mg/ml dimethylpimelimidate (Pierce).

Mitochondrial morphology analysis

MEF $p53^{+/+}$or $p53^{-/-}$ and OPCs were seeded at 50.000 and 20000 cells for 25 mm coverslip respectively, let growth for 24 h and then infected with a GFP targeted to the mitochondria insert in an adenoviral vector (Ad-mtGFP). 36h expression cells were treated as described then imaged with a Nikon Swept Field confocal equipped with CFI Plan Apo VC60XH objective (N.A. 1.4) and an Andor DU885 EM-CCD camera. Coverslip where placed in an incubated chamber with controlled temperature, CO_2 and humidity then z-stacks where acquired by 21 planes with 0.6 μm distance, to allow acquisition of the whole cell. Morphometric parameters where calculated on the best focused plane with NIS Elements (Nikon), while isosurface rendering and volume measurements were obtained with the 4D tools of MetaMorph (Universal Imaging).

Automated nuclei count analysis

MEF $p53^{+/+}$or $p53^{-/-}$ were seeded at 50.000 cells for 25 mm coverslip, let growth for 48 h and then treated with ADRIA, H_2O_2 or both. Coverslips where stained with Hoechst 10 μM then placed in an incubated chamber with controlled temperature and mounted on an Axiovert 200M microscope equipped with a motorized stage. Nuclei were acquired with a 10x Fluar objective (Zeiss) and a CoolSnap HQ CCD camera. 20 random fields were acquired with the random stage scan tools in MetaMorph and analyzed with the Nuclei count application.

High content throughput assay

OPCs culture where seeded on 96 well plates with glass bottom then after 7 days of cultures induce to differentiate substituting PDGF-AA and bFGF with 15 nM triiodothyronine for 5 days. Images where then acquired on Olympus Scan^R station, using a laser based hardware and an image based automatic autophocus. 80 field where acquired for each well using a 20x magnification, N.A. 0.75, while different fluorophores where exited by an MT20 illumination system and excitation filters used where 377/50, 498/20, 595/30 for DAPI, FITCH and TRITCH respectively allowing the shorter exposure time possible (5ms for Dapi, 20-50 for FITCH, 50-150 for TRITCH). Images where collected using an Orca-05G2 at full-frame, without binning. Cells where then scored and counted using the Scan^R analysis software.

SERCA activity

Analysis of SERCA activity was obtained on traces performed with an aequorin targeted to endoplasmic reticulum (erAEQ). Briefly time records from each single experiment were imported on Origin 6.0 and derivative was calculated. The first half of the filling phase was isolated and 5 points around the maximum value were collected for average calculation. This value was used as indicator of the max speed of Ca^{2+} import into Endoplasmic Reticulum and proportional to SERCA activity or expression.

Mitochondrial membrane potential measurements

Mitochondrial membrane potential ($\Delta\Psi_m$) was measured using 10 nM tetramethyl rhodamine methyl ester (TMRM) on a confocal microscope (model LSM 510; Carl Zeiss MicroImaging, Inc.). FCCP (carbonyl cyanide p-trifluoromethoxyphenylhydrazone), to collapses mitochondrial $\Delta\Psi$. The signal was collected as total emission >570 nm.

ROS measurements

Total release of ROS from mitochondria was estimated fluorimetrically by oxidation of Dihydroethidium, MitoSOX or DCF. Fluorescence was measured in multiwell plate reader (Infinite M200, Tecan, Austria) using 510 ± 10 nm excitation and 595 ± 35 nm emission wavelengths for MitoSOX and DHE while 513 ± 10 nm excitation and 530 ± 25 nm emission.

Statistical analysis of data

Statistical data are presented as mean ± S.D., significance was calculated by Student's t test, and correlation analysis was done with the SigmaPlot 5.0 software (SPSS Inc.).

References

1. Dyall SD, Brown MT, Johnson PJ. Ancient invasions: from endosymbionts to organelles. Science. 2004;304(5668):253-7. Epub 2004/04/10.
2. Frey TG, Mannella CA. The internal structure of mitochondria. Trends Biochem Sci. 2000;25(7):319-24. Epub 2000/06/29.
3. Vogel F, Bornhovd C, Neupert W, Reichert AS. Dynamic subcompartmentalization of the mitochondrial inner membrane. J Cell Biol. 2006;175(2):237-47. Epub 2006/10/18.
4. Rizzuto R, Pinton P, Carrington W, Fay FS, Fogarty KE, Lifshitz LM, et al. Close contacts with the endoplasmic reticulum as determinants of mitochondrial Ca2+ responses. Science. 1998;280(5370):1763-6. Epub 1998/06/20.
5. Benard G, Rossignol R. Ultrastructure of the mitochondrion and its bearing on function and bioenergetics. Antioxid Redox Signal. 2008;10(8):1313-42. Epub 2008/04/26.
6. Cereghetti GM, Scorrano L. The many shapes of mitochondrial death. Oncogene. 2006;25(34):4717-24. Epub 2006/08/08.
7. Santel A, Fuller MT. Control of mitochondrial morphology by a human mitofusin. J Cell Sci. 2001;114(Pt 5):867-74. Epub 2001/02/22.
8. James DI, Parone PA, Mattenberger Y, Martinou JC. hFis1, a novel component of the mammalian mitochondrial fission machinery. J Biol Chem. 2003;278(38):36373-9. Epub 2003/06/05.
9. Smirnova E, Griparic L, Shurland DL, van der Bliek AM. Dynamin-related protein Drp1 is required for mitochondrial division in mammalian cells. Mol Biol Cell. 2001;12(8):2245-56.
10. Yoon Y, Krueger EW, Oswald BJ, McNiven MA. The mitochondrial protein hFis1 regulates mitochondrial fission in mammalian cells through an interaction with the dynamin-like protein DLP1. Mol Cell Biol. 2003;23(15):5409-20. Epub 2003/07/16.
11. Yu T, Robotham JL, Yoon Y. Increased production of reactive oxygen species in hyperglycemic conditions requires dynamic change of mitochondrial morphology. Proc Natl Acad Sci U S A. 2006;103(8):2653-8. Epub 2006/02/16.
12. Csordas G, Hajnoczky G. SR/ER-mitochondrial local communication: calcium and ROS. Biochim Biophys Acta. 2009;1787(11):1352-62. Epub 2009/06/17.
13. Krebs HA. The citric acid cycle and the Szent-Gyorgyi cycle in pigeon breast muscle. Biochem J. 1940;34(5):775-9. Epub 1940/05/01.
14. Kennedy EP, Lehninger AL. Oxidation of fatty acids and tricarboxylic acid cycle intermediates by isolated rat liver mitochondria. J Biol Chem. 1949;179(2):957-72. Epub 1949/06/01.
15. Lambeth DO, Tews KN, Adkins S, Frohlich D, Milavetz BI. Expression of two succinyl-CoA synthetases with different nucleotide specificities in mammalian tissues. J Biol Chem. 2004;279(35):36621-4. Epub 2004/07/06.
16. Amemori S, Iwakiri R, Endo H, Ootani A, Ogata S, Noda T, et al. Oral dimethyl sulfoxide for systemic amyloid A amyloidosis complication in chronic inflammatory disease: a retrospective patient chart review. Journal of gastroenterology. 2006;41(5):444-9. Epub 2006/06/27.
17. Quinn PJ, Dawson RM. Interactions of cytochrome c and [14C]. Biochem J. 1969;115(1):65-75. Epub 1969/10/01.

18. Lenaz G, Genova ML. Structure and organization of mitochondrial respiratory complexes: a new understanding of an old subject. Antioxid Redox Signal. 2010;12(8):961-1008. Epub 2009/09/11.
19. Boyer PD. Catalytic site forms and controls in ATP synthase catalysis. Biochim Biophys Acta. 2000;1458(2-3):252-62. Epub 2000/06/06.
20. Ferguson SJ. ATP synthase: from sequence to ring size to the P/O ratio. Proc Natl Acad Sci U S A. 2010;107(39):16755-6. Epub 2010/09/23.
21. Kroemer G, Galluzzi L, Brenner C. Mitochondrial membrane permeabilization in cell death. Physiological reviews. 2007;87(1):99-163. Epub 2007/01/24.
22. Garrido C, Galluzzi L, Brunet M, Puig PE, Didelot C, Kroemer G. Mechanisms of cytochrome c release from mitochondria. Cell death and differentiation. 2006;13(9):1423-33. Epub 2006/05/06.
23. Hill MM, Adrain C, Martin SJ. Portrait of a killer: the mitochondrial apoptosome emerges from the shadows. Molecular interventions. 2003;3(1):19-26. Epub 2004/03/03.
24. Ravagnan L, Roumier T, Kroemer G. Mitochondria, the killer organelles and their weapons. Journal of cellular physiology. 2002;192(2):131-7. Epub 2002/07/13.
25. Pinton P, Ferrari D, Rapizzi E, Di Virgilio F, Pozzan T, Rizzuto R. The Ca2+ concentration of the endoplasmic reticulum is a key determinant of ceramide-induced apoptosis: significance for the molecular mechanism of Bcl-2 action. The EMBO journal. 2001;20(11):2690-701. Epub 2001/06/02.
26. Szalai G, Krishnamurthy R, Hajnoczky G. Apoptosis driven by IP(3)-linked mitochondrial calcium signals. The EMBO journal. 1999;18(22):6349-61. Epub 1999/11/24.
27. Danial NN, Korsmeyer SJ. Cell death: critical control points. Cell. 2004;116(2):205-19. Epub 2004/01/28.
28. Youle RJ, Karbowski M. Mitochondrial fission in apoptosis. Nature reviews Molecular cell biology. 2005;6(8):657-63. Epub 2005/07/19.
29. Szabadkai G, Simoni AM, Chami M, Wieckowski MR, Youle RJ, Rizzuto R. Drp-1-dependent division of the mitochondrial network blocks intraorganellar Ca2+ waves and protects against Ca2+-mediated apoptosis. Molecular cell. 2004;16(1):59-68. Epub 2004/10/08.
30. Ricchelli F, Sileikyte J, Bernardi P. Shedding light on the mitochondrial permeability transition. Biochimica et biophysica acta. 2011;1807(5):482-90. Epub 2011/03/08.
31. Baines CP, Kaiser RA, Purcell NH, Blair NS, Osinska H, Hambleton MA, et al. Loss of cyclophilin D reveals a critical role for mitochondrial permeability transition in cell death. Nature. 2005;434(7033):658-62. Epub 2005/04/01.
32. Basso E, Fante L, Fowlkes J, Petronilli V, Forte MA, Bernardi P. Properties of the permeability transition pore in mitochondria devoid of Cyclophilin D. The Journal of biological chemistry. 2005;280(19):18558-61. Epub 2005/03/29.
33. Nakagawa Y, Suzuki T, Kamimura H, Nagai F. Role of mitochondrial membrane permeability transition in N-nitrosofenfluramine-induced cell injury in rat hepatocytes. European journal of pharmacology. 2006;529(1-3):33-9. Epub 2005/12/06.
34. Rapizzi E, Pinton P, Szabadkai G, Wieckowski MR, Vandecasteele G, Baird G, et al. Recombinant expression of the voltage-dependent anion channel enhances the transfer of Ca2+ microdomains to mitochondria. The Journal of cell biology. 2002;159(4):613-24. Epub 2002/11/20.
35. Wieckowski MR, Szabadkai G, Wasilewski M, Pinton P, Duszynski J, Rizzuto R. Overexpression of adenine nucleotide translocase reduces Ca2+ signal transmission between the ER and mitochondria. Biochemical and biophysical research communications. 2006;348(2):393-9. Epub 2006/08/05.
36. Turrens JF. Mitochondrial formation of reactive oxygen species. The Journal of physiology. 2003;552(Pt 2):335-44. Epub 2003/10/17.

37. Pinton P, Rimessi A, Marchi S, Orsini F, Migliaccio E, Giorgio M, et al. Protein kinase C beta and prolyl isomerase 1 regulate mitochondrial effects of the life-span determinant p66Shc. Science. 2007;315(5812):659-63. Epub 2007/02/03.
38. Giorgio M, Migliaccio E, Orsini F, Paolucci D, Moroni M, Contursi C, et al. Electron transfer between cytochrome c and p66Shc generates reactive oxygen species that trigger mitochondrial apoptosis. Cell. 2005;122(2):221-33. Epub 2005/07/30.
39. Pinton P, Rizzuto R. p66Shc, oxidative stress and aging: importing a lifespan determinant into mitochondria. Cell Cycle. 2008;7(3):304-8. Epub 2008/02/01.
40. Giorgi C, De Stefani D, Bononi A, Rizzuto R, Pinton P. Structural and functional link between the mitochondrial network and the endoplasmic reticulum. Int J Biochem Cell Biol. 2009;41(10):1817-27. Epub 2009/04/25.
41. Vance JE. Phospholipid synthesis in a membrane fraction associated with mitochondria. Journal of Biological Chemistry. 1990;265(13):7248-56.
42. Mannella CA, Buttle K, Rath BK, Marko M. Electron microscopic tomography of rat-liver mitochondria and their interaction with the endoplasmic reticulum. Biofactors. 1998;8(3-4):225-8.
43. Kornmann B, Currie E, Collins SR, Schuldiner M, Nunnari J, Weissman JS, et al. An ER-mitochondria tethering complex revealed by a synthetic biology screen. Science. 2009;325(5939):477-81. Epub 2009/06/27.
44. Csordas G, Renken C, Varnai P, Walter L, Weaver D, Buttle KF, et al. Structural and functional features and significance of the physical linkage between ER and mitochondria. J Cell Biol. 2006;174(7):915-21.
45. Pizzo P, Pozzan T. Mitochondria-endoplasmic reticulum choreography: structure and signaling dynamics. Trends Cell Biol. 2007;17(10):511-7.
46. Piccini M, Vitelli F, Bruttini M, Pober BR, Jonsson JJ, Villanova M, et al. FACL4, a new gene encoding long-chain acyl-CoA synthetase 4, is deleted in a family with Alport syndrome, elliptocytosis, and mental retardation. Genomics. 1998;47(3):350-8.
47. Stone SJ, Vance JE. Phosphatidylserine synthase-1 and -2 are localized to mitochondria-associated membranes. J Biol Chem. 2000;275(44):34534-40.
48. Berridge MJ. The endoplasmic reticulum: a multifunctional signaling organelle. Cell Calcium. 2002;32(5-6):235-49.
49. Lebiedzinska M, Szabadkai G, Jones AW, Duszynski J, Wieckowski MR. Interactions between the endoplasmic reticulum, mitochondria, plasma membrane and other subcellular organelles. Int J Biochem Cell Biol. 2009;41(10):1805-16. Epub 2009/08/26.
50. Chen H, Detmer SA, Ewald AJ, Griffin EE, Fraser SE, Chan DC. Mitofusins Mfn1 and Mfn2 coordinately regulate mitochondrial fusion and are essential for embryonic development. J Cell Biol. 2003;160(2):189-200.
51. Hayashi T, Su TP. Sigma-1 receptor chaperones at the ER-mitochondrion interface regulate Ca(2+) signaling and cell survival. Cell. 2007;131(3):596-610.
52. Szabadkai G, Simoni AM, Chami M, Wieckowski MR, Youle RJ, Rizzuto R. Drp-1-dependent division of the mitochondrial network blocks intraorganellar Ca2+ waves and protects against Ca2+-mediated apoptosis. MolCell. 2004;16(1):59-68.
53. Kottgen M, Benzing T, Simmen T, Tauber R, Buchholz B, Feliciangeli S, et al. Trafficking of TRPP2 by PACS proteins represents a novel mechanism of ion channel regulation. Embo J. 2005;24(4):705-16.
54. Hajnoczky G, Csordas G, Krishnamurthy R, Szalai G. Mitochondrial calcium signaling driven by the IP3 receptor. JBioenergBiomembr. 2000;32(1):15-25.
55. Szabadkai G, Bianchi K, Varnai P, De Stefani D, Wieckowski MR, Cavagna D, et al. Chaperone-mediated coupling of endoplasmic reticulum and mitochondrial Ca2+ channels. The Journal of Cell Biology. 2006;175(6):901-11.
56. Berridge MJ, Lipp P, Bootman MD. The versatility and universality of calcium signalling. Nature reviews Molecular cell biology. 2000;1(1):11-21. Epub 2001/06/20.

57. Clapham DE. Intracellular calcium. Replenishing the stores. Nature. 1995;375(6533):634-5. Epub 1995/06/22.
58. Morgan AJ, Thomas AP. Single cell and subcellular measurement of intracellular Ca2+ concentration ([Ca2+]i). Methods Mol Biol. 1999;114:93-123. Epub 1999/03/19.
59. Jaffe LF, Creton R. On the conservation of calcium wave speeds. Cell calcium. 1998;24(1):1-8. Epub 1998/10/30.
60. Petersen OH, Burdakov D, Tepikin AV. Regulation of store-operated calcium entry: lessons from a polarized cell. European journal of cell biology. 1999;78(4):221-3. Epub 1999/06/01.
61. Inouye S, Noguchi M, Sakaki Y, Takagi Y, Miyata T, Iwanaga S, et al. Cloning and sequence analysis of cDNA for the luminescent protein aequorin. Proceedings of the National Academy of Sciences of the United States of America. 1985;82(10):3154-8. Epub 1985/05/01.
62. Shimomura O. Isolation and properties of various molecular forms of aequorin. The Biochemical journal. 1986;234(2):271-7. Epub 1986/03/01.
63. Pozzan T, Rizzuto R, Volpe P, Meldolesi J. Molecular and cellular physiology of intracellular calcium stores. Physiological reviews. 1994;74(3):595-636. Epub 1994/07/01.
64. Shimomura O, Kishi Y, Inouye S. The relative rate of aequorin regeneration from apoaequorin and coelenterazine analogues. The Biochemical journal. 1993;296 (Pt 3):549-51. Epub 1993/12/15.
65. Nomura M, Inouye S, Ohmiya Y, Tsuji FI. A C-terminal proline is required for bioluminescence of the Ca(2+)-binding photoprotein, aequorin. FEBS letters. 1991;295(1-3):63-6. Epub 1991/12/16.
66. Watkins NJ, Campbell AK. Requirement of the C-terminal proline residue for stability of the Ca(2+)-activated photoprotein aequorin. The Biochemical journal. 1993;293 (Pt 1):181-5. Epub 1993/07/01.
67. Hendrick JP, Hodges PE, Rosenberg LE. Survey of amino-terminal proteolytic cleavage sites in mitochondrial precursor proteins: leader peptides cleaved by two matrix proteases share a three-amino acid motif. Proceedings of the National Academy of Sciences of the United States of America. 1989;86(11):4056-60. Epub 1989/06/01.
68. Rizzuto R, Simpson AW, Brini M, Pozzan T. Rapid changes of mitochondrial Ca2+ revealed by specifically targeted recombinant aequorin. Nature. 1992;358(6384):325-7. Epub 1992/07/23.
69. Montero M, Brini M, Marsault R, Alvarez J, Sitia R, Pozzan T, et al. Monitoring dynamic changes in free Ca2+ concentration in the endoplasmic reticulum of intact cells. The EMBO journal. 1995;14(22):5467-75. Epub 1995/11/15.
70. Rizzuto R, Bastianutto C, Brini M, Murgia M, Pozzan T. Mitochondrial Ca2+ homeostasis in intact cells. The Journal of cell biology. 1994;126(5):1183-94. Epub 1994/09/01.
71. Brini M, Marsault R, Bastianutto C, Alvarez J, Pozzan T, Rizzuto R. Transfected aequorin in the measurement of cytosolic Ca2+ concentration ([Ca2+]c). A critical evaluation. The Journal of biological chemistry. 1995;270(17):9896-903. Epub 1995/04/28.
72. Kendall JM, Dormer RL, Campbell AK. Targeting aequorin to the endoplasmic reticulum of living cells. Biochemical and biophysical research communications. 1992;189(2):1008-16. Epub 1992/12/15.
73. Marsault R, Murgia M, Pozzan T, Rizzuto R. Domains of high Ca2+ beneath the plasma membrane of living A7r5 cells. The EMBO journal. 1997;16(7):1575-81. Epub 1997/04/01.
74. Miyawaki A, Griesbeck O, Heim R, Tsien RY. Dynamic and quantitative Ca2+ measurements using improved cameleons. Proceedings of the National Academy of Sciences of the United States of America. 1999;96(5):2135-40. Epub 1999/03/03.
75. Shimomura O, Johnson FH, Saiga Y. Extraction, purification and properties of aequorin, a bioluminescent protein from the luminous hydromedusan, Aequorea. JCell Comp Physiol. 1962;59:223-39.

76. Cody CW, Prasher DC, Westler WM, Prendergast FG, Ward WW. Chemical structure of the hexapeptide chromophore of the Aequorea green-fluorescent protein. Biochemistry. 1993;32(5):1212-8. Epub 1993/02/09.
77. Prasher DC, Eckenrode VK, Ward WW, Prendergast FG, Cormier MJ. Primary structure of the Aequorea victoria green-fluorescent protein. Gene. 1992;111(2):229-33. Epub 1992/02/15.
78. Tsien RY. The green fluorescent protein. Annu Rev Biochem. 1998;67:509-44. Epub 1998/10/06.
79. Chalfie M, Tu Y, Euskirchen G, Ward WW, Prasher DC. Green fluorescent protein as a marker for gene expression. Science. 1994;263(5148):802-5.
80. Cubitt AB, Heim R, Adams SR, Boyd AE, Gross LA, Tsien RY. Understanding, improving and using green fluorescent proteins. Trends Biochem Sci. 1995;20(11):448-55. Epub 1995/11/01.
81. De Giorgi F, Brini M, Bastianutto C, Marsault R, Montero M, Pizzo P, et al. Targeting aequorin and green fluorescent protein to intracellular organelles. Gene. 1996;173(1 Spec No):113-7.
82. Pollok BA, Heim R. Using GFP in FRET-based applications. Trends Cell Biol. 1999;9(2):57-60. Epub 1999/03/24.
83. Heim R, Prasher DC, Tsien RY. Wavelength mutations and posttranslational autoxidation of green fluorescent protein. ProcNatlAcadSciUSA. 1994;91(26):12501-4.
84. Heim R, Cubitt AB, Tsien RY. Improved green fluorescence. Nature. 1995;373(6516):663-4. Epub 1995/02/23.
85. Zolotukhin S, Potter M, Hauswirth WW, Guy J, Muzyczka N. A "humanized" green fluorescent protein cDNA adapted for high-level expression in mammalian cells. J Virol. 1996;70(7):4646-54. Epub 1996/07/01.
86. Ward WW, Cormier MJ. An energy transfer protein in coelenterate bioluminescence. Characterization of the Renilla green-fluorescent protein. J Biol Chem. 1979;254(3):781-8. Epub 1979/02/10.
87. Rutter GA, Kennedy HJ, Wood CD, White MR, Tavare JM. Real-time imaging of gene expression in single living cells. ChemBiol. 1998;5(11):R285-R90.
88. Heim R, Tsien RY. Engineering green fluorescent protein for improved brightness, longer wavelengths and fluorescence resonance energy transfer. CurrBiol. 1996;6(2):178-82.
89. Mitra RD, Silva CM, Youvan DC. Fluorescence resonance energy transfer between blue-emitting and red-shifted excitation derivatives of the green fluorescent protein. Gene. 1996;173(1 Spec No):13-7. Epub 1996/01/01.
90. Xu X, Gerard AL, Huang BC, Anderson DC, Payan DG, Luo Y. Detection of programmed cell death using fluorescence energy transfer. Nucleic Acids Res. 1998;26(8):2034-5. Epub 1998/06/06.
91. Mahajan NP, Harrison-Shostak DC, Michaux J, Herman B. Novel mutant green fluorescent protein protease substrates reveal the activation of specific caspases during apoptosis. Chem Biol. 1999;6(6):401-9. Epub 1999/06/22.
92. Romoser VA, Hinkle PM, Persechini A. Detection in living cells of Ca2+-dependent changes in the fluorescence emission of an indicator composed of two green fluorescent protein variants linked by a calmodulin-binding sequence. A new class of fluorescent indicators. J Biol Chem. 1997;272(20):13270-4. Epub 1997/05/16.
93. Xu Y, Piston DW, Johnson CH. A bioluminescence resonance energy transfer (BRET) system: application to interacting circadian clock proteins. Proc Natl Acad Sci U S A. 1999;96(1):151-6. Epub 1999/01/06.
94. Angers S, Salahpour A, Joly E, Hilairet S, Chelsky D, Dennis M, et al. Detection of beta 2-adrenergic receptor dimerization in living cells using bioluminescence resonance energy transfer (BRET). Proc Natl Acad Sci U S A. 2000;97(7):3684-9. Epub 2000/03/22.

95. Carrington WA, Lynch RM, Moore ED, Isenberg G, Fogarty KE, Fay FS. Superresolution three-dimensional images of fluorescence in cells with minimal light exposure. Science. 1995;268(5216):1483-7. Epub 1995/06/09.
96. Paemeleire K, Martin PE, Coleman SL, Fogarty KE, Carrington WA, Leybaert L, et al. Intercellular calcium waves in HeLa cells expressing GFP-labeled connexin 43, 32, or 26. Molecular biology of the cell. 2000;11(5):1815-27. Epub 2000/05/04.
97. ZhuGe R, Tuft RA, Fogarty KE, Bellve K, Fay FS, Walsh JV, Jr. The influence of sarcoplasmic reticulum Ca2+ concentration on Ca2+ sparks and spontaneous transient outward currents in single smooth muscle cells. The Journal of general physiology. 1999;113(2):215-28. Epub 1999/02/02.
98. Chang C, Simmons DT, Martin MA, Mora PT. Identification and partial characterization of new antigens from simian virus 40-transformed mouse cells. Journal of virology. 1979;31(2):463-71. Epub 1979/08/01.
99. Kress M, May E, Cassingena R, May P. Simian virus 40-transformed cells express new species of proteins precipitable by anti-simian virus 40 tumor serum. Journal of virology. 1979;31(2):472-83. Epub 1979/08/01.
100. Lane DP, Crawford LV. T antigen is bound to a host protein in SV40-transformed cells. Nature. 1979;278(5701):261-3. Epub 1979/03/15.
101. Linzer DI, Levine AJ. Characterization of a 54K dalton cellular SV40 tumor antigen present in SV40-transformed cells and uninfected embryonal carcinoma cells. Cell. 1979;17(1):43-52. Epub 1979/05/01.
102. Melero JA, Stitt DT, Mangel WF, Carroll RB. Identification of new polypeptide species (48-55K) immunoprecipitable by antiserum to purified large T antigen and present in SV40-infected and -transformed cells. Virology. 1979;93(2):466-80. Epub 1979/03/01.
103. Baker SJ, Fearon ER, Nigro JM, Hamilton SR, Preisinger AC, Jessup JM, et al. Chromosome 17 deletions and p53 gene mutations in colorectal carcinomas. Science. 1989;244(4901):217-21. Epub 1989/04/14.
104. Haupt Y, Maya R, Kazaz A, Oren M. Mdm2 promotes the rapid degradation of p53. Nature. 1997;387(6630):296-9. Epub 1997/05/15.
105. Vousden KH, Lane DP. p53 in health and disease. Nature reviews Molecular cell biology. 2007;8(4):275-83. Epub 2007/03/24.
106. Kamijo T, Bodner S, van de Kamp E, Randle DH, Sherr CJ. Tumor spectrum in ARF-deficient mice. Cancer research. 1999;59(9):2217-22. Epub 1999/05/08.
107. Lohrum MA, Ludwig RL, Kubbutat MH, Hanlon M, Vousden KH. Regulation of HDM2 activity by the ribosomal protein L11. Cancer cell. 2003;3(6):577-87. Epub 2003/07/05.
108. Christophorou MA, Ringshausen I, Finch AJ, Swigart LB, Evan GI. The pathological response to DNA damage does not contribute to p53-mediated tumour suppression. Nature. 2006;443(7108):214-7. Epub 2006/09/08.
109. Efeyan A, Collado M, Velasco-Miguel S, Serrano M. Genetic dissection of the role of p21Cip1/Waf1 in p53-mediated tumour suppression. Oncogene. 2007;26(11):1645-9. Epub 2006/09/12.
110. Jones RG, Plas DR, Kubek S, Buzzai M, Mu J, Xu Y, et al. AMP-activated protein kinase induces a p53-dependent metabolic checkpoint. Molecular cell. 2005;18(3):283-93. Epub 2005/05/04.
111. Matoba S, Kang JG, Patino WD, Wragg A, Boehm M, Gavrilova O, et al. p53 regulates mitochondrial respiration. Science. 2006;312(5780):1650-3. Epub 2006/05/27.
112. Polyak K, Xia Y, Zweier JL, Kinzler KW, Vogelstein B. A model for p53-induced apoptosis. Nature. 1997;389(6648):300-5. Epub 1997/09/26.
113. Rivera A, Maxwell SA. The p53-induced gene-6 (proline oxidase) mediates apoptosis through a calcineurin-dependent pathway. The Journal of biological chemistry. 2005;280(32):29346-54. Epub 2005/05/26.

114. Faraonio R, Vergara P, Di Marzo D, Pierantoni MG, Napolitano M, Russo T, et al. p53 suppresses the Nrf2-dependent transcription of antioxidant response genes. The Journal of biological chemistry. 2006;281(52):39776-84. Epub 2006/11/02.
115. Budanov AV, Sablina AA, Feinstein E, Koonin EV, Chumakov PM. Regeneration of peroxiredoxins by p53-regulated sestrins, homologs of bacterial AhpD. Science. 2004;304(5670):596-600. Epub 2004/04/24.
116. Hussain SP, Amstad P, He P, Robles A, Lupold S, Kaneko I, et al. p53-induced up-regulation of MnSOD and GPx but not catalase increases oxidative stress and apoptosis. Cancer research. 2004;64(7):2350-6. Epub 2004/04/03.
117. Yoon KA, Nakamura Y, Arakawa H. Identification of ALDH4 as a p53-inducible gene and its protective role in cellular stresses. Journal of human genetics. 2004;49(3):134-40. Epub 2004/02/27.
118. Marchenko ND, Zaika A, Moll UM. Death signal-induced localization of p53 protein to mitochondria. A potential role in apoptotic signaling. The Journal of biological chemistry. 2000;275(21):16202-12. Epub 2000/05/24.
119. Tomita Y, Marchenko N, Erster S, Nemajerova A, Dehner A, Klein C, et al. WT p53, but not tumor-derived mutants, bind to Bcl2 via the DNA binding domain and induce mitochondrial permeabilization. The Journal of biological chemistry. 2006;281(13):8600-6. Epub 2006/01/31.
120. Chipuk JE, Green DR. Cytoplasmic p53: bax and forward. Cell Cycle. 2004;3(4):429-31. Epub 2004/03/17.
121. Sot B, Freund SM, Fersht AR. Comparative biophysical characterization of p53 with the pro-apoptotic BAK and the anti-apoptotic BCL-xL. The Journal of biological chemistry. 2007;282(40):29193-200. Epub 2007/08/19.
122. Leu JI, Dumont P, Hafey M, Murphy ME, George DL. Mitochondrial p53 activates Bak and causes disruption of a Bak-Mcl1 complex. Nature cell biology. 2004;6(5):443-50. Epub 2004/04/13.
123. Wolff S, Erster S, Palacios G, Moll UM. p53's mitochondrial translocation and MOMP action is independent of Puma and Bax and severely disrupts mitochondrial membrane integrity. Cell research. 2008;18(7):733-44. Epub 2008/05/28.
124. Chipuk JE, Bouchier-Hayes L, Kuwana T, Newmeyer DD, Green DR. PUMA couples the nuclear and cytoplasmic proapoptotic function of p53. Science. 2005;309(5741):1732-5. Epub 2005/09/10.
125. Moll UM, Marchenko N, Zhang XK. p53 and Nur77/TR3 - transcription factors that directly target mitochondria for cell death induction. Oncogene. 2006;25(34):4725-43. Epub 2006/08/08.
126. Soussi T, Lozano G. p53 mutation heterogeneity in cancer. Biochemical and biophysical research communications. 2005;331(3):834-42. Epub 2005/05/04.
127. Mancini F, Di Conza G, Pellegrino M, Rinaldo C, Prodosmo A, Giglio S, et al. MDM4 (MDMX) localizes at the mitochondria and facilitates the p53-mediated intrinsic-apoptotic pathway. The EMBO journal. 2009;28(13):1926-39. Epub 2009/06/13.
128. Parant J, Chavez-Reyes A, Little NA, Yan W, Reinke V, Jochemsen AG, et al. Rescue of embryonic lethality in Mdm4-null mice by loss of Trp53 suggests a nonoverlapping pathway with MDM2 to regulate p53. Nature genetics. 2001;29(1):92-5. Epub 2001/08/31.
129. Migliorini D, Lazzerini Denchi E, Danovi D, Jochemsen A, Capillo M, Gobbi A, et al. Mdm4 (Mdmx) regulates p53-induced growth arrest and neuronal cell death during early embryonic mouse development. Molecular and cellular biology. 2002;22(15):5527-38. Epub 2002/07/09.
130. Marchenko ND, Wolff S, Erster S, Becker K, Moll UM. Monoubiquitylation promotes mitochondrial p53 translocation. The EMBO journal. 2007;26(4):923-34. Epub 2007/02/03.
131. Haglund K, Sigismund S, Polo S, Szymkiewicz I, Di Fiore PP, Dikic I. Multiple monoubiquitination of RTKs is sufficient for their endocytosis and degradation. Nature cell biology. 2003;5(5):461-6. Epub 2003/04/30.
132. Sigismund S, Polo S, Di Fiore PP. Signaling through monoubiquitination. Current topics in microbiology and immunology. 2004;286:149-85. Epub 2005/01/14.

133. Thrower JS, Hoffman L, Rechsteiner M, Pickart CM. Recognition of the polyubiquitin proteolytic signal. The EMBO journal. 2000;19(1):94-102. Epub 2000/01/05.
134. Endo H, Kamada H, Nito C, Nishi T, Chan PH. Mitochondrial translocation of p53 mediates release of cytochrome c and hippocampal CA1 neuronal death after transient global cerebral ischemia in rats. The Journal of neuroscience : the official journal of the Society for Neuroscience. 2006;26(30):7974-83. Epub 2006/07/28.
135. Kelly KJ, Plotkin Z, Vulgamott SL, Dagher PC. P53 mediates the apoptotic response to GTP depletion after renal ischemia-reperfusion: protective role of a p53 inhibitor. Journal of the American Society of Nephrology : JASN. 2003;14(1):128-38. Epub 2002/12/31.
136. Tsujimoto Y, Finger LR, Yunis J, Nowell PC, Croce CM. Cloning of the chromosome breakpoint of neoplastic B cells with the t(14;18) chromosome translocation. Science. 1984;226(4678):1097-9.
137. Chipuk JE, Moldoveanu T, Llambi F, Parsons MJ, Green DR. The BCL-2 family reunion. Mol Cell. 2010;37(3):299-310. Epub 2010/02/18.
138. Pinton P, Ferrari D, Magalhaes P, Schulze-Osthoff K, Di Virgilio F, Pozzan T, et al. Reduced loading of intracellular Ca(2+) stores and downregulation of capacitative Ca(2+) influx in Bcl-2-overexpressing cells. The Journal of Cell Biology. 2000;148(5):857-62.
139. Pinton P, Ferrari D, Rapizzi E, Di Virgilio FD, Pozzan T, Rizzuto R. The Ca2+ concentration of the endoplasmic reticulum is a key determinant of ceramide-induced apoptosis: significance for the molecular mechanism of Bcl-2 action. EMBO J. 2001;20(11):2690-701.
140. Foyouzi-Youssefi R, Arnaudeau S, Borner C, Kelley WL, Tschopp J, Lew DP, et al. Bcl-2 decreases the free Ca2+ concentration within the endoplasmic reticulum. ProcNatlAcadSciUSA. 2000;97(11):5723-8.
141. Palmer AE, Jin C, Reed JC, Tsien RY. Bcl-2-mediated alterations in endoplasmic reticulum Ca2+ analyzed with an improved genetically encoded fluorescent sensor. ProcNatlAcadSciUSA. 2004;101(50):17404-9.
142. Chami M, Prandini A, Campanella M, Pinton P, Szabadkai G, Reed JC, et al. Bcl-2 and Bax exert opposing effects on Ca2+ signalling, which do not depend on their putative pore-forming region. Journal of Biological Chemistry. 2004.
143. Bassik MC, Scorrano L, Oakes SA, Pozzan T, Korsmeyer SJ. Phosphorylation of BCL-2 regulates ER Ca2+ homeostasis and apoptosis. EMBO J. 2004;23(5):1207-16.
144. Rong YP, Aromolaran AS, Bultynck G, Zhong F, Li X, McColl K, et al. Targeting Bcl-2-IP3 receptor interaction to reverse Bcl-2's inhibition of apoptotic calcium signals. Mol Cell. 2008;31(2):255-65. Epub 2008/07/29.
145. Decrock E, Krysko DV, Vinken M, Kaczmarek A, Crispino G, Bol M, et al. Transfer of IP(3) through gap junctions is critical, but not sufficient, for the spread of apoptosis. Cell Death Differ. 2011. Epub 2011/11/26.
146. Giorgi C, Ito K, Lin HK, Santangelo C, Wieckowski MR, Lebiedzinska M, et al. PML regulates apoptosis at endoplasmic reticulum by modulating calcium release. Science. 2010;330(6008):1247-51. Epub 2010/10/30.
147. Bernardi R, Pandolfi PP. Structure, dynamics and functions of promyelocytic leukaemia nuclear bodies. Nature reviews Molecular cell biology. 2007;8(12):1006-16. Epub 2007/10/12.
148. Wang ZG, Ruggero D, Ronchetti S, Zhong S, Gaboli M, Rivi R, et al. PML is essential for multiple apoptotic pathways. Nature genetics. 1998;20(3):266-72. Epub 1998/11/07.
149. Marchi S, Rimessi A, Giorgi C, Baldini C, Ferroni L, Rizzuto R, et al. Akt kinase reducing endoplasmic reticulum Ca2+ release protects cells from Ca2+-dependent apoptotic stimuli. Biochemical and biophysical research communications. 2008;375(4):501-5. Epub 2008/08/30.
150. Jones AW, Szabadkai G. Ca(2)(+) transfer from the ER to mitochondria: channeling cell death by a tumor suppressor. Developmental cell. 2010;19(6):789-90. Epub 2010/12/15.

151. Giorgi C, De Stefani D, Bononi A, Rizzuto R, Pinton P. Structural and functional link between the mitochondrial network and the endoplasmic reticulum. Int J Biochem Cell Biol. 2009. Epub 2009/04/25.
152. Bernardi R, Papa A, Pandolfi PP. Regulation of apoptosis by PML and the PML-NBs. Oncogene. 2008;27(48):6299-312.
153. Rimessi A, Giorgi C, Pinton P, Rizzuto R. The versatility of mitochondrial calcium signals: From stimulation of cell metabolism to induction of cell death. Biochim Biophys Acta. 2008;1777(7-8):808-16.
154. Sano R, Annunziata I, Patterson A, Moshiach S, Gomero E, Opferman J, et al. GM1-ganglioside accumulation at the mitochondria-associated ER membranes links ER stress to Ca(2+)-dependent mitochondrial apoptosis. Mol Cell. 2009;36(3):500-11. Epub 2009/11/18.
155. Pinton P, Giorgi C, Siviero R, Zecchini E, Rizzuto R. Calcium and apoptosis: ER-mitochondria Ca2+ transfer in the control of apoptosis. Oncogene. 2008;27(50):6407-18.
156. Pinton P, Giorgi C, Pandolfi PP. The role of PML in the control of apoptotic cell fate: a new key player at ER-mitochondria sites. Cell Death Differ. 2011. Epub 2011/04/09.
157. Giorgi C, Agnoletto C, Baldini C, Bononi A, Bonora M, Marchi S, et al. Redox control of protein kinase C: cell- and disease-specific aspects. Antioxid Redox Signal. 2010;13(7):1051-85. Epub 2010/02/09.
158. Li J, Lee B, Lee AS. Endoplasmic reticulum stress-induced apoptosis: multiple pathways and activation of p53-up-regulated modulator of apoptosis (PUMA) and NOXA by p53. J Biol Chem. 2006;281(11):7260-70. Epub 2006/01/13.
159. Petersen OH, Michalak M, Verkhratsky A. Calcium signalling: past, present and future. Cell Calcium. 2005;38(3-4):161-9.
160. Clapham DE. Calcium signaling. Cell. 2007;131(6):1047-58.
161. Pinton P, Rimessi A, Romagnoli A, Prandini A, Rizzuto R. Biosensors for the detection of calcium and pH. Methods Cell Biol. 2007;80:297-325.
162. Yang M, Ellenberg J, Bonifacino JS, Weissman AM. The transmembrane domain of a carboxyl-terminal anchored protein determines localization to the endoplasmic reticulum. J Biol Chem. 1997;272(3):1970-5.
163. Mihara M, Erster S, Zaika A, Petrenko O, Chittenden T, Pancoska P, et al. p53 has a direct apoptogenic role at the mitochondria. MolCell. 2003;11(3):577-90.
164. Chipuk JE, Kuwana T, Bouchier-Hayes L, Droin NM, Newmeyer DD, Schuler M, et al. Direct activation of Bax by p53 mediates mitochondrial membrane permeabilization and apoptosis. Science. 2004;303(5660):1010-4. Epub 2004/02/14.
165. Nutt LK, Pataer A, Pahler J, Fang B, Roth J, McConkey DJ, et al. Bax and Bak promote apoptosis by modulating endoplasmic reticular and mitochondrial Ca2+ stores. J Biol Chem. 2002;277(11):9219-25. Epub 2001/12/14.
166. Marchenko ND, Moll UM. The role of ubiquitination in the direct mitochondrial death program of p53. Cell Cycle. 2007;6(14):1718-23. Epub 2007/07/17.
167. Zhao Y, Chaiswing L, Velez JM, Batinic-Haberle I, Colburn NH, Oberley TD, et al. p53 translocation to mitochondria precedes its nuclear translocation and targets mitochondrial oxidative defense protein-manganese superoxide dismutase. Cancer research. 2005;65(9):3745-50. Epub 2005/05/04.
168. Vaseva AV, Moll UM. The mitochondrial p53 pathway. Biochimica et biophysica acta. 2009;1787(5):414-20. Epub 2008/11/15.
169. Vaseva AV, Marchenko ND, Moll UM. The transcription-independent mitochondrial p53 program is a major contributor to nutlin-induced apoptosis in tumor cells. Cell Cycle. 2009;8(11):1711-9. Epub 2009/05/05.
170. Perfettini JL, Kroemer RT, Kroemer G. Fatal liaisons of p53 with Bax and Bak. Nature cell biology. 2004;6(5):386-8. Epub 2004/05/04.

171. Brandt-Rauf PW, Monaco R, Pincus MR. Conformational effects of environmentally induced, cancer-related mutations in the p53 protein. Proceedings of the National Academy of Sciences of the United States of America. 1994;91(20):9262-6. Epub 1994/09/27.
172. Ghafourifar P, Mousavizadeh K, Parihar MS, Nazarewicz RR, Parihar A, Zenebe WJ. Mitochondria in multiple sclerosis. Frontiers in bioscience : a journal and virtual library. 2008;13:3116-26. Epub 2007/11/06.
173. Schoenfeld R, Wong A, Silva J, Li M, Itoh A, Horiuchi M, et al. Oligodendroglial differentiation induces mitochondrial genes and inhibition of mitochondrial function represses oligodendroglial differentiation. Mitochondrion. 2010;10(2):143-50. Epub 2009/12/17.
174. Xu L, Guo YS, Liu YL, Wu SY, Yang C, Wu DX, et al. Oxidative stress in immune-mediated motoneuron destruction. Brain research. 2009;1302:225-32. Epub 2009/08/04.
175. Stadelmann C. Multiple sclerosis as a neurodegenerative disease: pathology, mechanisms and therapeutic implications. Current opinion in neurology. 2011;24(3):224-9. Epub 2011/04/02.
176. Forte M, Gold BG, Marracci G, Chaudhary P, Basso E, Johnsen D, et al. Cyclophilin D inactivation protects axons in experimental autoimmune encephalomyelitis, an animal model of multiple sclerosis. Proceedings of the National Academy of Sciences of the United States of America. 2007;104(18):7558-63. Epub 2007/04/28.
177. Todorich B, Pasquini JM, Garcia CI, Paez PM, Connor JR. Oligodendrocytes and myelination: the role of iron. Glia. 2009;57(5):467-78. Epub 2008/10/07.
178. Benarroch EE. Oligodendrocytes: Susceptibility to injury and involvement in neurologic disease. Neurology. 2009;72(20):1779-85. Epub 2009/05/20.
179. Gupta S, Knight AG, Gupta S, Knapp PE, Hauser KF, Keller JN, et al. HIV-Tat elicits microglial glutamate release: role of NAPDH oxidase and the cystine-glutamate antiporter. Neuroscience letters. 2010;485(3):233-6. Epub 2010/09/21.
180. Tong W, Shah D, Xu J, Diehl JA, Hans A, Hannink M, et al. Involvement of lipid mediators on cytokine signaling and induction of secretory phospholipase A2 in immortalized astrocytes (DITNC). Journal of molecular neuroscience : MN. 1999;12(2):89-99. Epub 1999/10/20.
181. Selmaj K, Raine CS, Cannella B, Brosnan CF. Identification of lymphotoxin and tumor necrosis factor in multiple sclerosis lesions. The Journal of clinical investigation. 1991;87(3):949-54. Epub 1991/03/01.
182. Musabak U, Demirkaya S, Genc G, Ilikci RS, Odabasi Z. Serum adiponectin, TNF-alpha, IL-12p70, and IL-13 levels in multiple sclerosis and the effects of different therapy regimens. Neuroimmunomodulation. 2011;18(1):57-66. Epub 2010/08/18.
183. Vladic A, Horvat G, Vukadin S, Sucic Z, Simaga S. Cerebrospinal fluid and serum protein levels of tumour necrosis factor-alpha (TNF-alpha) interleukin-6 (IL-6) and soluble interleukin-6 receptor (sIL-6R gp80) in multiple sclerosis patients. Cytokine. 2002;20(2):86-9. Epub 2002/11/26.
184. Martino G, Consiglio A, Franciotta DM, Corti A, Filippi M, Vandenbroeck K, et al. Tumor necrosis factor alpha and its receptors in relapsing-remitting multiple sclerosis. Journal of the neurological sciences. 1997;152(1):51-61. Epub 1997/12/12.
185. McCoy MK, Tansey MG. TNF signaling inhibition in the CNS: implications for normal brain function and neurodegenerative disease. Journal of neuroinflammation. 2008;5:45. Epub 2008/10/18.
186. Dopp JM, Mackenzie-Graham A, Otero GC, Merrill JE. Differential expression, cytokine modulation, and specific functions of type-1 and type-2 tumor necrosis factor receptors in rat glia. Journal of neuroimmunology. 1997;75(1-2):104-12. Epub 1997/05/01.
187. Moreau T, Coles A, Wing M, Isaacs J, Hale G, Waldmann H, et al. Transient increase in symptoms associated with cytokine release in patients with multiple sclerosis. Brain : a journal of neurology. 1996;119 (Pt 1):225-37. Epub 1996/02/01.
188. Nomura T, Abe Y, Kamada H, Shibata H, Kayamuro H, Inoue M, et al. Therapeutic effect of PEGylated TNFR1-selective antagonistic mutant TNF in experimental autoimmune

encephalomyelitis mice. Journal of controlled release : official journal of the Controlled Release Society. 2011;149(1):8-14. Epub 2009/12/29.
189. Caminero A, Comabella M, Montalban X. Tumor necrosis factor alpha (TNF-alpha), anti-TNF-alpha and demyelination revisited: an ongoing story. Journal of neuroimmunology. 2011;234(1-2):1-6. Epub 2011/04/09.
190. Arnett HA, Mason J, Marino M, Suzuki K, Matsushima GK, Ting JP. TNF alpha promotes proliferation of oligodendrocyte progenitors and remyelination. Nature neuroscience. 2001;4(11):1116-22. Epub 2001/10/16.
191. Cammer W. Effects of TNFalpha on immature and mature oligodendrocytes and their progenitors in vitro. Brain research. 2000;864(2):213-9. Epub 2000/05/10.
192. Chen Y, Balasubramaniyan V, Peng J, Hurlock EC, Tallquist M, Li J, et al. Isolation and culture of rat and mouse oligodendrocyte precursor cells. Nature protocols. 2007;2(5):1044-51. Epub 2007/06/05.
193. Ben-Hur T, Ben-Menachem O, Furer V, Einstein O, Mizrachi-Kol R, Grigoriadis N. Effects of proinflammatory cytokines on the growth, fate, and motility of multipotential neural precursor cells. Molecular and cellular neurosciences. 2003;24(3):623-31. Epub 2003/12/11.
194. Agresti C, Meomartini ME, Amadio S, Ambrosini E, Volonte C, Aloisi F, et al. ATP regulates oligodendrocyte progenitor migration, proliferation, and differentiation: involvement of metabotropic P2 receptors. Brain research Brain research reviews. 2005;48(2):157-65. Epub 2005/04/27.
195. Gavrieli Y, Sherman Y, Ben-Sasson SA. Identification of programmed cell death in situ via specific labeling of nuclear DNA fragmentation. The Journal of cell biology. 1992;119(3):493-501. Epub 1992/11/01.
196. Cohen RI, Almazan G. Rat oligodendrocytes express muscarinic receptors coupled to phosphoinositide hydrolysis and adenylyl cyclase. The European journal of neuroscience. 1994;6(7):1213-24. Epub 1994/07/01.
197. Murphy MP. How mitochondria produce reactive oxygen species. The Biochemical journal. 2009;417(1):1-13. Epub 2008/12/09.
198. Lee J, Giordano S, Zhang J. Autophagy, mitochondria and oxidative stress: cross-talk and redox signalling. The Biochemical journal. 2012;441(2):523-40. Epub 2011/12/23.
199. Gleyzer N, Scarpulla RC. PGC-1-related coactivator (PRC), a sensor of metabolic stress, orchestrates a redox-sensitive program of inflammatory gene expression. The Journal of biological chemistry. 2011;286(46):39715-25. Epub 2011/09/23.
200. Gilquin B, Cannon BR, Hubstenberger A, Moulouel B, Falk E, Merle N, et al. The calcium-dependent interaction between S100B and the mitochondrial AAA ATPase ATAD3A and the role of this complex in the cytoplasmic processing of ATAD3A. Molecular and cellular biology. 2010;30(11):2724-36. Epub 2010/03/31.
201. Hayashi T, Su TP. Sigma-1 receptors at galactosylceramide-enriched lipid microdomains regulate oligodendrocyte differentiation. Proceedings of the National Academy of Sciences of the United States of America. 2004;101(41):14949-54. Epub 2004/10/07.
202. Montero M, Lobaton CD, Moreno A, Alvarez J. A novel regulatory mechanism of the mitochondrial Ca2+ uniporter revealed by the p38 mitogen-activated protein kinase inhibitor SB202190. FASEB journal : official publication of the Federation of American Societies for Experimental Biology. 2002;16(14):1955-7. Epub 2002/10/09.
203. Cammer W, Zhang H. Maturation of oligodendrocytes is more sensitive to TNF alpha than is survival of precursors and immature oligodendrocytes. Journal of neuroimmunology. 1999;97(1-2):37-42. Epub 1999/07/17.
204. Rossi D, Volterra A. Astrocytic dysfunction: insights on the role in neurodegeneration. Brain research bulletin. 2009;80(4-5):224-32. Epub 2009/07/28.

205. Merrill JE. Tumor necrosis factor alpha, interleukin 1 and related cytokines in brain development: normal and pathological. Developmental neuroscience. 1992;14(1):1-10. Epub 1992/01/01.
206. Brown GC, Borutaite V. There is no evidence that mitochondria are the main source of reactive oxygen species in mammalian cells. Mitochondrion. 2012;12(1):1-4. Epub 2011/02/10.
207. Malinska D, Kulawiak B, Kudin AP, Kovacs R, Huchzermeyer C, Kann O, et al. Complex III-dependent superoxide production of brain mitochondria contributes to seizure-related ROS formation. Biochimica et biophysica acta. 2010;1797(6-7):1163-70. Epub 2010/03/10.
208. Higuchi M, Proske RJ, Yeh ET. Inhibition of mitochondrial respiratory chain complex I by TNF results in cytochrome c release, membrane permeability transition, and apoptosis. Oncogene. 1998;17(19):2515-24. Epub 1998/11/21.
209. Mariappan N, Elks CM, Fink B, Francis J. TNF-induced mitochondrial damage: a link between mitochondrial complex I activity and left ventricular dysfunction. Free radical biology & medicine. 2009;46(4):462-70. Epub 2008/12/02.
210. Ziabreva I, Campbell G, Rist J, Zambonin J, Rorbach J, Wydro MM, et al. Injury and differentiation following inhibition of mitochondrial respiratory chain complex IV in rat oligodendrocytes. Glia. 2010;58(15):1827-37. Epub 2010/07/29.
211. Vandamme W, Braet K, Cabooter L, Leybaert L. Tumour necrosis factor alpha inhibits purinergic calcium signalling in blood-brain barrier endothelial cells. Journal of neurochemistry. 2004;88(2):411-21. Epub 2003/12/24.
212. Wieckowski MR, Giorgi C, Lebiedzinska M, Duszynski J, Pinton P. Isolation of mitochondria-associated membranes and mitochondria from animal tissues and cells. Nat Protoc. 2009;4(11):1582-90. Epub 2009/10/10.